Master's thesis

NTNU
Norwegian University of Science and Technology
Faculty of Engineering
Department of Energy and Process Engineering

Omar Volpato

Design of an Integrated Energy System using a Cascade High Temperature Heat Pump with Zeotropic Refrigerants.

Master's thesis in Chemical and Process Engineering
Supervisor: Trygve Magne Eikevik
Co-supervisor: Ganesan Palanichamy
December 2023

NTNU
Norwegian University of
Science and Technology

Omar Volpato

Design of an Integrated Energy System using a Cascade High Temperature Heat Pump with Zeotropic Refrigerants.

Master's thesis in Chemical and Process Engineering
Supervisor: Trygve Magne Eikevik
Co-supervisor: Ganesan Palanichamy
December 2023

Norwegian University of Science and Technology
Faculty of Engineering
Department of Energy and Process Engineering

NTNU
Norwegian University of Science and Technology

Norwegian University of Science and Technology Engineering

Faculty of Engineering Department of Energy and Process

EPT-P-2023

MASTER'S THESIS

for

student Omar Volpato

Autumn 2023

Design of an integrated energy system using a cascade high temperature heat pump with zeotropic refrigerants.

Design av et integrert energisystem ved bruk av en kaskade høytemperatur varmepumpe med zeotropiske kjølemidler.

Background and objective

Combined cooling, heating, and power generation system meets the need of low-carbon neighborhood to fully absorb renewable energy. A development of load peak-shaving technology of renewable energy based on solar energy with thermal energy storage (TES), as well as the new solar-thermal converting devices, with high-temperature heat pump and compact energy storage system (PCM). In the scenario of 100% clean energy, to achieve a high proportion of renewable energy acceptance by energy supply systems in large public buildings or small-scale neighborhoods. In such systems it is necessary to develop a high-temperature electric heat pump using green or natural working fluid, in which the hot side outlet temperature can reach to 100°C, the temperature rise can exceed 50°C, and the COP of the heating system can exceed 3.6. Evaluate different system solutions and alternative natural working fluids to be able to fulfill the requirement.

- System development
- Transient operations
- Compressor optimization

The project is in cooperation with Shanghai Jiao Tong University.

The following tasks are to be considered:

1. Literature review of high-temperature heat pumps in integrated systems
2. Furter development of the software programming for optimization of transient operations.
3. Consider different green zeotropic mixtures as working fluids.
4. Select a case (architecture) for the system.
5. Investigate the influence on the seasonal coefficient of performance related to the design point of the system.
6. Investigate the potential of the high-temperature heat pump in the integrated system using dynamic simulation.
7. Make a proposal for further work.

Abstract

In the face of an escalating global energy demand, this thesis deals with the pivotal challenge of designing and modelling a self-sustainable integrated energy system. At its core, the system harnesses the power of a cascade high-temperature heat pump utilizing zeotropic refrigerants. The heat pump design is specifically sized to generate hot water for district heating with a temperature higher than 100°C, coupled with a Coefficient of Performance (COP) surpassing 3.6. This innovative system is tested in Oslo through a Matlab simulation, underlying the practical applicability to real-world scenarios. The results of this research demonstrate a noteworthy achievement: the proposed system not only meets the two design specifications, but is also a sustainable and efficient source of energy. The simulation is performed over a year on an hourly basis. The system proves capable of providing enough heat to satisfy the district heating demand for 9/12 months of the year while also achieving self-sustainability during its operation. In addition, the deployment of zeotropic mixtures as refrigerants adds an extra layer of efficiency and adaptability to the system thanks to their temperature glide. This remarkable success is a significant jump forward in clean and sustainable energy solutions, particularly for district heating. It demonstrates the potential of high temperature heat pumps to effectively address the energy needs of our world.

Sammendrag

I møte med en eskalerende global etterspørsel etter energi, tar denne avhandlingen for seg den sentrale utfordringen med å designe og modellere et selvstendig integrert energisystem. Ved kjernen utnytter systemet kraften fra en kaskadevarmepumpe med høy temperatur som bruker zeotropiske kjølemidler. Varmepumpedesignet er spesifikt dimensjonert for å generere varmt vann til fjernvarme med en temperatur over 100 °C, koblet med en ytelsesfaktor (COP) som overstiger 3,6. Dette innovative systemet testes i Oslo gjennom en Matlab-simulering, som understreker den praktiske anvendbarheten i virkelige scenarier. Resultatene av denne forskningen viser en bemerkelsesverdig prestasjon: det foreslåtte systemet oppfyller ikke bare de to designspesifikasjonene, men er også en bærekraftig og effektiv energikilde. Simuleringen utføres over et år på timesbasis. Systemet viser seg å være i stand til å levere nok varme for å tilfredsstille fjernvarmebehovet i 9 av 12 måneder i året, samtidig som det oppnår selvstendighet under driften. I tillegg legger bruken av zeotropiske blandinger som kjølemidler til et ekstra lag av effektivitet og tilpasningsevne til systemet takket være deres temperaturglidning. Denne bemerkelsesverdige suksessen representerer et betydelig skritt fremover innen rene og bærekraftige energiløsninger, spesielt for fjernvarme. Den demonstrerer potensialet til høytemperatur varmepumper for å effektivt imøtekomme energibehovene til vår verden.

Sommario

Di fronte a una crescente richiesta globale di energia, questa tesi affronta la sfida cruciale della progettazione e modellazione di un sistema energetico integrato autosufficiente. Al suo nucleo, il sistema sfrutta la potenza di una pompa di calore ad alta temperatura a cascata che utilizza refrigeranti zeotropici. Il progetto è dimensionato specificatamente per generare acqua calda per il riscaldamento urbano con una temperatura superiore a 100°C, associata ad un Coefficiente di Prestazione (COP) che supera 3.6. Questo sistema innovativo è testato ad Oslo attraverso una simulazione Matlab, sottolineando l'applicabilità pratica scenari reali. I risultati di questo lavoro di ricerca dimostrano una conquista notevole: il sistema proposto non solo soddisfa le due specifiche di progettazione, ma è anche una fonte di energia sostenibile ed efficiente. La simulazione è eseguita durante un intero anno su base oraria. Il sistema si dimostra in grado di fornire abbastanza calore da soddisfare la domanda di riscaldamento urbano per 9/12 mesi, garantendo contemporaneamente l'autosufficienza termica durante il suo funzionamento. Inoltre, l'impiego di miscele zeotropiche come refrigeranti aggiunge un ulteriore strato di efficienza e adattabilità al sistema, grazie al loro *glide*. Questo notevole successo rappresenta un significativo passo avanti nelle soluzioni energetiche pulite e sostenibili, in particolare per il riscaldamento urbano. Dimostra il potenziale delle pompe di calore ad alta temperatura nell'affrontare in modo efficace le esigenze energetiche del nostro mondo.

Preface

Embarking on an academic journey often takes unexpected turns, and mine led me to the enriching experience of Erasmus+ mobility. As I stand at the completion of this thesis, I am filled with gratitude for the unique opportunities and perspectives that this international adventure has provided. I would like to express my gratitude to my esteemed supervisor, Trygve M. Eikevik and my co-supervisor postdoctoral fellow, Ganesan Palanichamy. Your unwavering support, insightful guidance, and boundless patience have been instrumental in shaping this research, even across borders.

After my semester abroad at NTNU I would like to thank my family, always supporting me from home. I am also profoundly grateful to my housemates who generously dedicated their time to correct and revise my work. Your willingness to engage in scholarly discourse, despite the non-academic nature of our living arrangements, has been invaluable. I would also like to express my gratitude to the University of Padova for granting me the opportunity to participate in the Erasmus+ program. This experience has not only broadened my academic horizons but has also enriched my personal and professional development in ways I could have never imagined. In closing, I dedicate this work to those who have accompanied me on this long journey. My hope is that this thesis will contribute, in some small measure, to the ever-expanding mosaic of knowledge.

Omar Volpato

Università degli Studi di Padova (UniPd)

Norges Teknisk-Naturvitenskapelige Universitet (NTNU)

19/12/2023

Table of Contents

List of Figures

List of Tables

List of Abbreviations

AHX	Auxiliary Heat Exchanger
ASHRAE	American Society of Heating, Refrigerating and Air Conditioning Engineering
BFD	Block Flow Diagram
BHE	Borehole Heat Exchanger
BTES	Borehole Thermal Energy Storage
CFC	ChloroFluoroCarbon
CO_2	Carbon Dioxide
COP	Coefficient of Performance
DH	District Heating
GSHP	Ground Source Heat Pump
HFC	HydroFluoroCarbon
HP	Heat Pump
HTHP	High Temperature Heat Pump
HS	High Stage
HX	Heat Exchanger
IES	Integrated Energy System
IHX	Internal Heat Exchanger
ISO	International Organization for Standardization
LDC	Load-Duration Curve
LMTD	Logarithmic Mean Temperature Difference
LS	Low Stage
NIST	National Institute of Standard and Technology
NTNU	Norges Teknisk-Naturvitenskapelige Universitet
ODP	Ozone Depletion Potential
PCM	Phase-Change Material
PCM-TES	Phase-Change Material Thermal Energy Storage
PFD	Process Flow Diagram
PV	PhotoVoltaic

PVT	PhotoVoltaic/Thermal
SAHP	Solar Assisted Heat Pump
SDG	Sustainable Development Goals
TCM	Thermo-Chemical Materials
TES	Thermal Energy Storage
VHTHP	Very High Temperature Heat Pump
VLE	Vapor-Liquid Equilibrium

Nomenclature

A	Area [m^2]
B	Battery capacity [kWh]
c_p	Specific heat capacity [kJ/(kg*K)]
COP	Coefficient of performance [-]
D	Heat demand [kW]
E	Error on the LMTD [K]
h	Enthalpy [kJ/kg]
H	BTES capacity [kWh]
I_t	Solar irradiance [W/m^2]
$\dot{m}$	Mass flow rate [kg/s]
P	Pressure [bar]/[kPa]
$\dot{P}_{el}$	Electrical power from PVT [kW]
$\dot{P}_{th}$	Thermal power from PVT [kW]
$\dot{Q}$	Heat flow [kW]
r	Compression ratio [-]
s	Entropy [kJ/(kg*K)]
S	PCM-TES capacity [kWh]
T	Temperature [K]/[°C]
T_a	Air temperature [K]/[°C]
U	Global heat transfer coefficient [W/(m^2*K)]
V_c	Compressor size [m^3/h]
$\dot{W}$	Work flow [kW]
ΔT_{ml}	Logarithmic mean temperature difference [K]
η	Efficiency [-]
θ	Temperature difference [K]
ρ	Mass density [kg/m^3]

1. Introduction

1.1. Background and Motivation

The world has been witnessing an unprecedented surge in the demand of energy prompted by rapid population growth, industrialization and technological progress. The investigation and development of sustainable and efficient solutions have become of primary importance to face this escalating need for energy. In the prospect of energy systems, the alignment with global initiatives such as the Sustainable Development Goals (SDGs) is now more pressing than ever. This thesis explores the possibility of building an integrated energy system with a particular emphasis on key SDGs, such as affordable and clean energy (SDG 7), industry, innovation, and infrastructure (SDG 9), and climate action (SDG 13). In the past decades, the use of fossil fuels for heating purposes has been the predominant solution worldwide; however, in the Net Zero Emissions by 2050 scenario, the use of green energy source must become the preferred choice for a substantial reduction of CO_2 emissions in the atmosphere. The utilization of a heat pump for heat generation brings many benefits, both in terms of energy efficiency and mitigation of greenhouse gases release. Industrial processes that require heating and waste heat disposal can benefit from the development of high temperature heat pumps. Both investment and operational cost of boilers and cooling towers can be potentially saved with a single more efficient and less complex energy system, at the same time reducing the environmental footprint. Furthermore, the employment of zeotropic refrigerants adds a layer of complexity and innovation to the conventional heat pump paradigm, enhancing the energy-efficiency thanks to their varying compositions and thermodynamic properties. Understanding and optimizing the interactions within this integrated system becomes crucial as it directly contributes to SDG 13. This exploration is not merely an academic pursuit; it is a stride towards a future where energy systems seamlessly align with environmental stewardship, economic viability, and technological innovation, all the while reflecting the interconnected objectives of the SDGs. The following chapters will delve into the theoretical foundations, design considerations, and empirical analyses necessary to comprehend and implement this integrated energy system, emphasizing its potential to significantly reduce CO2 emissions and contribute to a sustainable future.

1.2. About the Project

This work is part of the bigger project “Key technologies and demonstration of combined cooling, heating and power generation for low-carbon neighborhoods/buildings with clean energy” (ChiNoZEN). The project is the result of the cooperation of Norwegian and Chinese researchers within energy topics. The ChiNoZEN project supports the transition to a reliable, affordable, publicly accepted and sustainably built environment, aiming at reducing fossil fuel dependency in the face of increasingly scarce resources, growing energy needs, and threatening climate change. The project delivers new knowledge, solutions and innovative technologies for low-carbon buildings and neighborhoods. The key result of the ChiNoZEN project is a combined cooling, heating and power generation system able to meet the needs of low-carbon communities to fully absorb nearby available renewable energy. The project is funded by the Research Council of Norway and the Ministry of Science and Technology in China, and has a variety of industry and academic partners in China and Norway (NTNU Department of Energy and Process Engineering, 2020).

Previous research works on the high temperature heat pump field are used as a starting point for this thesis. Many concepts and parameters for modelling the plant are taken from the master’s theses written by Ryssdal and Skoglund. From the theoretical point of view, Ganesan’s publications on high temperature heat pumps with zeotropic refrigerants have been illuminating. [1] [2] [3] [4]

2. Literature Review

2.1. Heat Pumps

A patent for an optimized heat pump system was granted to Slack and his collaborators in 2017. They designed a system for space heating or cooling including a heat pump with a refrigeration circuit for transferring heat between a source and a sink for heating and cooling operations. An interface receives user inputs, including an indication of discomfort based on temperature. The controller creates a profile for a minimum and a maximum comfortable temperature level, and controls the heat pump to perform heating and cooling operations in accordance with the profiles for comfortable temperature levels. The controller may also generate an optimized heat demand plan in accordance with predictions of outdoor and indoor temperature, cost, and demand. The plan is then optimized to cost-effectively maintain the temperature of the heated space within the comfortable temperature range defined by the profiles. [5]

Olympios et al. presented a methodology for identifying optimal designs for a low-temperature air-source heat pump with a single-stage compressor, based on the vapor-compression cycle suitable for domestic heating applications. They accounted explicitly for a trade-off between cost and efficiency, as well as for the influence of the outside air temperature during off-design operation. This was achieved through the development of comprehensive design and off-design heat-pump models, composed of dedicated heat exchanger models, screw compressor efficiency maps and costing correlations. Cost and performance of twelve different heat pump configurations with the same heat output were explicitly captured. The possible heat pump designs were integrated into a whole-energy system model representing the UK electricity and heat system, allowing the best configuration to be identified. The results showed that the best design and off-design performance was ensured using refrigerants R-152a and R-410a. From a system perspective, high-performance heat pumps require significantly less installed electricity generation capacity (20 GW) to decarbonize domestic heat by 2050, and therefore produce lower and more realistic power grid expansion rates. However, the use of a larger heat exchanger does not compensate overall for the increased technology cost, with low-performance HP being associated with the lowest system transition cost, which is about £35 billion lower than that achieved by higher-performance units. In their future work, Olympios et al. will consider more working fluid and component sizes, which will require the use of sophisticated surrogate models suitable for integrating the heat pump optimization problem within the whole-energy system optimization model. [6]

2.2. High Temperature Heat Pumps

Hays' design for a high temperature heat pump (2002) has been influential in the field. The invention relates generally to the utilization of waste heat in industrial applications, and in buildings, and more particularly the use of heat pumps to enable such low-level (<200°F) waste heat utilization, which is enormous. Basically, the invention is embodied in heat pump apparatus comprising a low temperature heat exchanger to produce vapor of a first fluid with the heat transferred from a second fluid, a high temperature heat exchanger to heat the second fluid to useful high temperatures from the condensation of the first fluid. A compressor increases pressure and temperature of the vapor, while an expansion valve lowers pressure and temperature of the first fluid producing a mixture of vapor and liquid. [7]

Bamibegtan et al. conducted a theoretical analysis to evaluate available and potential fluids with thermodynamic properties that are applicable for HTHPs. They showed that certain hydrocarbons and halocarbons are the most promising fluid candidates for waste heat upgrade from low to high temperatures, up to 125°C. The restrictions of safety and environmental impacts imposed by the Kigali's amendment to the Montreal protocol were considered. From the study resulted that R-600 and R-1233zd(E), show the highest potential for the immediate future implementation in HTHPs. R-600, though with lower COP compared to the heavier hydrocarbons, has a broad operating range and is therefore more flexible for different operating conditions. Also it is thermodynamically closer to R-600a and R-290 which have well developed compressor technology, and can be used directly in these compressors with little modifications. On the other hand, R-1233zd(E) showed a high COP with favorable autoignition temperature compared to R-601; nevertheless, its stability and compatibility must be tested and verified at the operating conditions, since its decomposition products are highly toxic and have negative effects on the environment. In their further research, Bamigbetan et al. will include experimental verification of the performances of the simulated fluids via laboratory scale tests, to obtain a better understanding of the fluids in operation at high temperature during compression. Furthermore, they will investigate the impact of fluid dependent effects like pressure drop, lubrication compatibility and lubrication stability on the process. [8]

Urbanucci et al. investigated the integration of high-temperature heat pumps within a trigeneration system. The heat pump uses the low-temperature heat from the condenser of the absorption chiller as heat source to produce hot water at around 90°C. The cooling tower or the air cooler can be replaced depending on the case. The technical viability of current heat pump technology and the performance of different working fluids were assessed by developing a numerical model of the heat pump cycle, apprising also the implementation of internal heat exchangers. The advantages of the novel trigeneration system with respect to traditional systems for energy production were shown via exergy analysis; the COP of the heat pump cycle was found a crucial parameter for the exergy performance. A levelized cost of electricity methodology was adopted to assess the economic viability of the proposed energy system, showing that the integration of the high-temperature heat pump within a trigeneration system can be economically profitable compared to conventional technologies. Urbanucci et al. integrated the proposed trigeneration system into an existing separate-production plant of a pharmaceutical factory as a case study. The profitability was investigated through the economic optimization of the investment with a two-level algorithm. The adopted system allows around huge global cost saving: 40% with respect to separate energy production and 10% with respect to traditional cogeneration and trigeneration processes, providing also the flexibility to cover variable energy demands. [9]

2.3. Cascade Heat Pumps

A design for a cascade heat pump system and with control system was developed by Choi (2011). A cascade type heat pump system was provided to immediately generate high temperature water for heating, or supplying it to maximize spatial utilization as separate water heating equipment is not necessary. The cascade heat pump system includes a first heat pump unit, a second heat pump unit, a cooling-and-heating unit, and a hot water supplying unit. The cooling-and-heating unit includes a heat storage tank and a second fluid line for cooling and heating. [10]

Yerdesh et al. studied the application of a two-stage cascade heat pump cycle operating with two different refrigerants to provide a sustainable solution to lift the condenser temperature above 70 ℃. They made this study because both heating capacity and coefficient of performance of a single stage vapor compression heat pump cycle are significantly reduced at low temperatures. Many refrigerant pairs were numerically tested for low and high temperature cycles, using Engineering Equation Solver software for the calculation of thermal performance. R-32/R-134a and R-410A/R-134a showed the highest vapor compression cycle COP of 1.98, from -30 ℃ ambient air temperature and +60 ℃ heating circuit temperature range. The above-mentioned refrigerants will be eventually suppressed in near future by Paris Agreement. R-32/R-290 and R-744/R-290 working fluids combinations were proposed as environmentally friendly alternative in the cascade cycle; they also allow the compressors to operate at a lower pressure ratio. Yerdesh et al. made some proposals for further work, including a cascade system optimal operation control algorithm, cascade heat pump components and overall system thermodynamic optimization, a study of intermediate cascade heat exchanger operational conditions, and an energy and exergy study. [11]

Jung et al. investigated experimentally cascade multi-functional heat pump, combining a heat pump using R-410A for air heating with a water heating unit using R-134a for hot water supply. The results were compared with those of a single-stage multi-functional heat pump using R-410A for air and water heating. The performance of the cascade multi-functional heat pump was measured by varying the refrigerant charge amount, valve opening, water flow rate, and water inlet temperature. The adoption of the water heating unit in the cascade multi-functional heat pump showed more stable air and water heating operations, and yielded higher water outlet temperatures, up to 76.6°C (at the water inlet temperature of 40.0°C and water flow rate of 120 kg/h). The air heating capacity of the cascade multi-functional heat pump remained relatively constant even with variations of the water inlet temperature and water flow rate, while that of the single-stage multi-functional heat pump varied significantly. On the other hand, when the water temperature was lower than 45°C, the COP of the cascade multi-functional heat pump was lower than the single-stage multi-functional heat pump. [12]

Boahen and Choi proposed a new cycle to enhance performance of the cascade heat pump by adopting an auxiliary heat exchanger (AHX) in desuperheater, heater and parallel positions at the low stage (LS) side. Compared to the conventional cycle, heating capacity and coefficient of performance (COP) of the new cascade cycle with AHX in desuperheater position increased up to 7.4% and 14.9% respectively. This strong improvement is due to the higher heat transfer to secondary fluid of the HS cycle in the AHX, and lowest pressure difference of the LS cycle. [13]

2.4. Zeotropic Heat Pumps

Yilmaz presented the performance analysis of an air-to-water vapor compression heat pump system using pure refrigerants and zeotropic refrigerant mixtures. The considered heat pump system was composed of compressor, condenser, air cooled evaporator, expansion valve, receiver tank, superheater/subcooler, refrigerant mixture unit and some auxiliary and measurement devices. Comparisons were made between the pure refrigerants R-12, R-22, R-114 and refrigerant mixtures R-12/R-114, R-12/R-22 based on the COP and second law efficiency; the effect of the evaporator source inlet temperature was also presented. Yilmaz concluded from his study that COP and second law efficiency increase with increasing evaporator source inlet temperature for both pure refrigerants and refrigerant mixtures; the results for pure refrigerants can be improved by using appropriate mixtures of the refrigerants. Moreover, the mixture ratio affects significantly the COP and second law efficiency of heat pumps, and this last factor can be used to identify the highest efficiency mixtures of refrigerants. [14]

Navarro-Esbrí et al. presented a semi-empirical assessment of a two-stage cascade cycle for high temperature heat pumps applications to produce hot water up to 150°C from a water flow at 35°C and 25°C. They assessed the energy performance of a cascade system through a validated semi-empirical model, considering several novel mixtures for both stages. The experimental results from two single-stage heat pump prototypes (R-1234ze(E) and R-1336mzz(Z)) with different temperature lifts were used for this study. The best refrigerant combinations, ensuring up to 14% COP increase respect to the base experimental results, were R-152a/600 (0.08/0.92) and R-1233zd(E)/161 (0.88/0.12) for the low stage and high stage, respectively. The LS mixture is however highly flammable, a possible replacement that satisfies the flammability concern is R-1234ze(E)/R-32 (0.7/0.3), which has a lower COP than the first proposed combination but still higher than the baseline. The COP increase of the proposed mixtures is remarkable but not excellent; however, the increase in the volumetric heating capacity is up to 30%. Future studies must consider different structures for obtaining better results in terms of efficiency. [15]

2.5. Solar/Ground-assisted Heat Pumps

Sezen and Gungor reviewed 77 recent studies on solar-assisted heat pump (SAHP) systems, which have been a popular research topic in last decades because of their proven improved performance by integrating solar energy to system. In their work, Sezen and Gungor classified the systems according to their configurations to provide an infrastructure for comparison, examining the effect of solar radiation and ambient temperature on SAHP systems performance and identifying the ambient condition ranges preferable for each system. The complexity of systems was expressed with type and number of components used, and the costs of the systems are compared considering the payback period. The reviewed studies revealed that, below solar irradiation of 400 W/m^2, direct expansion systems should be preferred because of their utilization of solar and air simultaneously as heat source. Indirect expansion systems are more complex than direct expansion systems and this limits their preferability; however, replacing the solar-side evaporator with a solar air preheater, thereby integrating the existing solar system and air source heat pump system, can simplify the indirect expansion systems. With low-cost external cooling devices, the temperature rise problem that prevents the use of PVT panels in indirect systems can be eliminated. [16]

Olabi et al. investigated the advancements, applications, research trends related to ground source heat pumps (GSHPs), and the challenges and barriers that face their development based on a bibliometric analysis. The results showed that in recent years, a considerable growth in GSHP's research has been recognized, with a focus on heating more than cooling, because GSHP is more suitable for cold regions. Moreover, GSHPs can play a significant role in achieving the sustainable development goals (SDGs), particularly for affordable and clean energy (SDG 7) and climate action (SDG 13). Based on the interpretation of the bibliometric analysis, Olabi et al. deduced that most of the challenges and barriers to GSHPs are related to their capital cost, groundwater contamination, regulations, subsidies, and incentives. An important point to clarify is that GSHP systems are highly sophisticated; as a result, installation, maintenance, and repair of these systems need the assistance of trained professionals. GSHPs however can create several jobs: engineers and designers for system design and installation, technicians for installation and maintenance, marketing personnel to promote GSHPs, researchers and scientists to develop the technology, and project managers to oversee installation and commissioning. Recent advancements in GSHPs are focusing on the development of new materials and designs to increase the efficiency of heat transfer from/to the ground/heat pump; this can lead to smaller GSHP systems that use less energy and are more cost-effective. [17]

Lazzarin and Noro studied the performance of a PVT dual source heat pump, operating with the ground as source/sink in a refurbished building located in Northern Italy. Dual or multisource heat pumps were conceived to obviate the defects of a single source, such as outside air, ground, water, or solar radiation. Concerning the latter, the use of Photovoltaic/Thermal (PVT) modules allows not only to partially recover the otherwise lost heat, but also to cool the PV and increase its electrical efficiency. The use of glazed PVT increases thermal efficiency of the collector, and the coupling of ground allows to keep the electrical efficiency at high values without the risk of cells damage due to overheating. When the heat pump does not need heat or operates for summer air conditioning, the ground is the heat sink for both the heat pump and for the PVT cooling. Lazzarin and Noro designed the plant by means of dynamic simulation considering five alternatives with increasing solar field area (20-40-60 m^2) and decreasing number of boreholes (5-4-3 of 100 m each), and compared them with a traditional solution (NG boiler + air/water chiller). The most efficient solution was found to be the alternative 60 m^2 PVT + 300 m boreholes. Increasing the solar field to a certain extent permits in facts the reduction of the ground field extension with better performances and lower costs, as confirmed also by previous Authors' study. Very high efficiency and low primary energy consumption were demonstrated for the whole plant, thanks also to the high energy independency from the grid. [18]

3. Theory

In this chapter a theoretical description of the subsystems used for building the integrated energy system (IES) is given. Specifically, the principles governing cascade heat pump is extensively illustrated, together with a thermodynamic elucidation of the use of zeotropic refrigerants in the heat pump cycle. Furthermore, a basic description of the functioning of photovoltaic/thermal panels, thermal energy storage and borehole storage is provided in the next subsections.

3.1. Heat Pumps

Heat pumps (HP) are a promising technology for heating (and cooling) domestic buildings that provide exceptionally high efficiencies compared with fossil fuel combustion. The HP has evolved to become a mature technology over the past three decades. They use an external energy source, often electricity, to remove heat from a cold location called heat source and pump it to a warmer one called heat sink, by continuously circulating a refrigerant.

A heat source can be a gas, air, water (surface water, underground water or discharged hot water) or the ground; a heat sink can be space heating (radiant panels, warm air, convective systems, etc.) for low-temperature heating systems, or water heating for high temperature heating systems. The main classification of HPs is related to the way in which external energy is driven into the system; a HP can use electrical energy (electro-

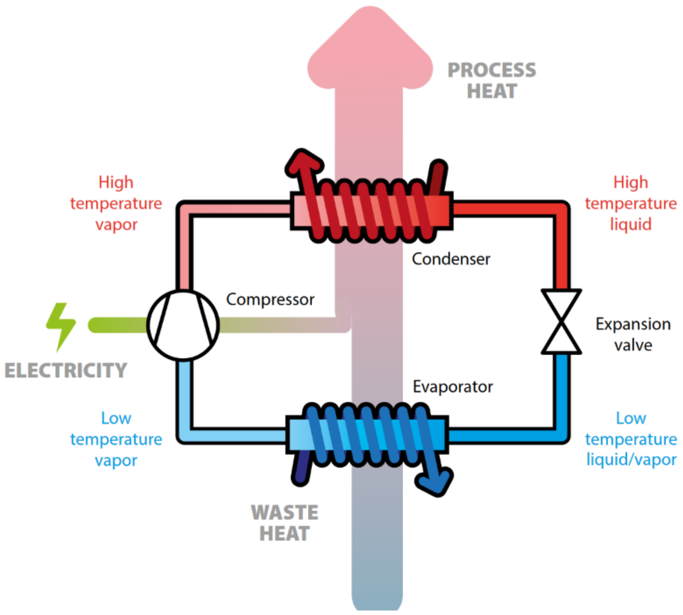

Figure 1: Scheme of a generic vapor compression heat pump.

compressor), mechanical energy (mechanical compression with expansion turbines), thermo-mechanical energy (steam ejector), thermal energy (absorption cycle), or thermo-electrical energy (Peltier effect). Most of the HPs used nowadays are based on a vapor-compression cycle, namely they are electrically driven; they include four basic units: an evaporator, a condenser, a compressor, and an expansion valve (see Figure 1). [19] [20] [21]

A HP cycle can be visualized from a thermodynamic point of view in a temperature-entropy (T-s) diagram or in a pressure-enthalpy (P-h) diagram.

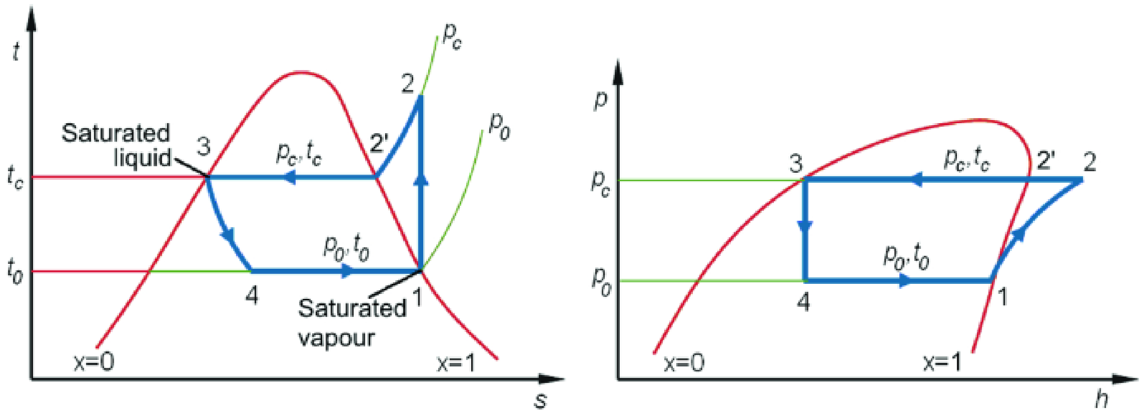

Figure 2: Temperature-entropy (T-s) diagram (left) and pressure-enthalpy (P-h) diagram (right) of the theoretical HP cycle

The theoretical vapor-compression HP cycle, shown in Figure 2, assumes isentropic compression, with no superheating of the vapor nor subcooling of the liquid; it is composed of the following reversible transformations of a closed system:

a) $(1 \rightarrow 2)$: Isentropic compression of the cold saturated vapor in the compressor, which increases pressure and temperature from (p_0, t_0) to (p_c, t_2).
b) $(2 \rightarrow 2')$: Isobaric cooling of the hot superheated vapor in the condenser at the pressure p_c, which reduces the temperature from t_2 to t_c.
c) $(2' \rightarrow 3)$: Isobaric condensation of the hot saturated vapor in the condenser at the pressure p_c.
d) $(3 \rightarrow 4)$: Isenthalpic expansion of the hot saturated liquid in the valve, which reduces pressure and temperature of the hot saturated liquid from (p_c, t_c) to (p_0, t_0).
e) $(4 \rightarrow 1)$: Isobaric evaporation of the biphasic fluid in the evaporator at the pressure p_0.

The specific compression work delivered to the system is given by Equation 3.1:

$$w = h_2 - h_1 \tag{3.1}$$

The specific heat gained by the system during the evaporation is given by Equation 3.2:

$$q_e = h_1 - h_4 \tag{3.2}$$

The specific heat lost by the system during the condensation is given by Equation 3.3:

$$q_c = h_2 - h_3 \tag{3.3}$$

Where the h_i represent the specific enthalpy of the fluid at the point i in the diagrams in Figure 2.

The efficiency of a HP cycle is usually represented in terms of the coefficient of performance (COP), which is defined as the ratio between the useful heat supplied by the system and the work supplied to the system; its definition is reported in Equation 3.4:

$$COP_{HP} = \frac{q_c}{w_c} > 1 \tag{3.4}$$

In the case of a real vapor-compression HP cycle, all the transformations are no longer reversible. The compression step is polytropic and pressure and heat losses are present in pipes and equipment; it is shown in Figure 3.

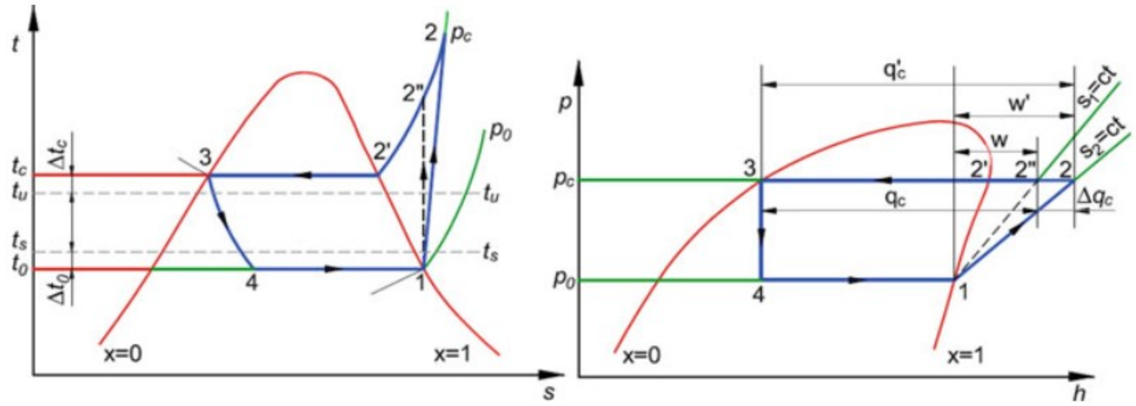

Figure 3: Temperature-entropy (T-s) diagram (left) and pressure-enthalpy (P-h) diagram (right) of the real HP cycle.

The isentropic efficiency of the compression step can be calculated according to Equation 3.5:

$$\eta_S = \frac{w}{w'} = \frac{w' - \Delta q_c}{w'} = 1 - \frac{\Delta q_c}{w'} < 1 \tag{3.5}$$

Where $w'$is the adiabatic irreversible compression work and Δq_c is the increase in the specific thermal load due to the non-ideality of the compression process. The real coefficient of performance of the HP system is therefore given by Equation 3.6:

$$COP'_{HP} = \frac{q'_c}{w'} = \frac{q_c + \Delta q_c}{w + \Delta q_c} = \frac{q_c + \left(\frac{1}{\eta_S} - 1\right) w}{w + \left(\frac{1}{\eta_S} - 1\right) w} = (COP_{HP} - 1)\eta_S + 1 < COP_{HP} \quad (3.6)$$

Where q'_c is the real specific thermal load of condensation in the real cycle. A real HP process has always a lower COP compared to the ideal case, which represents the upper limit of efficiency. In addition, the overall COP of the heating system is further diminished mainly because of mechanical and electrical losses of the compression equipment. Usually, the COP of a heat pump system ranges between 2 and 6. [22]

3.2. High Temperature Heat Pumps

There is not a generally accepted temperature level to distinguish between high temperature heat pumps (HTHP) and regular heat pumps. Another possible classification criteria, proposed by Arpagaus et al., is based on the heat source and sink temperature levels: HTHPs have a source temperature between 40 and 60°C and a sink temperature between 80 and 100°C, if the temperature levels are higher, it is the case of a very high temperature heat pumps (VHTHP). This concept was presented by Bobelin et al. In this work no distinction will be made between HTHPs, and VHTHPs; their operations are in fact identical. The only difference between high temperature heat pumps and regular heat pumps is in the heat source delivery temperature, obviously higher for the former. HTHPs are extensively used in industry to remove waste heat at 30-70°C, a level significantly higher if compared to outdoor air, seawater, groundwater or geothermal heat. [23] [24]

3.3. Cascade Heat Pumps

Cascade heat pumps are used in many industrial applications when the temperature difference between heat source and heat sink is too high to ensure the transfer of heat with a satisfactory efficiency. In cascade systems two or more HP cycles are nested together by means of cascade heat exchangers (see Figure 4). In this way the compression ratio of each cycle is much lower than the total one, ensuring a higher compression efficiency.

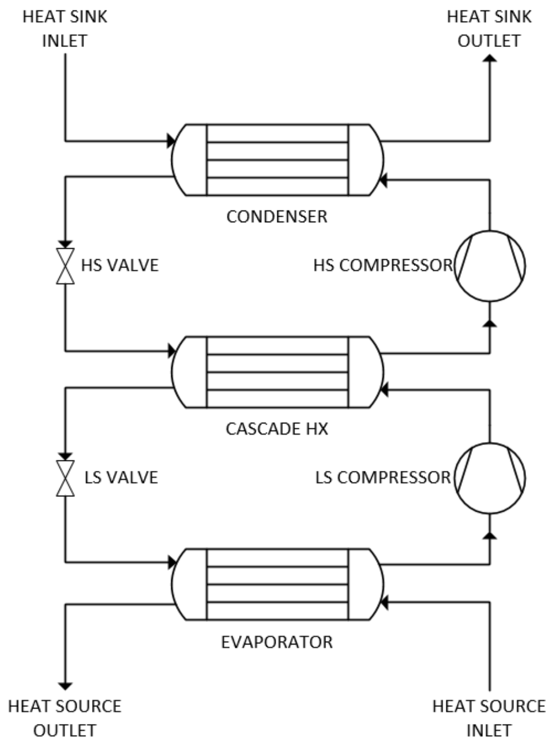

Figure 4: General scheme of a two-stage cascade HP.

The latent heat of vaporization of a refrigerant is lower at higher pressures, reaching zero at the critical point; therefore, the use of the same refrigerant for both high and low stages usually is not the optimal solution. The refrigerants used in a cascade HP have an increasing critical point by increasing the stage. The coefficient of performance for a cascade heat pump can be calculated according to Equation 3.7:

$$COP_{Cascade\ HP} = \frac{q_c}{\sum_i w_i} \tag{3.7}$$

Where w_i is the compression work in the i-th stage. [22]

3.4. Zeotropic Mixtures

A zeotropic mixture (or non-azeotropic mixture) is a mixture of two or more substances with different boiling points. The boiling point of a zeotropic mixture at a given pressure and composition is not unique, but ranges between the bubble point and the dew point, therefore a temperature glide exists at every composition except for the pure components. When a liquid zeotropic mixture vaporizes, it produces the first bubble of gas at the bubble point and consumes the last drop of liquid at the dew point, vice-versa during condensation. An azeotropic mixture presents at least one composition, called azeotrope, in which the bubble point and the dew point are equal, namely its temperature glide is zero, and it behaves as a pure refrigerant (see Figures 5-6).

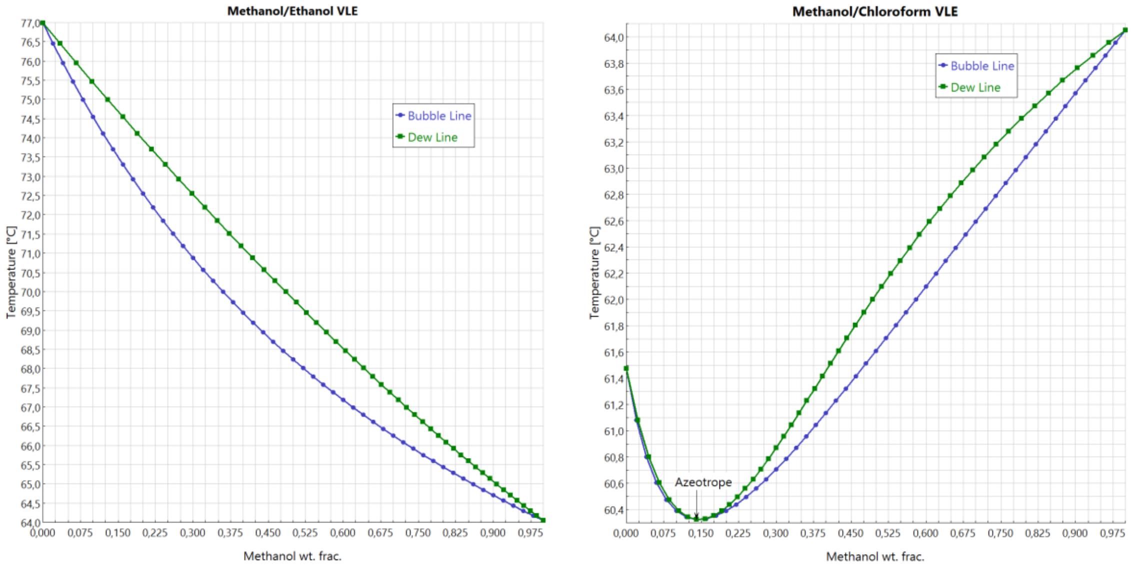

Figures 5-6: Example of VLE for a zeotropic mixture (left) and for an azeotropic mixture (right).

Normally pure refrigerants are used as working fluids in heat pumps. In those cases the HP can be seen thermodynamically as a reversed Carnot cycle, made of two isothermal and two isentropic transformations. When a zeotropic mixture is used, the heat pump resembles a modified Lorentz cycle, made of an isothermal, an isobaric and two isentropic transformations (see Figure 7).

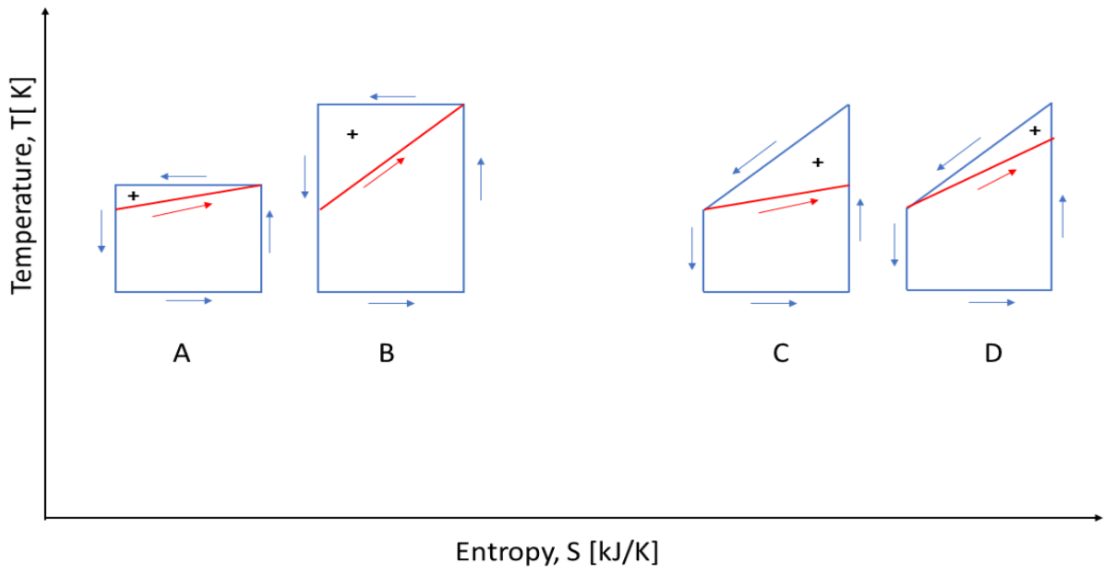

Figure 7: Sketch of the reverse Carnot cycle (left) and modified Lorentz cycle (right).

According to Stene, the modified Lorentz cycle has lower thermodynamic losses with respect to the reverse Carnot cycle, because of the better temperature profiles coupling between refrigerant and the counterflow secondary fluid. In Figure 7 the energy loss is represented graphically by a + sign. It results in an optimal composition of the zeotropic mixture that can be found ensuring the best coupling with the secondary fluid, minimizing the energy losses. [2] [25]

3.5. Photovoltaic/Thermal Panels (PVT)

Solar energy is a renewable energy that derives from the sun's radiation. It is abundant and widely distributed on earth, it is available for the whole year without costs almost everywhere, and it is clean because it does not generate pollution. For these reasons, solar energy is nowadays considered as one of the most valuable alternatives to the use of fossil fuels. As the world's need for energy is continuously increasing, also the technology for collecting solar energy makes steady progress in increasing the efficiency and reducing the costs of these systems.

Photovoltaic panels (PV) can be used to convert the sun radiation into electrical energy. Their basic building block is the solar cell, these cells are connected to form a module, which are in turn arranged to form an array with a flat surface. Each cell is made by contacting two layers of semiconductor materials with opposite charges: a p-type positive layer (an intrinsic semiconductor doped with an electron-acceptor element) and a n-type negative layer (an intrinsic semiconductor doped with an electron-donor element) separated by a p-n junction as shown in Figure 8. When the cell is exposed to solar radiation, photons hitting the surface knock electrons loose, which then travel through a

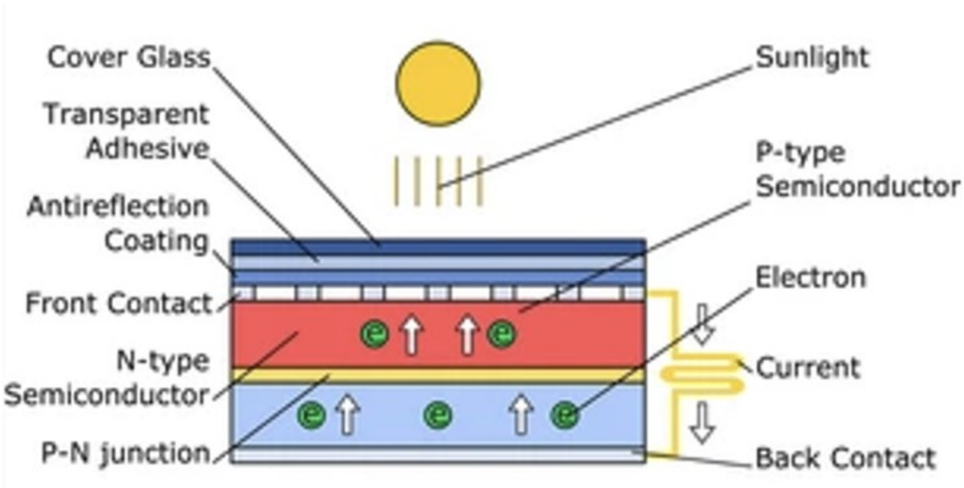

Figure 8: Simplified scheme of a solar cell.

circuit from one layer to the other, generating electricity. The surface of PV panels is usually coated by an anti-reflecting protective material, often tempered glass, which maximizes the amount of light absorbed by the cells, protecting them from the action of atmospheric agents.

The electrical power produced by a PV panel is given by Equation 3.8:

$$P_{el} = \eta_{el} I_t A_{PV} \tag{3.8}$$

Where I_t is the incident solar radiation, A_{PV} is the total area of the PV panel, and η_{el} is the electrical efficiency of the PV panel. The electrical efficiency is therefore defined as the fraction of the incident radiation energy that is converted into electrical energy by the solar cells (Equation 3.9).

$$\eta_{el} = \frac{P_{el}}{I_t A_{PV}} < 1 \tag{3.9}$$

The value of η_{el} is usually quite low, Dhilipan et al. made a comparison of different types of solar cells; overall the efficiency is around 20%. Furthermore, the electrical efficiency is lower at higher temperatures of the PV module; the temperature of the solar cells can increase because of the external air temperature or due to the conversion of a part of the solar radiation into heat. A common and unexpensive method employed to decrease the temperature of the cells is the forced air circulation. This is an efficient solution only when the air temperature is low enough to rapidly remove the heat generated. [26] [27]

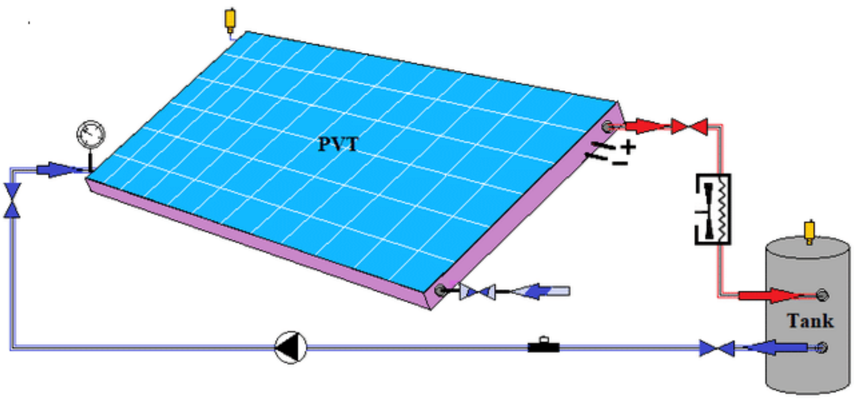

Figure 9: Simplified scheme of a photovoltaic/thermal (PVT) system.

When the air temperature is above 20°C for long periods of the year, which is common at low latitudes, the air heat removal works less effectively and the circulation of a refrigerant fluid is used instead. The refrigerant, which usually is water, flows through a heat exchanger in thermal contact with the rear part of the PV modules (see Figure 9). If the heat stored in the refrigerant fluid is used for heating purposes, then the system becomes a photovoltaic/thermal system (PVT), it offers a dual energy output and it can be effective in cost reduction. [28] [29]

The thermal power produced by a PVT panel is given by Equation 3.10:

$$P_{th} = \eta_{th} I_t A_{PVT} \tag{3.10}$$

Where A_{PVT} is the total area of the PVT panel and η_{th} is the thermal efficiency of the PVT panel. The thermal efficiency is therefore defined as the fraction of the incident radiation energy that is converted into heat by the solar/thermal system (Equation 3.11).

$$\eta_{el} = \frac{P_{th}}{I_t A_{PVT}} < 1 \tag{3.11}$$

The thermal efficiency of a PVT system is generally higher than its electrical efficiency. According to Sevela and Olesen, it can reach a maximum of 42%. [30]

3.6. Thermal Energy Storages (TES)

The accumulation of energy is paramount for several applications, many industrial and domestic processes require a continuous energy input. The energy supply can be intermittent during the day or the year due to impractical production or to its high cost. Therefore, a system for the storage of energy enables an efficient use of it, storing energy when is abundant or cheap and releasing it when is scarce or costly, makes the process independent of the energy supply.

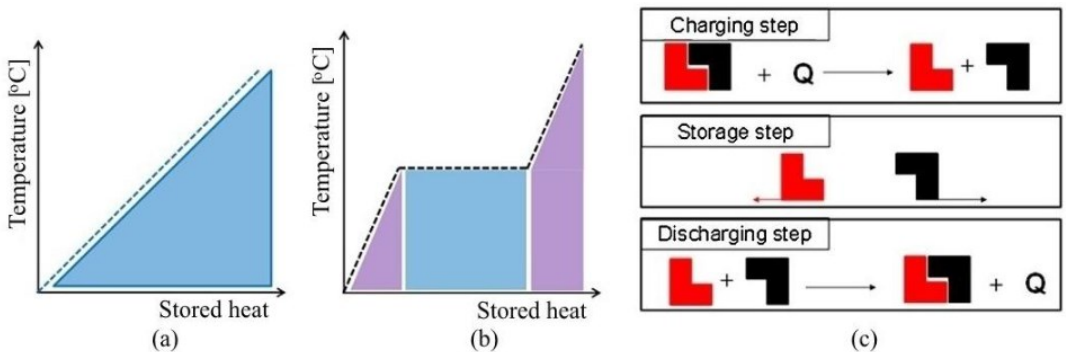

Figure 10: Different types of TES: sensible heat TES (left), latent heat TES (center), thermo-chemical TES (right).

Energy can be stored in various forms: as electricity in battery accumulators, as a compressed fluid in a mechanical energy storage, as a heavy lifted object in a gravitational energy storage or as heat in a thermal energy storage (TES). In this last case, heat can be stored inside a storage medium as sensible heat, latent heat, or thermo-chemical heat (see Figure 10). [31]

A sensible heat TES stores heat by increasing the temperature of the medium; the amount of heat stored by a mass m of the medium whose temperature increases from T_1 to T_2 is given by Equation 3.12:

$$Q = m\Delta h(T_1 \rightarrow T_2) = m \int_{T_1}^{T_2} c_p dT \qquad (3.12)$$

Where c_p is the specific heat capacity of the medium. The most used medium in sensible heat TES is water, which can store a high amount of heat with a small change in temperature, due to its high specific heat. Many other materials can be used as medium, both organic liquids and solids e.g., rock, sand, cast iron, etc.

A latent heat TES stores heat by changing the phase of the medium, possibly increasing its temperature too. The amount of heat stored by a mass m of a medium whose temperature increases from T_1 to T_2, changing from phase α to phase β at the temperature T_{pc} is given by Equation 3.13:

$$\begin{aligned} Q &= m\left[\Delta h^{\alpha}(T_1 \rightarrow T_{pc}) + f\Delta h^{\alpha\rightarrow\beta}(T_{pc}) + \Delta h^{\beta}(T_{pc} \rightarrow T_2)\right] \\ &= m \int_{T_1}^{T_{pc}} c_p^{\alpha} dT + f\Delta h^{\alpha\rightarrow\beta}(T_{pc}) + m \int_{T_{pc}}^{T_2} c_p^{\beta} dT \end{aligned} \qquad (3.13)$$

Where c_p^{α} and c_p^{β} are the specific heat capacities of phases α and β respectively, f is the fraction of medium that has changed phase and $\Delta h^{\alpha\rightarrow\beta}(T_{pc})$ is the latent heat associated to the phase change $\alpha \rightarrow \beta$ at the temperature T_{pc}. The media used in latent heat TES are called phase-change materials (PCM), the phase change is usually the transition between solid and liquid phase, i.e., melting. PCMs can be classified into organic, inorganic, and eutectic materials, each one with advantages and disadvantages.

In conclusion, a thermo-chemical TES stores heat by causing an endothermic chemical reaction within the medium. The amount of heat stored by a mass m of a medium involved in an endothermic chemical reaction is given by Equation 3.14:

$$Q = m\Delta h_R \qquad (3.14)$$

Where Δh_R is the heat of reaction. The media used in thermo-chemical TES are called thermo-chemical materials (TCM), usually the chemical reaction involved is the decomposition of the reactants. [32]

3.7. Borehole Thermal Energy Storage (BTES)

A borehole thermal energy storage system (BTES) is a specific type of sensible heat TES, which stores thermal energy in the ground. It represents a very promising and inexpensive technology for heating and cooling requirements. Furthermore, it is often coupled with a heat pump system in regions where there is the necessity for a long-term thermal energy storage. It consists of a well drilled into the ground usually not deeper than 250 m, in which a working fluid, typically water, circulates in an open or closed loop inside a pipe network fixed by filling the borehole with grout material. The pipe network can have different designs, either with coaxial pipes or with U-shaped pipes (see Figure 11), it constitutes the borehole heat exchanger (BHE). [33] [34]

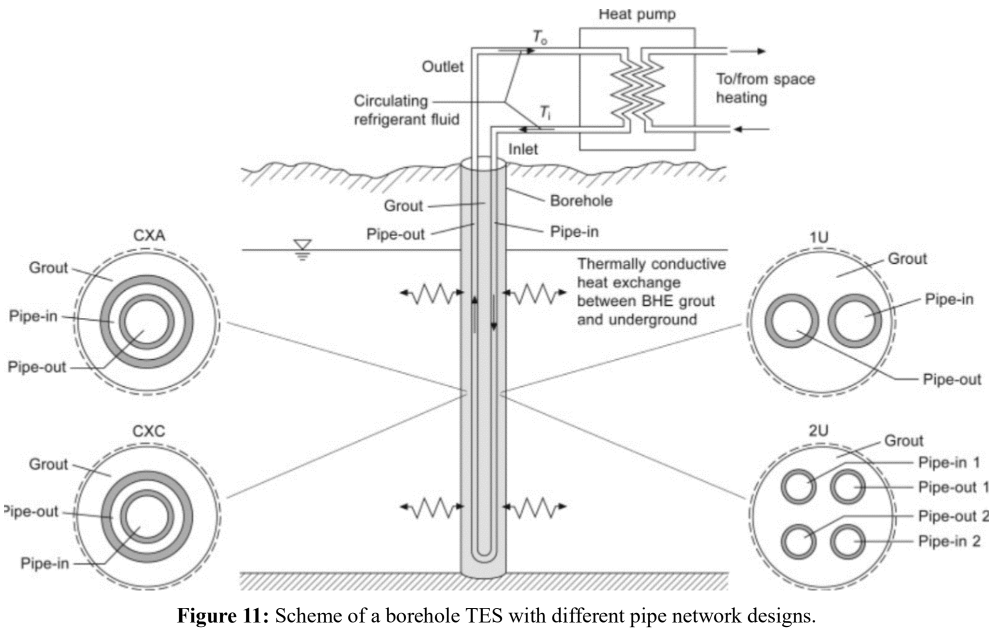

Figure 11: Scheme of a borehole TES with different pipe network designs.

Heat can be stored or extracted from the ground through the BHE, the heat transport mechanism in the ground is conduction/convection, thus it is regulated by the specific heat capacity and the thermal conductivity of the ground, whose values strongly depend on the type of soil and on the presence of underground moisture. Different soils can have very different specific heat capacity and thermal conductivity, the typical range are 0.7−1 kJ/(kg*K), and 1−5 W/(m*K) respectively. [35]

4. Simulation Approach

4.1. General

A model describing the integrated energy system is built using Matlab. The zeotropic cascade heat pump is the core of the plant; therefore, it is the section modelled with the highest degree of detail. For each part of the plant some simplifying assumptions are made. They are presented and explained in the following specific sections of the document. Most of the principles for the simulation approach are taken from previous works on the topic, specifically the master's theses made by Ryssdal and Skoglund. [1] [2]

The city of Oslo is the base location for building the system, meteorologic data (air temperature and solar irradiation) on hourly base were retrieved using Meteonorm for year 2005. For the detailed simulation of the heat pump, the thermodynamic properties of the fluids are calculated using Refprop v9.1, coupled with Matlab. Refprop is a software developed by NIST (National Institute of Standards and Technology) for the evaluation of pure component and mixture thermodynamic and transport phenomena properties based on the most accurate models currently existing. [36]

It is assumed that the compressors are the only unit operation of the plant that require electrical energy to work, the consumption of all the other electrically-driven devices is neglected. The heat demand for district heating is divided into water heating and space heating demands. A base demand of 50 kW for water heating, independent of outside air

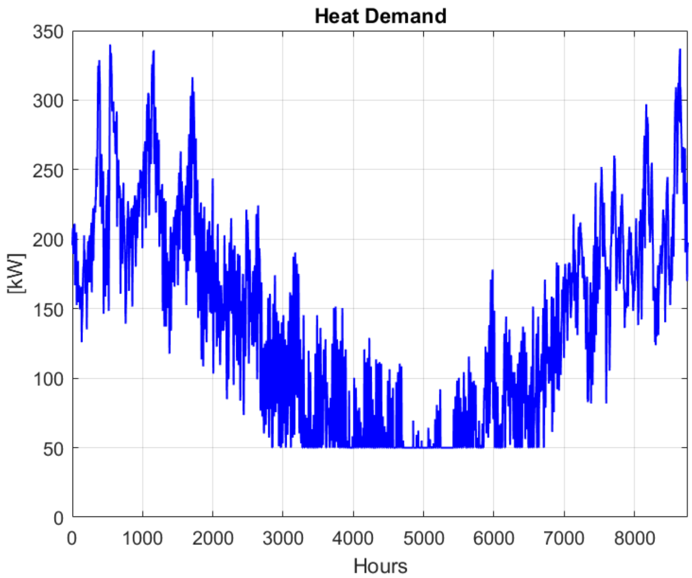

Figure 12: Heat demand for district heating throughout the year 2005 in Oslo.

temperature, is assumed; while, a temperature dependency exists for the space heating demand: it increases of 10.25 kW for every Celsius degree below 15°C. The mathematical relationship defining the heat demand is reported in Equation 4.1.

$$D = \begin{cases} 50\ kW & if\ T_a \geq 15°C \\ [50 + 10.25(15 - T_a)]\ kW & if\ T_a < 15°C \end{cases} \tag{4.1}$$

Where T_a is the outside air temperature. The trend of the heat demand in Oslo during year 2005 is shown in Figure 12.

4.2. Zeotropic Cascade High Temperature Heat Pump

4.2.1. Configuration

The zeotropic cascade high temperature heat pump consists of a low stage and a high stage, both comprise an evaporator, a condenser, two equal parallel compressors and an expansion valve. The two stages are nested together by means of a cascade heat exchanger, which serves as condenser for the low stage and as evaporator for the high stage. For both stages an internal heat exchanger (IHX) can be present. It permits to integrate the vapor superheating at the evaporator outlet with the liquid subcooling at the condenser outlet. Once the temperature levels in those points are known, it will be possible to determine if the IHXs are applicable; superheater and subcooler with external utilities are used otherwise. A configuration with two parallel compressors for both stages is useful for load and capacity control, one of the compressors can be shut-off when the heat demand is low, increasing the plant's energy efficiency. A PFD of the heat pump section obtained after sizing is shown in Figure 13.

The following assumptions are made for modelling the heat pump:

- In the cascade heat exchanger, the low stage and the high stage refrigerants exchange the same heat capacity.
- Saturated vapor is present at the outlet of the evaporators.
- Saturated liquid is present at the outlet of the condensers.
- The expansion process is isenthalpic.
- The pressure drops and the heat losses in the system are neglected.
- All the heat exchangers have a counter-flow configuration.

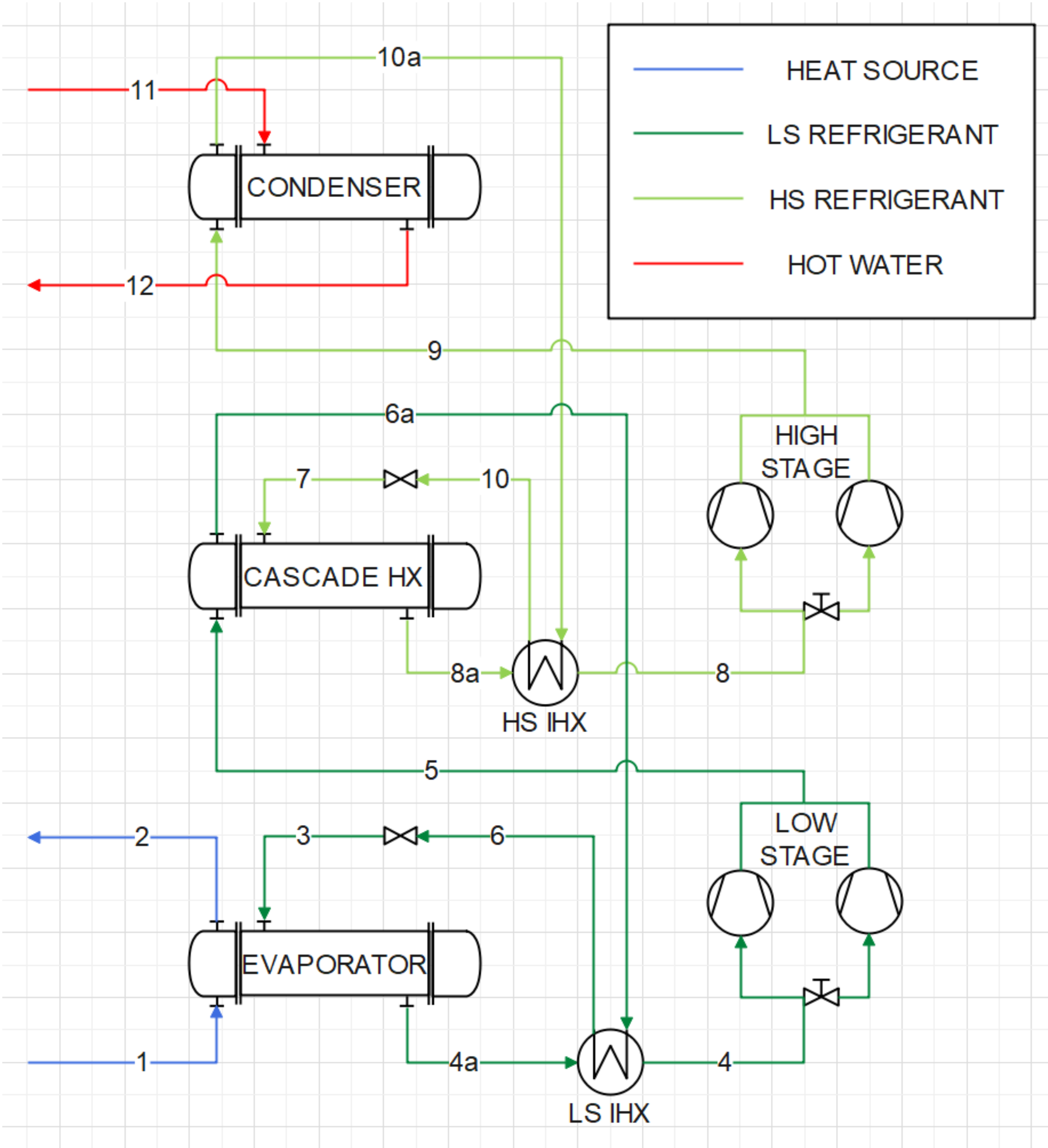

Figure 13: PFD of the heat pump section.

4.2.2. Refrigerant Selection

A two-stage cascade heat pump requires the selection of two refrigerants such that the critical point of the one used in the high stage has a higher critical point than the one used in the low stage. Natural working fluids such as ammonia, carbon dioxide, light alkanes and alkenes, thanks to their negligible ODP, have a lower impact on the environment compared to synthetic refrigerants (HFCs and CFCs). Therefore, natural working fluids must be the primary choice as refrigerants. Sarkar and Bhattacharyya made a comparison in terms of performance between pure hydrocarbons and CO_2/hydrocarbon blends utilized as refrigerants in a heat pump. Results showed that, due to gliding temperature during evaporation and condensation, the zeotropic blends (specifically CO_2/butane and CO_2/isobutane) can be employed very effectively in heat pumps, instead of their pure counterparts. Ganesan and Eikevik showed that CO_2/butane and CO_2/pentane zeotropic mixtures with higher content of CO_2 result in higher power consumption of the compressor and lower COP of the heat pump. This generally happens if the heat source temperature is above 20°C (see Figures 14-15). Zeotropic mixtures with a small content of CO_2 (lower than 10%) should be selected. [37] [3]

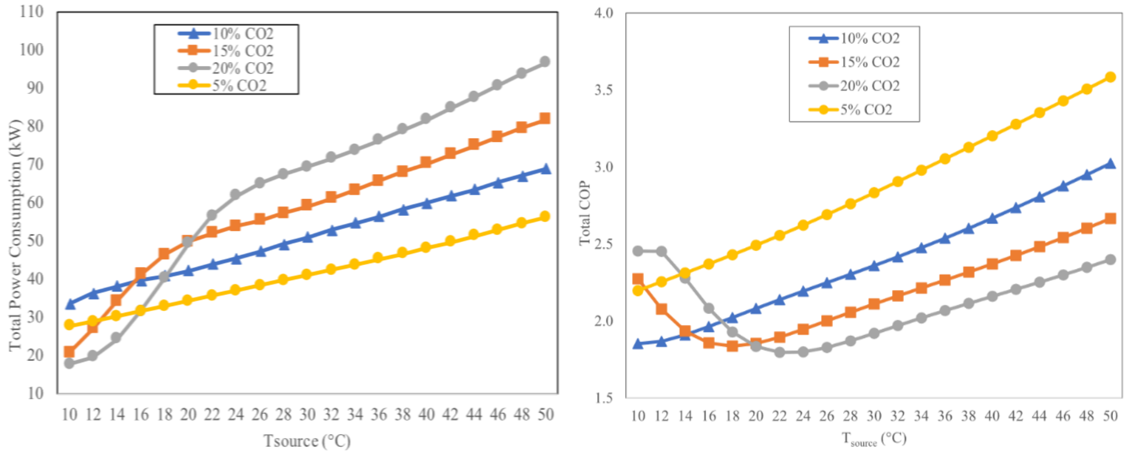

Figures 14-15: Impact of the source temperature on power consumption (left) and COP (right) of the HP, at various CO2 contents.

As suggested by Skoglund, the key approach to select the refrigerant mixtures is to minimize the pressure levels and at the same time having a good temperature profile match in the main heat exchangers between the contacted fluids. In his thesis work, Skoglund used pure propane and 5/95% CO_2/butane mixture as low stage and high stage refrigerants respectively. He reported that the condensation pressure levels obtained in the cascade heat pump were 2,440 kPa and 1,800 kPa. From the cost estimation point of view, the capital investment of a operation unit increases significantly if the pressure inside is higher than 10-12 bar, because thicker walls or special materials are needed; thus, a reasonable assumption is to set the condensation pressures lower than 12 bar. [2] [38] [39]

CO_2/butane and CO_2/pentane blends are selected for low stage and high stage respectively, their vapor-liquid equilibria and temperature glides at different composition are shown in Figures 16-17. As it can be seen, if the CO_2 mass fraction is increased from 0 to 10%, then the bubble temperature of both blends decreases much faster than the dew temperature, which only varies from 50 to 45°C. Given the mixture pressure, its dew temperature can reasonably be assumed constant, for a CO_2 content lower than 10%.

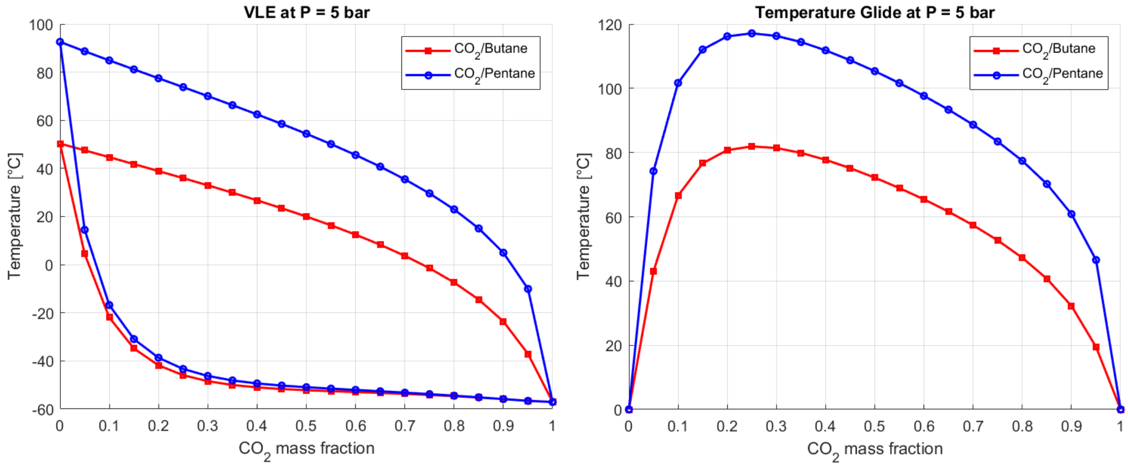

Figures 16-17: VLE (left) and temperature glide (right) at 5 bar for CO2/butane and CO2/pentane blends.

Focusing first on the high stage refrigerant, it contacts the hot water inside the condenser; an inlet temperature of 70°C is assumed for hot water, while, for the design specification, it has to exit at least at 100°C. It is desirable to have a difference of around 5-10°C between contacted fluids in the heat exchangers, thus the high stage condensation pressure should be around 7 bar, leading to a CO_2/pentane dew temperature between 103 and 106°C (see Figure 18). Inside the condenser the temperature profiles of the contacted fluids should be close to each other, but must not cross; therefore, as shown in Figure 18, the best mixture to select is 2/98% CO_2/pentane, ensuring the best fluid coupling.

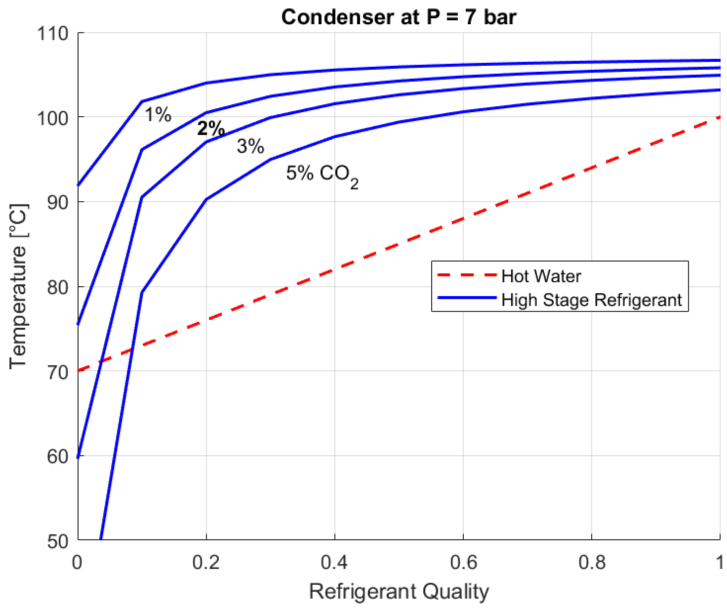

Figure 18: Temperature coupling in the condenser between hot water and CO2/pentane mixtures at different compositions.

Similarily, the refrigerant to be used in the low stage can be selected. This time it contacts the heat source in the evaporator, for which an inlet temperature of 40°C and an outlet temperature of 30°C are assumed. The evaporation pressure that ensures a temperature difference between the fluids at the evaporator outlet of 5-10°C is around 3 bar, resulting in a dew temperature of the mixture of 30°C. In this case the refrigerant enters the exchanger as a liquid/vapor mixture with roughly a 10% vapor quality, because it is expandend in the valve. For that reason, not all the latent heat of vaporization is exchanged. As it can be seen in Figure 19, the closest line to the heat source one, that does not cross it, is relative to the 1/99% CO_2/butane mixture. However, during the heat

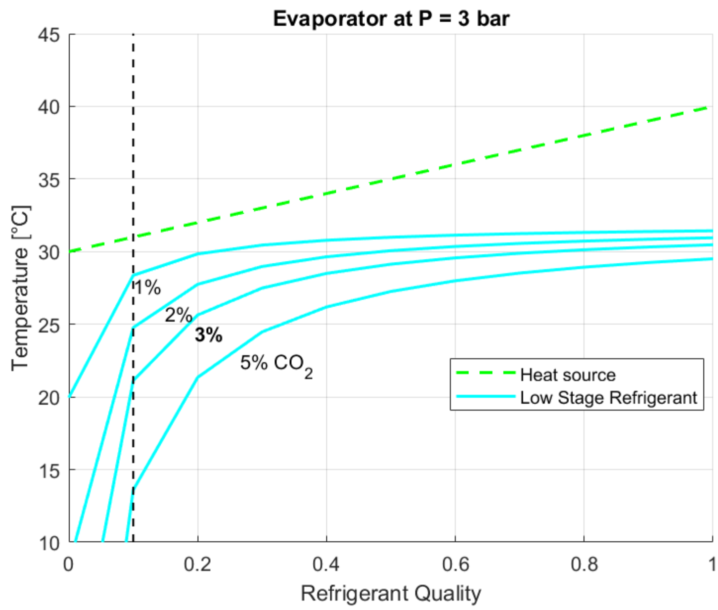

Figure 19: Temperature coupling in the evaporator between heat source and CO2/butane mixtures at different compositions.

exchange, the temperature difference between the fluids gets too low (less than 3°C), the same happens for the 2/98% mixture; therefore, the refrigerant ensuring the best coupling for the low stage is the 3/97% CO_2/butane mixture.

The choice of the correct refrigerant can be verified after the heat pump is sized, by looking the actual temperature trends inside the heat exchangers.

4.2.3. Sizing

Once the two zeotropic refrigerants are selected for both stages, the cascade heat pump can be sized, based on two main design specifications: hot water temperature higher than 100°C and COP of the heat pump higher than 3.6. From the air temperature data in Oslo in year 2005, the heat demand for district heating can be calculated on an hourly basis with Equation 4.1 (see Figure 12). By sorting the heat demand in a complementary cumulative form, the load-duration curve (LDC) for the heat pump can be drawn (see Figure 20). The area below the LDC represents the total heat demand in the whole year, a heat pump delivering heat to such system should cover at least 90% of the total demand.

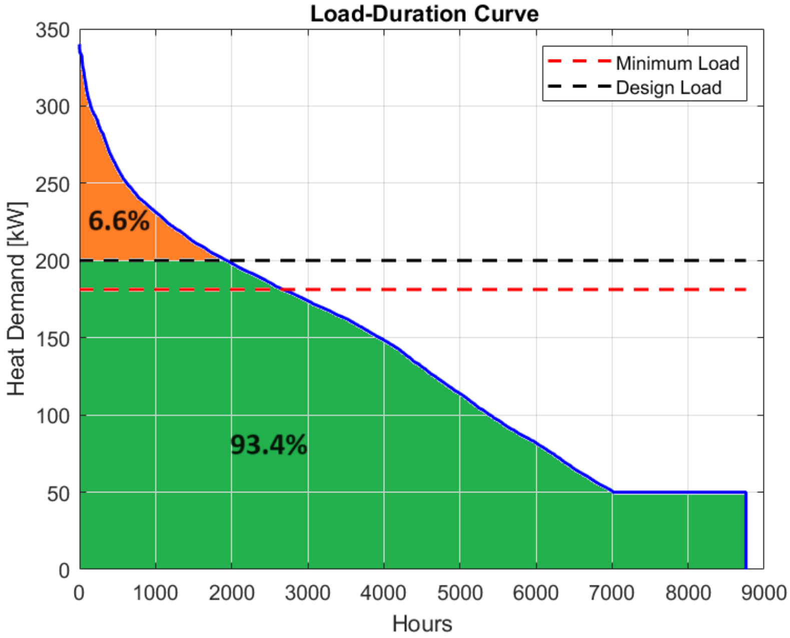

Figure 20: Load-duration curve of the heat pump, with minimum load and selected design load.

By numerically integrating the LDC, it results that the minimum capacity of a heat pump operating at maximum load is 181.2 kW. Hence, the heat pump is sized to deliver 200 kW when operating full load. This will cover 93.4% of the total heat demand, leaving the system with insufficient heating for 1950 hours during the year.

Inlet and outlet temperatures of both heat source and heat sink are decided at this level. The values of condensation pressure of both stages and evaporation pressure of the low stage are assigned such that a good temperature coupling will result, given the previously selected refrigerants. To complete the set of information required for sizing, the mass flow rates of the two refrigerants are assumed to be the same. The degrees of superheating for both stages and the temperature difference between the stages are imposed. A superheating degree of 12°C is enough to avert refrigerant condensation inside the compressors, while a difference of 8°C between the dew point of the refrigerants in the cascade heat exchanger should ensure a good temperature profile coupling. The values assumed for the all the above-mentioned sizing parameters are reported in Table 1.

Sizing Parameter	Value
Heat source inlet temperature (T_1)	40°C
Heat source outlet temperature (T_2)	30°C
Heat sink inlet temperature (T_{11})	70°C
Heat skink outlet temperature (T_{12})	100°C
Low stage evaporation pressure (P_e^{LS})	3 bar
Low stage condensation pressure (P_c^{LS})	9 bar
High stage condensation pressure (P_c^{HS})	7.5 bar
Superheating degrees $\left(T_{sup}^{LS}\right)$ & $\left(T_{sup}^{HS}\right)$	12°C
Temperature difference between stages $\left(T_{diff}\right)$	8°C

Table 1: Values assumed for the sizing parameters.

The state property values are computed in all the points of the heat pump, starting from the low stage. The compression steps are not considered to be ideal, instead they have an efficiency lower than 100%. Both isentropic and volumetric efficiencies of the compressors depend on the compression ratio of the vapor. As described in Ryssdal's work, a power series correlation is assumed, it is reported in Equations 4.2-4.3. [1]

$$\eta_S = -0.00000461\, r^6 + 0.00027131\, r^5 - 0.00628605\, r^4 + 0.07370258\, r^3 - 0.46054399\, r^2 + 1.40653347\, r - 0.87811477 \tag{4.2}$$

$$\eta_V = 0.0011\, r^2 - 0.0487\, r + 0.9979 \tag{4.3}$$

Where r is the compression ratio, either of the low stage or of the high stage compressor. Once all the state properties are calculated, based on the 200 kW of condenser capacity to be obtained, the mass flow rate of the refrigerants and the capacities of cascade heat exchanger and evaporator can be calculated according to Equations 4.4-4.7.

$$\dot{m}_{ref}^{HS} = \frac{\dot{Q}_c}{h_9 - h_{10a}} \tag{4.4}$$

$$\dot{Q}_{che} = \dot{m}_{ref}^{HS}(h_{8a} - h_7) \tag{4.5}$$

$$\dot{m}_{ref}^{LS} = \frac{\dot{Q}_{che}}{h_5 - h_{6a}} \tag{4.6}$$

$$\dot{Q}_e = \dot{m}_{ref}^{LS}(h_{4a} - h_3) \tag{4.7}$$

Where the h_i is the specific enthalpy in point i (see Figure 13 for number reference). The electrical power duties of the compressors can be calculated according to Equations 4.8-4.9.

$$\dot{W}_c^{LS} = \dot{m}_{ref}^{LS}(h_5 - h_4) \tag{4.8}$$

$$\dot{W}_c^{HS} = \dot{m}_{ref}^{HS}(h_9 - h_8) \tag{4.9}$$

For the calculation of the heat exchangers' area, a value for all the global heat transfer coefficients must be assumed. For the three main heat exchangers, the same values as in Skoglund's work are taken, they are reported in Table 2. [2]

Heat exchanger	**Global heat transfer coefficient [W/(m²K)]**
Condenser	1400
Cascade Heat Exchanger	1800
Evaporator	1600
Internal Heat Exchangers	1000

Table 2: Values assumed for the global heat transfer coefficients.

From the capacities of the heat exchangers and the temperature levels of the fluid inside them, the areas can be calculated according to Equation 4.10.

$$A_{HX} = \frac{\dot{Q}_{HX}}{U_{HX}\Delta T_{ml}^{HX}} \tag{4.10}$$

Where U_{HX} represents the global heat transfer coefficient of a generic heat exchanger and ΔT_{ml}^{HX} is the logarithmic mean temperature difference of the fluids, whose definition is given in Equation 4.11.

$$\Delta T_{ml}^{HX} = \frac{\theta_{HX}^{in} - \theta_{HX}^{out}}{\ln\left(\frac{\theta_{HX}^{in}}{\theta_{HX}^{out}}\right)} \tag{4.11}$$

Where θ_{HX}^{in} and θ_{HX}^{out} represent the temperature difference between the contacted fluids at the inlet and outlet of a generic heat exchanger.

The areas of all the heat exchangers of the heat pump resulting from the sizing procedure are listed in Table 3, together with their scaling to commercial values.

Heat Exchanger	Exchange Area [m^2]
Condenser	12.69 → 13
Cascade HX	12.76 → 13
Evaporator	13.83 → 14
Low stage IHX	1.16 → 1.2
High stage IHX	3.70 → 3.7

Table 3: Exchanger area of all the heat exchangers resulting from sizing, with the scaling to commercial values.

The last information that derives from the sizing procedure is the size of the compressors. The formula used for the calculation considers the volumetric efficiency η_V, it is reported in Equation 4.12.

$$V_c = 3{,}600\ \frac{\dot{m}_{ref}}{\eta_V \rho_{in}} \tag{4.12}$$

Where $\dot{m}_{ref}$ is the mass flow rate of the vapor refrigerant to be compressed, ρ_{in} is its mass density and the factor 3,600 is for the conversion between seconds and hours. The flow of refrigerant is split between two equal parallel compressors; therefore, the size of a single compressor is half of the one deriving from Equation 4.12. The values are reported in Table 4 and scaled to the commercial values.

Compressor	Size [m^3/h]
Low Stage	158.72 → 160
High Stage	164.13 → 165

Table 4: Compressor sizes resulting from sizing, with the scaling to commercial values.

The mass flow rates of both heat source and heat sink can be used as inputs for the heat pump, their values result from Equation 4.13-4.14, and are reported in Table 5.

$$\dot{m}_{hs} = \frac{\dot{Q}_e}{c_p(T_1 - T_2)} \tag{4.13}$$

$$\dot{m}_{hw} = \frac{\dot{Q}_c}{c_p(T_{12} - T_{11})} \tag{4.14}$$

Stream	Mass Flow Rate [kg/s]
Heat Source	4.11
Heat Sink	1.59

Table 5: Mass flow rate of heat source and heat sink.

Finally the COP of the heat pump can be estimated according to Equation 4.15.

$$COP = \frac{\dot{Q}_c}{\dot{W}_c^{LS} + \dot{W}_c^{HS}} \tag{4.15}$$

The resulting COP of the heat pump is around 3.15, which is lower than the threshold imposed by the design specification. The energy efficiency of the system, thus the COP, can be increased by applying an energy integration procedure.

4.2.4. Operational Modes

The design of the heat pump is based on the heating capacity that it must deliver for district heating, namely 90% of the total annual demand when the heat pump operates on full load. When the demand of energy is low, it is not necessary to operate the heat pump at full load mode, a part load mode is selected instead. When the heat pump operates on part load, it produces a fraction of the full load capacity, at the same time consuming a fraction of the full load compression duty. The heat pump can operate on part load also when the available power is insufficient for the full load mode.

The sizing procedure presented in Section 4.2.3, assumed that the heat pump operated on part load mode produces half the capacity of when it operates on full load. In that case, a simple way to switch between full load and part load is to shut-off one of the parallel compressors, which halves the mass flow rate of refrigerant, the power consumption, and the condenser capacity. To maintain constant temperature levels between the two operational modes in the heat exchangers, the exchange areas of all the heat exchangers must be halved. This in practice can be obtained by physically closing to the refrigerants flow part of the exchangers.

4.2.5. Energy Integration

For the designed heat pump a simple energy integration within the system is applicable. It is useful to improve the energy efficiency, and to meet the specification imposed on the COP. According to the sizing procedure applied, the high stage IHX cannot completely subcool the refrigerant exiting the condenser from 80°C to 54°C, because the heat transfer is not permitted with the same refrigerant to be superheated from 65°C to 77°C. An external utility would be necessary to perform the subcooling. An energy integration solution that avoids the use of other utilities and at the same time increases the COP, is to split the subcooling in two steps. The first part of the subcooling can be performed in the condenser, assuming the hot water entering at 60°C and lowering the refrigerant temperature to 65°C. With 5°C of difference the temperature coupling is maintained good. The remaining part of the subcooling, from 65°C to 54°C can be conducted with a process stream at least 10°C colder, that needs to be heated. An example is the heat source leaving the evaporator, which must be re-heated from 30°C to 40°C, hence the IHX is not eliminated but simply moved. The superheating of the high stage refrigerant now remains undetermined. A simple solution, that would in turn increase the COP, is to carry out the superheating inside the cascade heat exchanger, thus contacting the two refrigerants. The heat pump scheme after energy integration is shown in Figure 21.

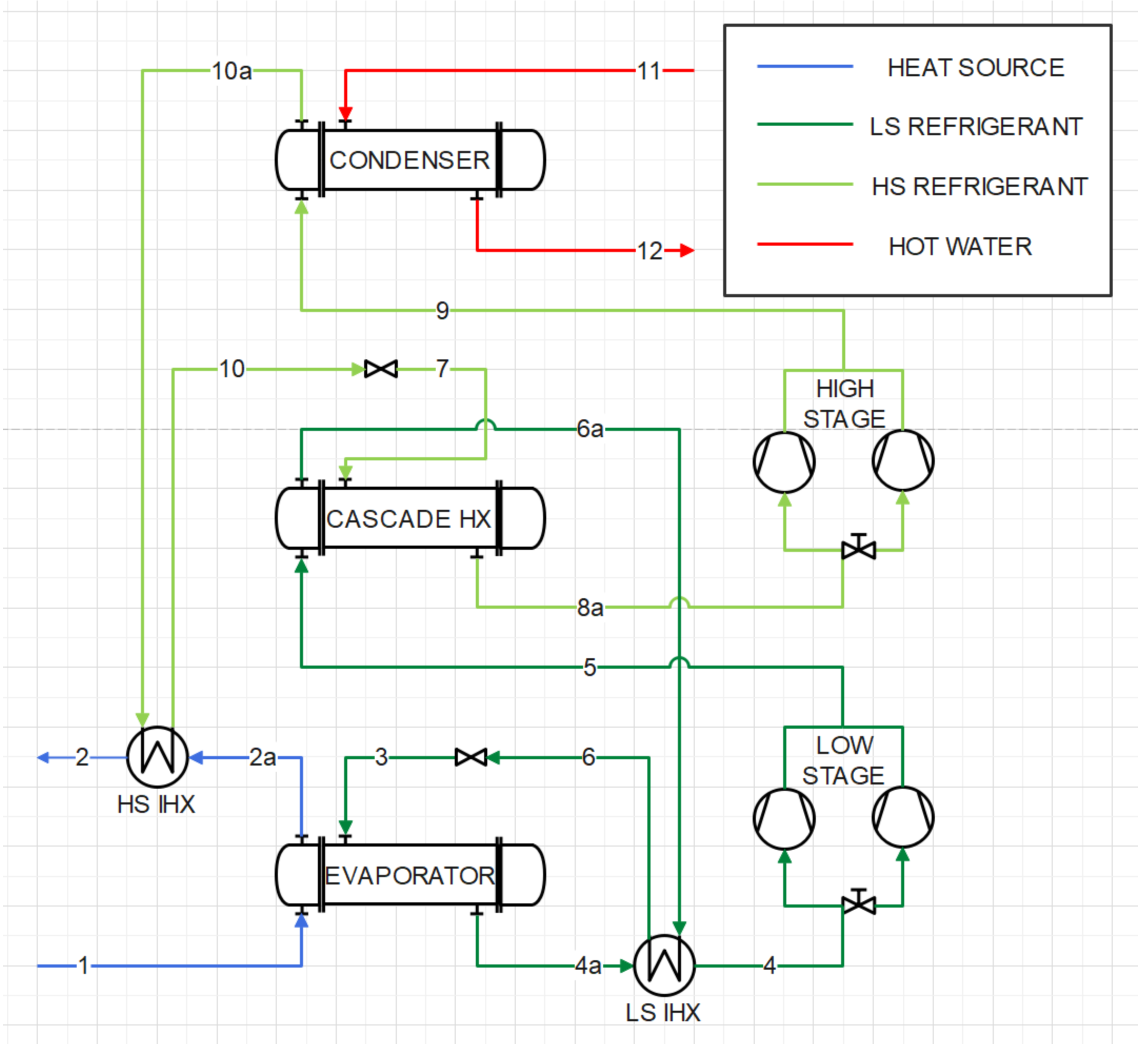

Figure 21: PFD of the heat pump section after energy integration.

After energy integration the values of the design parameters have changed. The new values, for both full load and part load, are listed in Table 6.

Design Parameter	Full Load	Part Load
Condenser Area [m^2]	18.57 → 22	9.28 → 11
Cascade HX Area [m^2]	11.65 → 12	5.82 → 6
Evaporator Area [m^2]	12.63 → 13	6.32 → 6.5
Low Stage IHX Area [m^2]	1.06 → 1.1	0.53 → 0.55
High Stage IHX Area [m^2]	0.48 → 0.5	0.24 → 0.25
LS Compressor Size [m^3/h]	289.88 → 290	144.94 → 145
HS Compressor Size [m^3/h]	296.96 → 300	148.48 → 150

Table 6: Values of the design parameters of the heat pump after energy integration, for full load and part load.

The new flow parameters of heat source and heat sink streams are listed in Table 7.

Stream	Flow Parameter	Full Load	Part Load
Heat Source	Inlet Temperature	40°C	40°C
	Mass Flow Rate	3.76 kg/s	1.88 kg/s
Heat Sink	Inlet Temperature	60°C	60°C
	Mass Flow Rate	1.19 kg/s	0.60 kg/s

Table 7: Values of the inlet flow parameter of heat source and heat sink for full load and part load.

After energy integration the value of the COP estimated with sizing is 3.51, it is still lower than 3.6, but now it can easily meet the design specification by slightly increasing the condenser area, which means increasing the heat capacity of the heat pump. Choosing a condenser area of 22 m^2, rather than 19 m^2, will allow the COP to overcome the threshold of 3.6.

4.2.6. Algorithm

The zeotropic cascade high temperature heat pump, that has been sized with energy integration, can then be simulated. Given the input conditions (mass flow rate and inlet temperature of both heat source and heat sink), all the output variables (condenser capacity, compressor work, COP, and hot water outlet temperature) of the heat pump system are calculated with an iterative procedure.

Each iteration starts with an estimate of the low stage evaporation temperature T_e^{LS}, the low stage condensation temperature T_c^{LS} and the high stage condensation temperature T_c^{HS}. Note that, since the refrigerants are zeotropic mixtures, evaporation and condensation temperatures are not unique; the evaporation temperature is taken equal to the mixture's dew point, while the condensation temperature is taken equal to the mixture's bubble point. All the state properties of the heat pump are calculated, with specified superheating degree and temperature difference between the stages. Then the capacities of all the main heat exchangers can be computed. Every heat exchanger is characterized by a logarithmic mean temperature difference (LMTD), which has two mathematical expressions: one is the actual logarithmic mean of the temperature differences between inlet and outlet, the other comes from the global energy balance of the heat exchanger. The three equations based on the exchanger LMTDs are reported in Equations 4.16-4.18.

$$\Delta T_{ml}^{c} = \frac{\dot{Q}_c}{U_c A_c} = \frac{(T_9 - T_{12}) - (\boldsymbol{T_c^{HS}} - T_{11})}{\ln\left(\frac{T_9 - T_{12}}{\boldsymbol{T_c^{HS}} - T_{11}}\right)} \tag{4.16}$$

$$\Delta T_{ml}^{che} = \frac{\dot{Q}_{che}}{U_{che} A_{che}} = \frac{(T_5 - T_{8a}) - (\boldsymbol{T_c^{LS}} - T_7)}{\ln\left(\frac{T_5 - T_{8a}}{\boldsymbol{T_c^{LS}} - T_7}\right)} \tag{4.17}$$

$$\Delta T_{ml}^{e} = \frac{\dot{Q}_e}{U_e A_e} = \frac{(T_1 - \boldsymbol{T_e^{LS}}) - (T_2 - T_3)}{\ln\left(\frac{T_1 - \boldsymbol{T_e^{LS}}}{T_2 - T_3}\right)} \tag{4.18}$$

The system of algebraic equations composed by Equations 4.16-4.18 cannot be solved through an analytical method but require a numerical solution. The Matlab solver fsolve, specifically made for the numerical solution of systems of non-linear equations is used. Fsolve solves the function minimization problem shown in Equation 4.19.

$$\min_{T_e^{LS}, T_c^{LS}, T_c^{HS}} \{|E_c(T_e^{LS}, T_c^{LS}, T_c^{HS})|, |E_{che}(T_e^{LS}, T_c^{LS}, T_c^{HS})|, |E_e(T_e^{LS}, T_c^{LS}, T_c^{HS})|\} \tag{4.19}$$

Where the function E_i are the errors specific for each heat exchanger, defined as the difference between the two definitions of LMTD (Equations 4.16-4.18). The iterative procedure is therefore carried out inside fsolve, without the need of building a while cycle in the code. It returns the approximated values of T_e^{LS}, T_c^{LS} and T_c^{HS} such that the errors E_c, E_{che} and E_e are below the default tolerance of fsolve i.e., 10^{-6}. This approach for solving the zeotropic heat pump system is more suitable than the one proposed by Ryssdal and used by Skoglund in their works, because it accounts for the variation of temperature during evaporation and condensation of the refrigerants. [1] [2]

4.2.7. Heat Pump Results

The simulation of the heat pump using the algorithm described in Section 4.2.6, allows the calculation of all the outlet parameters of the heat pump, both for the full load and the part load operations. They are reported in Table 8. An energy efficiency of 85% is assumed for the compressors.

Parameter	Full Load Value	Part Load Value
Heat Pump Heat Capacity	200.6 kW	100.4 kW
Heat Pump Power Consumption	55.8 kW (65.6 kW)	27.8 kW (32.7 kW)
Hot Water Outlet Temperature	**100.3°C**	**100.4°C**
Coefficient of Performance (COP)	**3.60**	**3.61**

Table 8: Results of the heat pump operation for both full load and part load operations.

Given the exact values of the state properties in the heat pump system, the heat pump operation can be easily visualized in the T-s and P-h diagrams shown in Figures 22-23.

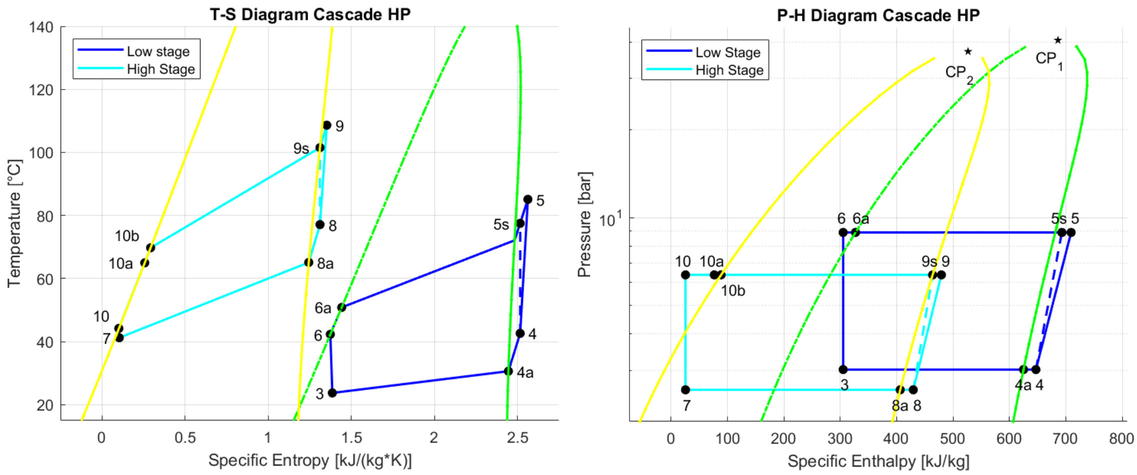

Figures 22-23: T-s (left) and P-h (right) diagrams representing the heat pump.

Since the type of the heat exchangers have not been decided, it is assumed that the heat flux between contacted fluids is uniform and independent of the phase changes. The heat exchangers are divided in slices. A fraction of the total heat flow is transferred inside each slice, allowing to track the temperature profiles of the fluids and in turn the LMTDs values. All the profiles inside the three main heat exchangers (evaporator, cascade heat exchanger and condenser) are shown in Figures 24-29.

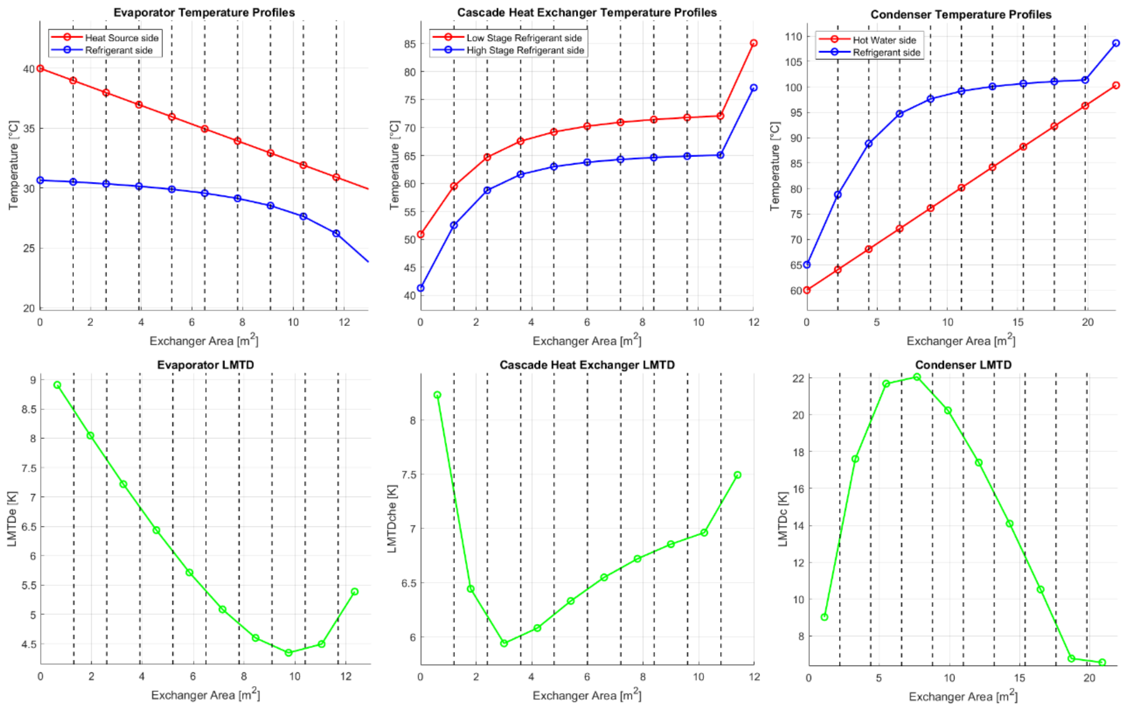

Figures 24-29: Temperature profiles (top) and LMTDs (bottom) inside the three main heat exchangers.

From Figures 24-29, it is clear that the refrigerants selected ensures a good temperature profile coupling, so that the internal LMTDs are never below 4°C. Inside the condenser the LMTD between high stage refrigerant and hot water reaches 22°C; this value is very high, and it is not possible to decrease it, due to the shape of the gliding temperature of the CO_2/pentane mixture (see Figure 18). However, once the type of heat exchanger is assumed, information about the fluid dynamics and the heat transfer inside can be deducted, enabling a more detailed description of the internals.

4.3. Photovoltaic/Thermal (PVT) Model

4.3.1. Configuration

Photovoltaic/thermal (PVT) panels are used to collect solar energy from the sun and convert it into electrical and thermal energy, useful to drive the compressors and re-heat the heat source of the heat pump. The photovoltaic/thermal panels are described using a very simple model: the solar incident radiation that hits the solar collector is converted into both electrical energy and thermal energy with certain electrical and thermal efficiencies. With the solar irradiance data collected with Meteonorm, specific for Oslo in the year 2005, the electrical and thermal generation data on a hourly base can be obtained. Thermal and electrical efficiencies are not considered to be constant. Instead they vary depending on the system conditions, and they are calculated according to the methods presented in the work of Herrando et al. [40]

Starting with the thermal efficiency of the PVT collector, there is not a standard approach for the assessment its performance. ISO and ASHRAE are two methods based on steady-state testing of the PVT panels. In this thesis, the ISO method is preferred. It models the PVT thermal efficiency according to Equation 4.20.

$$\eta_{th} = \eta_O - a_1 T_r - a_2 I_t {T_r}^2 \tag{4.20}$$

Where η_O is the optical efficiency, a_1 is the linear heat loss coefficient, a_2 is the quadratic heat loss coefficient, I_t is the total solar irradiance per unit of area and T_r is the reduced temperature, whose definition is given by Equation 4.21.

$$T_r = \frac{\overline{T_f} - T_a}{I_t} \tag{4.21}$$

In which $\overline{T_f}$ is the average cooling fluid temperature, namely the arithmetic mean between inlet and outlet heat source temperatures and T_a is the air temperature. When the total solar irradiance I_t is zero or close to zero, then mathematically the thermal efficiency would tend to minus infinity; to avoid this possibility, the thermal efficiency is set to zero when the sun is low.

For what concerns the electrical efficiency, it strongly depends on the PV cell temperature according to Equation 4.22.

$$\eta_{th} = \eta_{ref}\left[1 - \beta_0\left(T_{PV} - T_{ref}\right)\right] \tag{4.22}$$

Where η_{ref} is the reference PV module efficiency tested at the reference temperature T_{ref} of 25°C and at a solar irradiance of 1000 W/m^2, β_0 is the temperature coefficient of the PV module, while T_{PV} is the surface temperature of the PV module, which is assumed to be 20°C higher than the air temperature.

The PVT panel type will not be specified, but the total area of the panels is assumed to be 4000 m^2 and the values of all the coefficients needed for the calculation of the PVT module efficiencies are taken from previous works, listed in Table 9. [1] [2]

PVT Feature	Value
Optical Efficiency η_O	0.51
Linear Heat Loss Coefficient a_1	4.93 W/(m^{2}K)
Quadratic Heat Loss Coefficient a_2	0.021 W/(m^{2}K^2)
Reference Electrical Efficiency η_{ref}	0.147
Temperature Coefficient β_0	-0.0045 K^{-1}
Reference Temperature T_{ref}	25°C
Total Panels Area A_{PVT}	4000 m^2

Table 9: PVT module features.

4.3.2. Algorithm

At the kth time iteration, the air temperature and solar irradiance data ($T_a^{(k)}$ and $I_t^{(k)}$) are the inputs to the PVT model. The model calculates the electrical and thermal efficiencies ($\eta_{el}^{(k)}$ and $\eta_{th}^{(k)}$) using Equations 4.20-4.22, if the thermal efficiency results to be negative, it is set to zero. Eventually, knowing the total area of the PVT panels, the model calculates the electrical and thermal power generated according to Equations 4.23-4.24.

$$\dot{P}_{el}^{(k)} = \eta_{el}^{(k)} I_t^{(k)} A_{PVT} \tag{4.23}$$

$$\dot{P}_{th}^{(k)} = \eta_{th}^{(k)} I_t^{(k)} A_{PVT} \tag{4.24}$$

4.4. Battery Model

4.4.1. Configuration

A solar-assisted heat pump cannot be independent from the electrical grid if one or more batteries are not integrated in the system. The energy that can be obtained from the sun with a solar collector is discontinuous during the day, due to day/night switch, variable cloud coverage, and other atmospheric factors. It is also variable throughout the year, particularly in Nordic countries, because of the difference in daytime duration between summer and winter. A battery is an energy accumulator that can store a certain amount of electrical energy and release it when needed. In this thesis work it is simulated according to a greatly simplified model. A battery type will not be specified and, for sake of simplicity, the maximum capacity and the charging/discharging efficiencies will be the only two parameters characterizing the battery accumulator. Their values are reported in Table 10.

Battery Feature	Value
Maximum Capacity B_{max}	1000 kWh
Charging/Discharging Efficiency η_B	80%

Table 10: Battery features.

4.4.2. Algorithm

Initially the energy stored in the battery accumulator is set to be 75% of the total capacity B_{max}. At every time iteration, the battery either charges or discharges depending on the heat pump demand and on the PVT supply ($\dot{W}_c^{(k)}$ and $\dot{P}_{el}^{(k)}$). During charging, the amount of electrical energy stored at the k^th iteration is given by Equation 4.25.

$$\begin{aligned} B^{(k)} &= B^{(k-1)} + \eta_B \int_{t_{k-1}}^{t_k} \left(\dot{P}_{el} - \dot{W}_c\right) dt \\ &= B^{(k-1)} + \eta_B \left(\dot{P}_{el}^{(k)} - \dot{W}_c^{(k)}\right) \cdot 1h \end{aligned} \tag{4.25}$$

During discharging Equation 4.26 is used instead.

$$\begin{aligned} B^{(k)} &= B^{(k-1)} - (2 - \eta_B) \int_{t_{k-1}}^{t_k} \left(\dot{W}_c - \dot{P}_{el}\right) dt \\ &= B^{(k-1)} - (2 - \eta_B) \left(\dot{W}_c^{(k)} - \dot{P}_{el}^{(k)}\right) \cdot 1h \end{aligned} \tag{4.26}$$

4.5. Borehole Thermal Energy Storage (BTES) Model

4.5.1. Configuration

A borehole thermal energy storage (BTES) is integrated in the system to store the thermal energy produced by the PVT panels. The thermal energy obtained from the PVT collector is subjected to significant variations. Like the electrical energy, it is necessary to collect it in a storage system. The BTES is not designed in detail, the number and the features of the pipes in the borehole heat exchanger (BHE) have not been decided and the heat transfer within the BHE is not investigated. Furthermore, a strong assumption is made on the BTES: the heat stored in it never gets below 1% of the maximum capacity, because a small amount of heat can be extracted from the ground. The BTES will be characterized only by its total storage capacity and by a loading/unloading efficiency. Their values are reported in Table 11.

BTES Feature	Value
Maximum Capacity H_{max}	100,000 kWh
Loading/Unloading Efficiency η_H	90%

Table 11: BTES features.

4.5.2. Algorithm

The simulation of the BTES system is based on the same simplified model as the battery accumulator. Initially the energy stored in the BTES is set to be 75% of the total capacity H_{max}. At every time iteration, the BTES is either loaded or unloaded depending on the heat pump demand and on the PVT supply ($\dot{Q}_e^{(k)}$ and $\dot{P}_{th}^{(k)}$). During loading, the amount of thermal energy stored at the k[th] iteration is given by Equation 4.27.

$$\begin{aligned} H^{(k)} &= H^{(k-1)} + \eta_H \int_{t_{k-1}}^{t_k} \left(\dot{P}_{th} - \dot{Q}_e\right) dt \\ &= H^{(k-1)} + \eta_H \left(\dot{P}_{th}^{(k)} - \dot{Q}_e^{(k)}\right) \cdot 1h \end{aligned} \quad (4.27)$$

During unloading Equation 4.28 is used instead.

$$\begin{aligned} H^{(k)} &= H^{(k-1)} - (2-\eta_H) \int_{t_{k-1}}^{t_k} \left(\dot{Q}_e - \dot{P}_{th}\right) dt \\ &= H^{(k-1)} - (2-\eta_H)\left(\dot{Q}_e^{(k)} - \dot{P}_{th}^{(k)}\right) \cdot 1h \end{aligned} \quad (4.28)$$

4.6. Phase-Change Material Thermal Energy Storage (PCM-TES) Model

4.6.1. Configuration

A thermal energy storage, based on phase-change materials (PCM-TES), can be integrated into the system to store the surplus energy produced by the heat pump with respect to the heat demand of district heating. Conversely, in the winter months, when the heat pump capacity is insufficient, heat can be withdrawn from the TES to satisfy the demand. As for the other energy storage systems, also the PCM-TES is not designed in detail, the phase-change material is not selected and again only the maximum capacity and the loading/unloading efficiencies are assumed. The values are reported in Table 12.

PCM-TES Feature	**Value**
Maximum Capacity S_{max}	1000 kWh
Loading/Unloading Efficiency η_S	90%

Table 12: PCM-TES features.

4.6.2. Algorithm

The model describing the PCM-TES system is analogous to the ones previously presented for battery and BTES. Initially the energy stored in the PCM-TES is set to be 75% of the total capacity S_{max}. At every time iteration, the PCM-TES is either loaded or unloaded depending on the district heating demand and on the heat pump capacity ($D^{(k)}$ and $\dot{Q}_c^{(k)}$). During loading, the amount of thermal energy stored at the k[th] iteration is given by Equation 4.29.

$$\begin{aligned} S^{(k)} &= S^{(k-1)} + \eta_S \int_{t_{k-1}}^{t_k} (\dot{Q}_c - D) dt \\ &= S^{(k-1)} + \eta_S \left(\dot{Q}_c^{(k)} - D^{(k)}\right) \cdot 1h \end{aligned} \tag{4.29}$$

During unloading Equation 4.30 is used instead.

$$\begin{aligned} S^{(k)} &= S^{(k-1)} - (2 - \eta_S) \int_{t_{k-1}}^{t_k} (D - \dot{Q}_c) dt \\ &= S^{(k-1)} - (2 - \eta_S)\left(D^{(k)} - \dot{Q}_c^{(k)}\right) \cdot 1h \end{aligned} \tag{4.30}$$

4.7. District Heating Model

In this thesis, the district heating will not be modelled because the number and the type of building supplied with the heat produced by the heat pump are not decided upon. A mathematical expression is assumed for the heat demand composed of a water heating and a space heating contributions (Equation 4.1). The whole district heating system will be treated as if it was a heat exchanger. At every time iteration, the hot water leaving the heat pump ceases the sensible heat defined by the heat demand to the district heating, returning to the heat pump condenser at a lower temperature. Hence, the temperature reduction of the hot water at the k^th iteration can be calculated according to Equation 4.31.

$$\Delta T_{DH}^{(k)} = \frac{D^{(k)}}{m_{hw}^{(k)} c_p} \tag{4.31}$$

4.8. Integrated Energy System

4.8.1. Configuration

The integrated energy system is built by joining together all the subsystems presented in the previous Sections. The resulting plant scheme is shown in Figure 30.

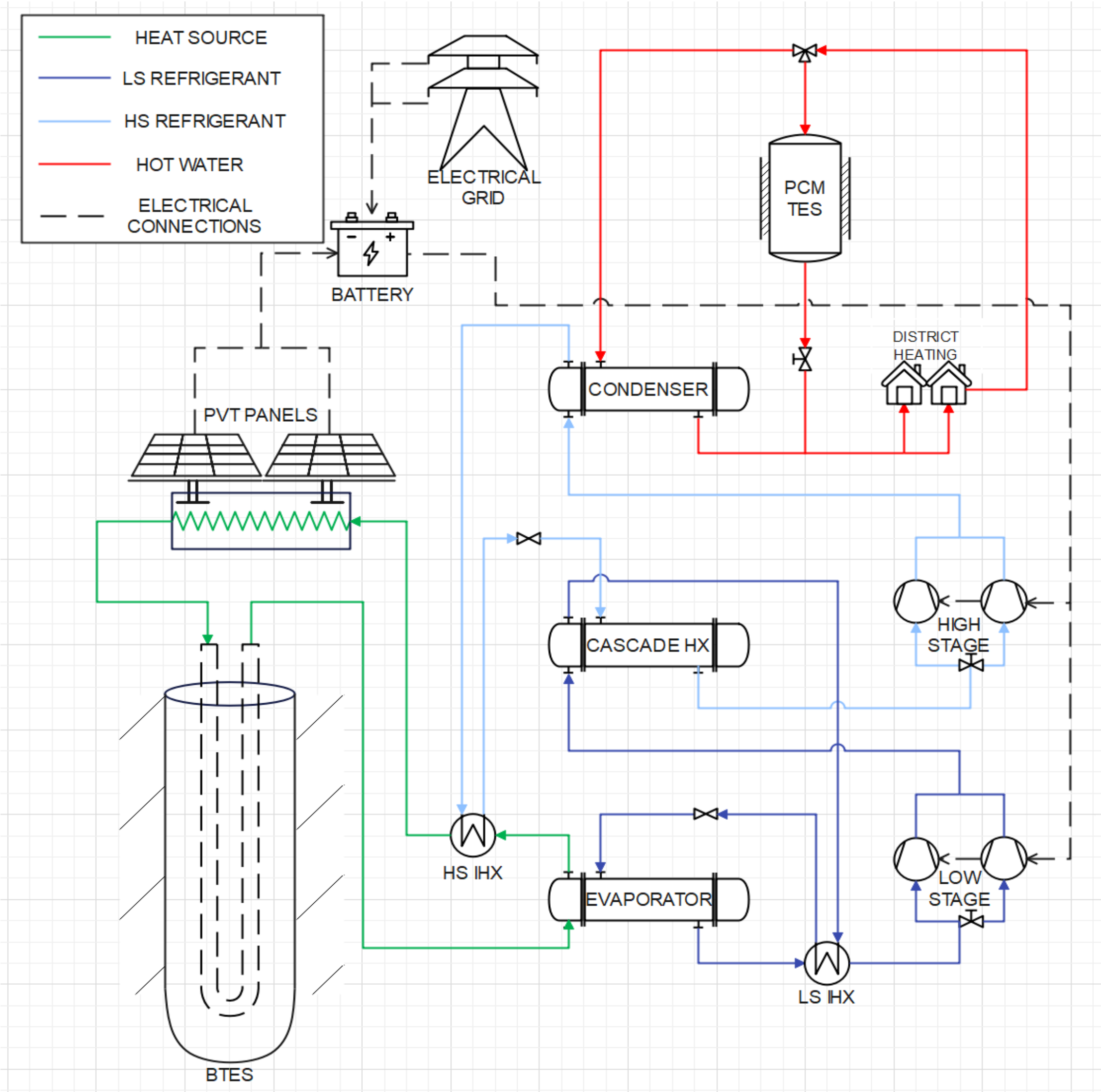

Figure 30: PFD of the integrated energy system.

The heat pump has a double connection with the PVT panels. The first connection is thermal through the BTES, with which the heat source exiting the evaporator is re-heated in the PVT collector, before to return to the heat pump. The surplus or the deficit of thermal energy is either supplied or withdrawn from the BTES. The second connection is electrical through the battery accumulator. The electrical energy generated by the PVT collector is used to drive the heat pump compressors. When a surplus or deficit of electrical energy results, the battery is either charged or uncharged. Moreover, the heat pump has a thermal connection with the district heating via the PCM-TES. Similarly to the previous cases, the hot water produced by the heat pump is supplied to the district heating, then returned to the heat pump condenser at a lower temperature. If the heat demand overcomes the condenser capacity, the remaining part of thermal energy is furnished by the PCM-TES, otherwise the thermal energy surplus is stored. A connection to the external electrical grid is present, the system can either import or export electrical energy to the outside when the battery capacity is minimal or maximal respectively.

4.8.2. Algorithm

The integrated energy system works according to an algorithm that combines all the models developed for the subsystems. First the weather data (air temperature and solar irradiance) on an hourly basis specific for Oslo in year 2005 are retrieved. From there it is possible to calculate heat demand for district heating, electrical and thermal power generation from the PVT panels throughout the year. The system is then initialized. For battery, BTES and PCM-TES the initial values of capacity are set. For all the time iteration, namely from the first to the last hours of year 2005, many system parameters are calculated: heat pump operational mode, condenser and evaporator capacities, power consumption, battery stored energy, BTES stored energy, PCM-TES stored energy, power imported or exported to the electrical grid and heat supplied to district heating. At the beginning of an iteration, if the PCM-TES is at its maximum capacity, the heat pump is shut-off, because the thermal energy surplus produced would be wasted. In that case the heat demand is satisfied with the solely heat stored in the PCM-TES. Both capacities and power consumption are null, thus battery and BTES are loaded. If thermal energy can still be stored in the PCM-TES, then the operational mode of the heat pump at that time iteration is decided depending on the available electrical energy (power generated by the

PVT panels plus energy stored in the battery). If the available electrical energy is sufficient, the heat pump runs on full load, and the battery can be either charged or uncharged. Otherwise, if the available electrical energy is enough to run the heat pump on part load, said operation is selected and again the battery can either be charged, when surplus electrical energy is produced, or uncharged instead. If at a certain iteration there is not enough available energy to run the heat pump on part load, energy is imported from

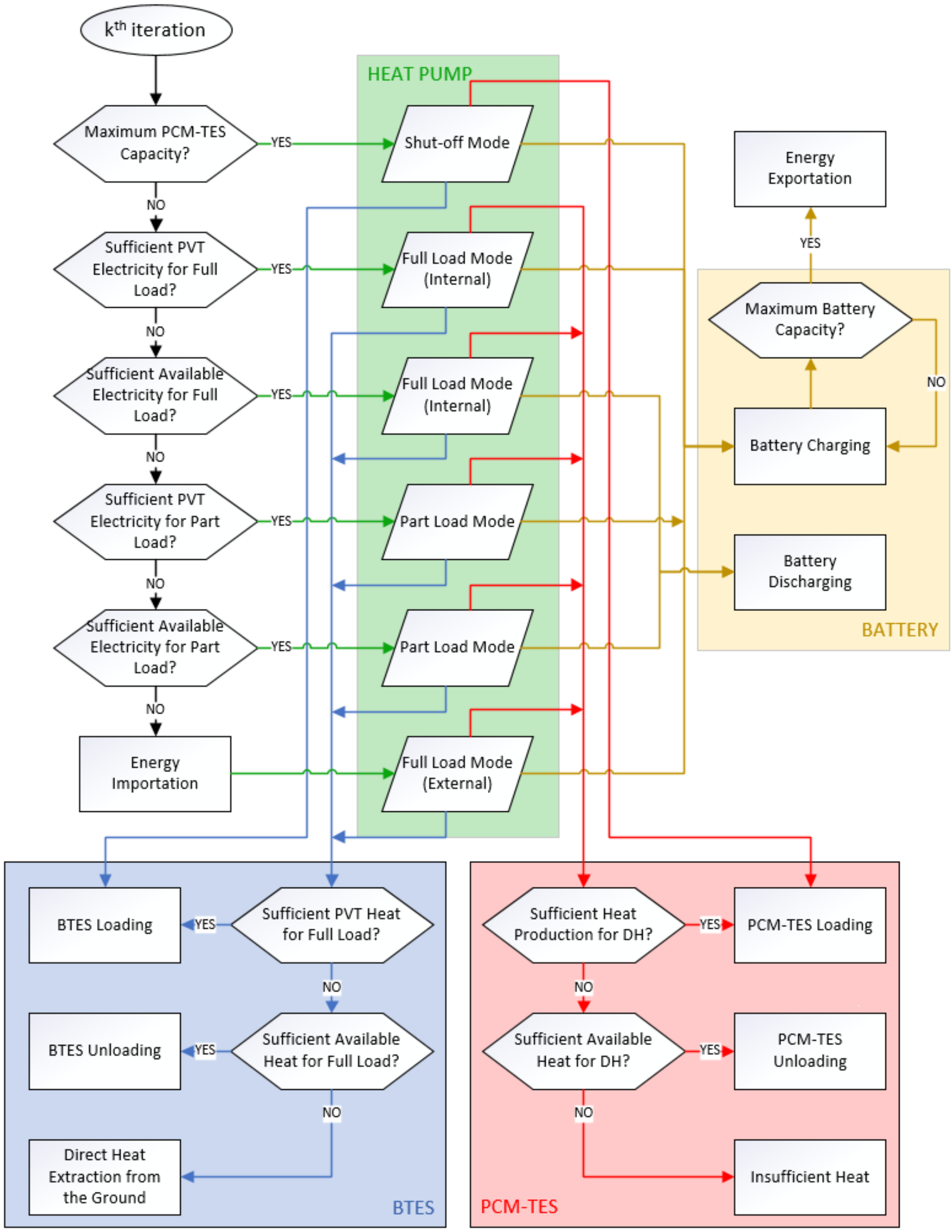

Figure 31: BFD of the algorithm used to simulate the integrated energy system (the sections are highlighted with different colors.

the external and the heat pump is run on full load, charging the battery too. Every time the battery is charged, the maximum capacity might be reached, in that case the electrical energy that cannot be stored is exported to the outside through the electrical grid. When the BTES reaches its maximum capacity, then the thermal energy that would be added is assumed to be completely wasted. On the other hand, when the BTES reaches its minimum capacity, the heat source is assumed to be re-heated to 40°C, regardless of the thermal energy missing. Finally, when the PCM-TES reaches its maximum, the heat pump is shut-off to avoid thermal energy dissipation. The BFD of the integrated energy system algorithm is shown in Figure 31.

5. Results

5.1. Yearly Results

The results obtained through the Matlab code bult for modelling the integrated energy system are presented in this chapter on a yearly basis. However, due to the very high number of time iterations (8760), the results displayed in a plot may be difficult to interpret. Results specific for winter, summer, and spring/fall are presented separately in the following chapters to facilitate both visualization and discussion.

5.1.1. Air Temperature and Solar Irradiation

From the weather data obtained using Meteonorm, the plot shown in Figure 32-33 can be obtained by averaging the air temperature and solar irradiance for every week. The average temperature between winter and summer varies significantly: the air temperature usually remains above 15°C during the summer and between 0 and -5°C during the winter.

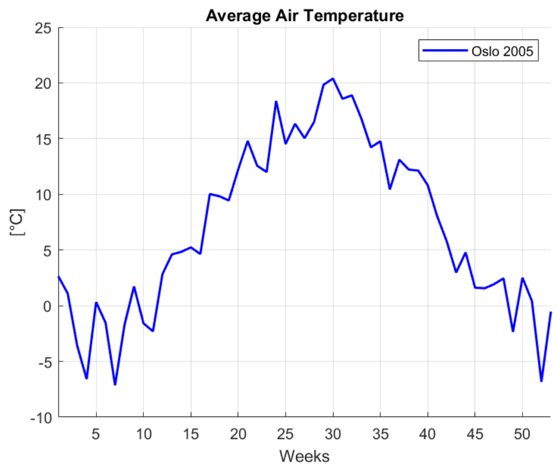

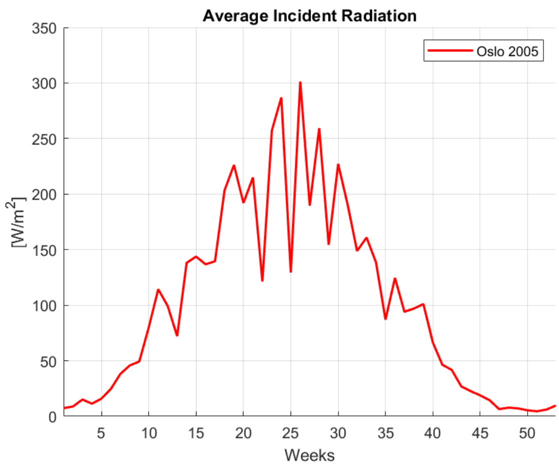

Figures 32-33: Weekly averaged air temperature (left) and solar irradiance (right) in Oslo during the year 2005.

The average solar irradiance shows an extreme variation during the year. This is due to the high latitude of Oslo, which ensures more than 200 monthly sunshine hours in the summer, but only 50 during the winter. Since the average trend is shown, the local maxima and minima of temperature cannot be seen in Figures 32-33. They are shown in Table 13. Because both air temperature and solar irradiance vary from year to year, they might not be accurate for 2023 or later years. Nevertheless, according to Michaels et al., yearly temperatures follow trends and the average temperatures in each month rarely vary with more than two degrees; thus, the values are assumed to be representative for the simulation at this point in the project. [41] [42]

Descriptor	Air temperature	Solar Irradiance
Maximum	+29.8°C	868 kW/m^2
Minimum	-13.3°C	0 kW/m^2
Winter Average	-1.9°C	35 kW/m^2
Summer Average	+15.9°C	166 kW/m^2
Yearly Average	+7.1°C	102 kW/m^2

Table 13: Maximum, minimum and average air temperature in Oslo during the year 2005.

5.1.2. Integrated Energy System Performance

The simulation of the integrated energy system for the whole year gives results in terms of the performance of all the subsystems. For what concerns the heat pump, it can run on

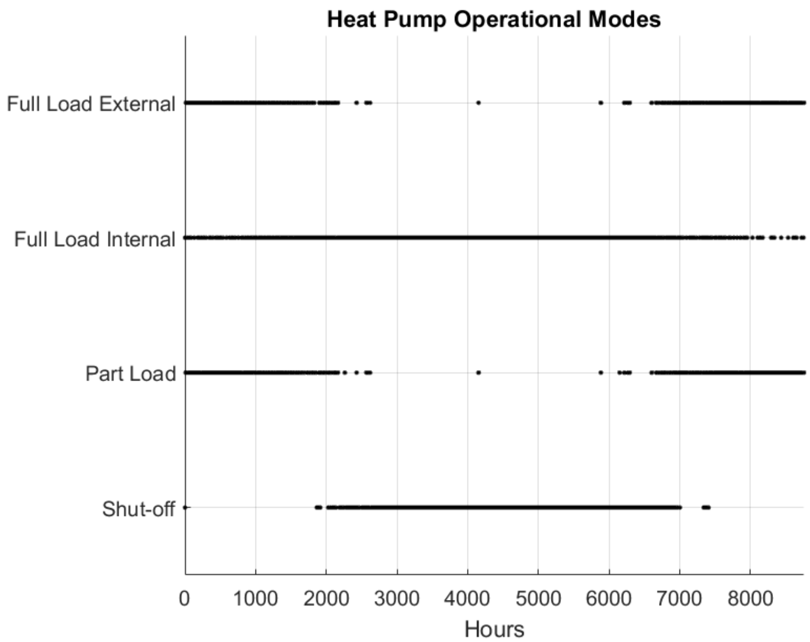

Figure 34: Heat pump operational modes during the year.

Period	Hours Full Load		Hours Part Load	Hours Shut-off
	Internal	External		
January	53 (7.2%)	370 (49.7%)	321 (43.1%)	0 (0.0%)
April	540 (75.0%)	14 (1.9%)	13 (1.8%)	153 (21.3%)
July	380 (51.1%)	0 (0.0%)	0 (0.0%)	364 (48.9%)
October	220 (29.5%)	217 (29.2%)	197 (26.5%)	110 (14.8%)
Year	3497 (39.9%)	1770 (20.2%)	1540 (17.6%)	1953 (22.3%)

Table 14: Hours of full load, part load and shut-off operation in different periods of the year.

three different operational modes, depending on the overall energy availability and demand of the system. The trend with which the operational mode is changed during the year is shown in Figure 34. The quantification of the hours in each mode, also divided for specific periods of the year, is reported in Table 14.

For the sake of clarity, a distinction has been made between the system's full load operation driven by the directly available electrical energy (internal full load) and the full load operation driven by the electrical energy provided by the external grid (external full load). The heat pump works on full load for the whole year, but it alternates its operational mode with the part load mode roughly during the winter, or with the shut-off mode in the warm months. In the winter the full load operation of the heat pump is mainly sustained by the external grid. In the spring and in the summer the system does not rely heavily on the grid, while in the fall it is equally driven by the power generated by the PVT panels and the power imported from the external grid.

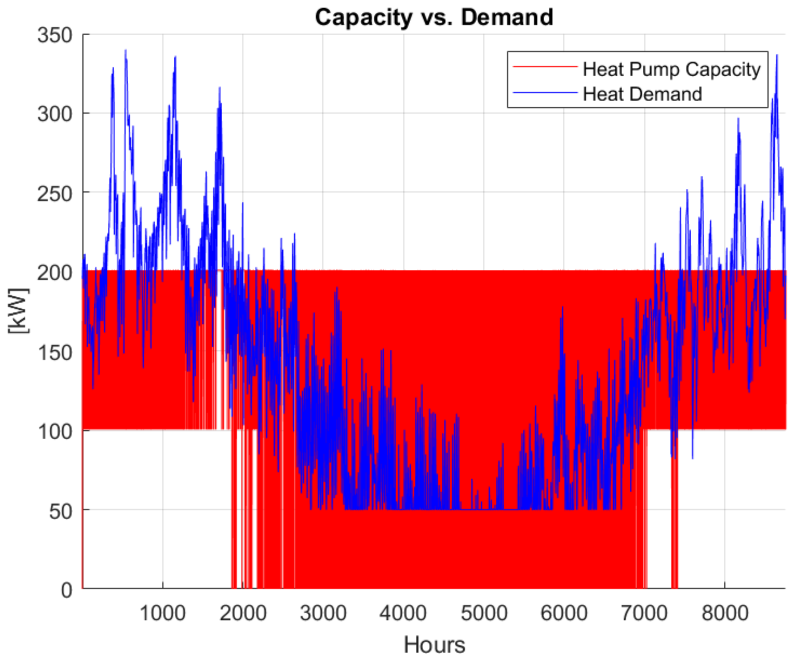

Figure 35: Heat pump capacity and heat demand during the year.

In Figure 35 the heat capacity of the heat pump is displayed together with the heat demand of district heating, the three operational modes of the heat pump are clearly distinguishable. The full load supplies 200 kW, the part load supplies 100 kW, while in shut-off mode the capacity is null. The heat demand highly exceeds the full load capacity of the heat pump in the winter months, the maximum heat demand of 340 kW is attained when the air reaches its minimum temperature on January 22nd. In the summer the heat demand rarely surpasses 100 kW, therefore the heat pump can always deliver sufficient heat to district heating.

The total thermal energy produced weekly by the heat pump is shown in Figure 36. It is higher in the winter and always above 25 MWh per week, with a peak of 33 MWh. It is lower in the summer and maintains an energy production between 15 and 20 MWh.

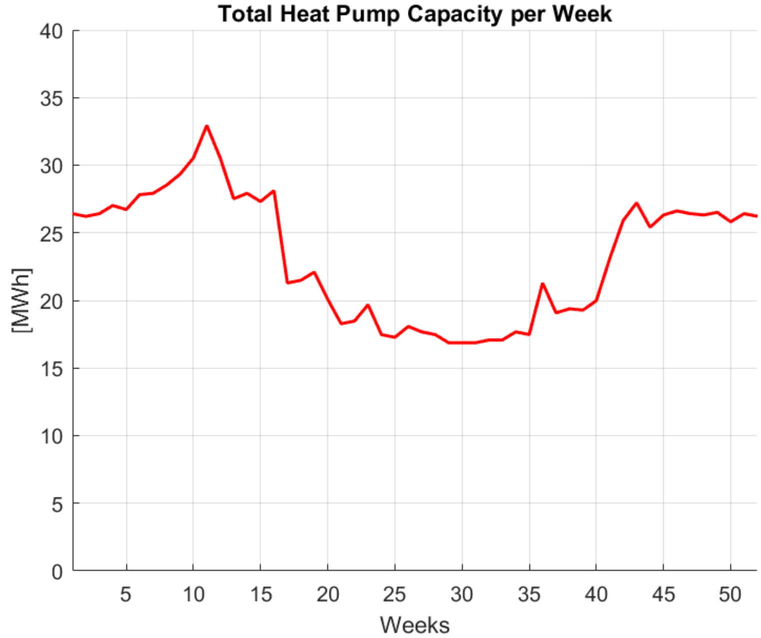

Figure 36: Total heating capacity generated by the heat pump per week.

In Figure 37 the weekly averaged heat demand is compared to the weekly averaged heat available for district heating. The availability of heat, namely the one stored in PCM-TES

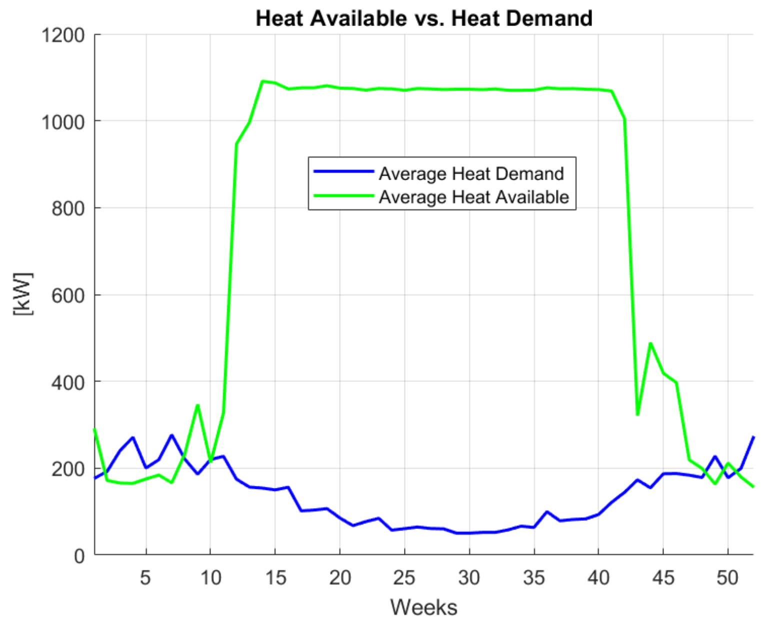

Figure 37: Weekly averaged heat demand and heat available during the year.

plus the one produced on time by the heat pump, is always much higher than the demand in the summer, and in large part of spring and fall. In the winter, on the other hand, there are few weeks during which the heat demand surpasses the heat available. The results shown in Figure 37 are quantified in Table 15, in terms of number of hours of insufficient heat and amount of insufficient heat.

Period	Hours Insufficient Heat	Total Insufficient Heat [MWh]
January	538 (72.3%)	49.02
April	0 (0.0%)	0.00
July	0 (0.0%)	0.00
October	80 (10.8%)	4.80
Year	2242 (25.6%)	183.73

Table 15: Hours and total amount of insufficient heat in different periods of the year.

Taking January as a reference for the winter months, for 72.3% of the integrated energy system operation, the heat available is insufficient to fulfill the district heating demand. Only in the month of January, 49.02 MWh of thermal energy has not been delivered. Overall, one quarter of the year is characterized by insufficient heat, which sums up to a total lack of 183.73 MWh.

Period	Total Energy Produced by the PVT Panels [MWh]	Total Energy Consumed by the Heat Pump [MWh]
January	4.67	37.86
April	60.81	36.45
July	96.62	24.71
October	19.00	34.81
Year	547.48	392.56

Table 16: Total electrical energy produced by the PVT panels and consumed by the heat pump for various periods of the year.

Results specific to the production and consumption of electrical energy are reported in Table 16. During the winter, little energy is produced by the PVT collector, due to the short duration of the days, with a total energy consumption of the heat pump that is more than 8 times larger. Conversely, in the month of July, 20 times more electrical energy is generated by the PVT panels than in January and with a lower consumption by the heat pump. Considering the whole year, 72% of the electrical energy deriving from the sun is spent to drive the heat pump. The remaining part is either exported to the grid or wasted due to the charging/discharging efficiency of the battery.

The results concerning the thermal energy production by the heat pump and the delivery to district heating are shown in Table 17. In the winter all the heat produced is supplied to the district heating and a small part is wasted due to the loading/unloading efficiency of the PCM-TES. During the summer only 54% of the heat is delivered. The remaining part is stored in the PCM-TES, again with a certain efficiency.

Period	Total Heat Produced by the Heat Pump [MWh]	Total Heat Supplied to District Heating [MWh]
January	116.57	116.45
April	112.18	101.21
July	76.06	41.38
October	107.17	99.14
Year	1208.24	1040.03

Table 17: Total heat produced by the heat pump and supplied to district heating for various periods of the year.

The amount of energy (electrical and thermal) lost by loading and unloading the accumulators (battery, BTES, PCM-TES) is investigated too. The results are reported in Table 18. The battery is the accumulator that is wasting the biggest amount of energy, but it is also the one having the lowest loading/unloading efficiency, i.e. 80%. Most of the electrical energy loss occurs in April, while in winter and summer the loss is lower. The thermal energy loss caused by the BTES does not show a large variability during the year, it is slightly higher in the cold period. Conversely, the thermal energy loss caused by the PCM-TES is very low in the month of January and higher in the warm period.

Period	Energy Loss by the Battery [MWh]	Energy Loss by the BTES [MWh]	Energy Loss by the PCM-TES [MWh]
January	4.87	6.73	0.88
April	9.30	4.77	4.17
July	4.91	4.74	4.19
October	6.02	7.00	3.89
Year	72.01	51.27	37.81

Table 18: Total energy loss by the accumulators (Battery, BTES and PCM-TES) for various periods of the year.

The last outcome deriving from the simulation of the integrated energy system is the import/export of electrical energy from/to the grid. The results are shown in Table 19. Most of the importation of external energy occurs during the winter, when the exportation is null. In the fall the amount of energy imported is higher than the one exported, while in the spring the opposite is true. Eventually, in the summer, no electrical energy is imported from the grid, a substantial exportation takes place instead. Considering the whole year, the balance between exportation and importation is positive, with a net production of 85 MWh.

Period	Total Energy Imported from the Grid [MWh]	Total Energy Exported to the Grid [MWh]
January	36.90	0.00
April	1.40	15.79
July	0.00	67.03
October	21.70	0.91
Year	177.00	262.77

Table 19: Total electrical energy imported and exported to the grid for various periods of the year.

5.2. Winter Results

The results of the integrated energy system simulation specific for the wintertime are presented for the month of January, taken as a reference winter month. The heat pump is the core of the integrated energy system and it has two energy inlets: a thermal and an electrical one. Additionally, it has one thermal energy outlet; each input/output contains an energy production, an energy storage and an energy consumption subsystem.

The results for the electrical input comprise the electrical PVT generation, the battery storage and the compressors consumption of the heat pump. They are shown in Figure 38. During January little electrical energy is produced by the PVT solar collector. Rarely the power generated by itself is sufficient to sustain the heat pump, whose power consumption oscillates between 32 and 65 kW. The initial battery capacity is 750 kWh (75% of the maximum), and runs out in a few hours by feeding the heat pump; then the capacity never exceeds 60 kWh for the whole month of January.

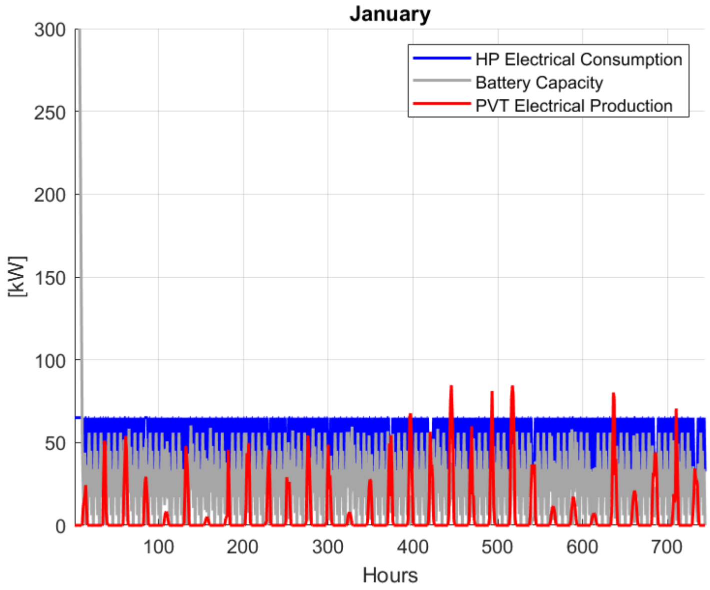

Figure 39: Trends of heat pump consumption, battery capacity, and PVT production of electrical energy in January.

Figure 39 shows the results of the thermal input of the integrated energy system. Two y-axes are present for helping with the visualization.

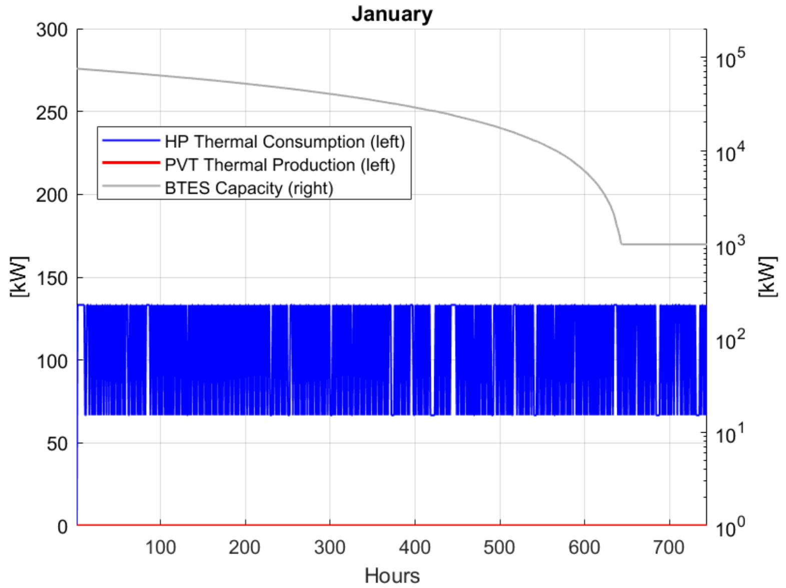

Figure 38: Trends of heat pump consumption, BTES capacity, and PVT production of thermal energy in January.

The thermal energy produced by the PVT panels is null for the whole month of January. In fact the air temperature is too low, and does not result in a positive thermal efficiency of the PVT collector. The heat pump is therefore thermally driven only by the heat stored in the BTES, which initially is 75 MWh (75% of the maximum), then decreases rapidly until reaching the 1% capacity before the end of January and simultaneously remains constant, since a continuous 1 MW of thermal energy is supplied by the ground.

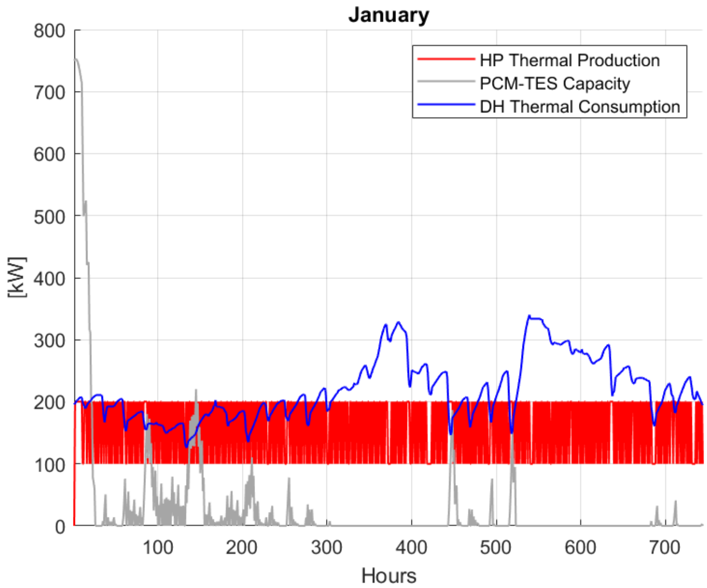

Figure 40: Trends of district heating consumption, PCM-TES capacity, and heat pump production of thermal energy in January.

The trends specific for the thermal energy outlet of the overall system, namely district heating consumption, PCM-TES capacity, and heat pump generation, are shown in Figure 40. In the first part of January, the heat demand is comparable with the full load capacity of the heat pump. After half of the month it increases, exceeding 300 kW for some hours. The PCM-TES capacity initially is 750 kWh (75% of the maximum), but, since the part load operation is adopted many times, the heat available in the storage is drained rapidly. A small amount of heat is stored in the PCM-TES during the short periods when the heat demand remains lower than the heat supplied by the heat pump.

5.3. Summer Results

July is the reference month for the summertime operation of the integrated energy system. The presentation of the summer results is made according to the system's input/output structure, starting with the electrical energy input. Figure 41 shows the trends of PVT generation, battery capacity, and heat pump electrical consumption.

Thanks to the longer daylight period and stronger solar irradiance during the month of July, the PVT collector produces much more electrical energy than in the winter. The production has spikes of 500 kW, allowing the battery to be completely full for many hours. The heat pump is alternatively on full load mode or shut-off. The active operation is sustained by the battery during the night. Due to bad weather conditions over five to

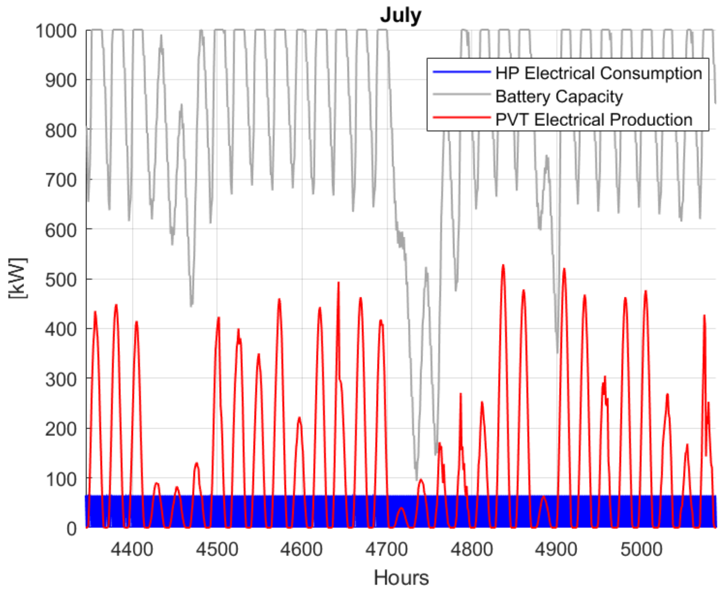

Figure 41: Trends of heat pump consumption, battery capacity, and PVT production of electrical energy in July.

six days the production does not reach 100 kW. Correspondingly, the battery capacity drops down significantly, but it is not drained completely.

The results specific for the thermal energy input in the month of July are shown in Figure 42, two different y-axes are used for a better visualization. Like the electrical case, the production of thermal energy by the PVT collector is much higher in the summer than in winter. In the warmer days, with high solar irradiance, there are peaks in production up to 1500 kW. In July, apart from a few days, the full load thermal energy requirement of the heat pump is always at least six to eight times smaller than the heat production of the PVT panels. Consequently, the BTES capacity never gets below 90% of its maximum.

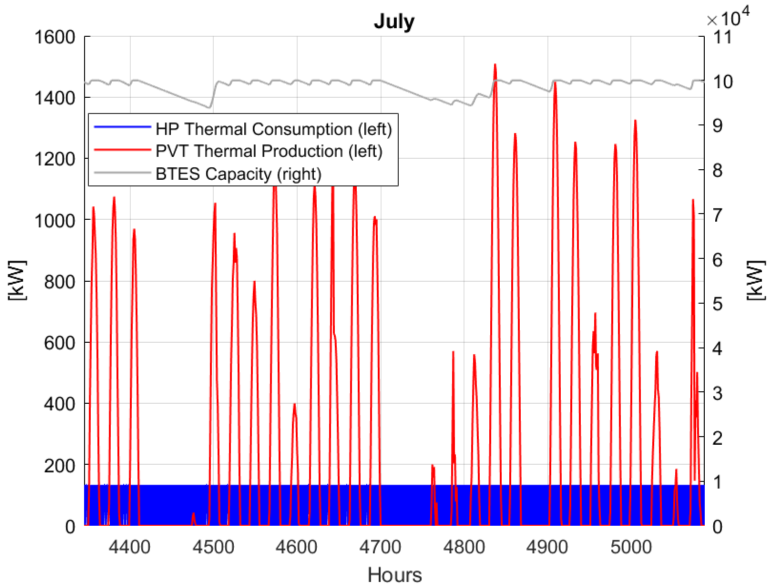

Figure 42: Trends of heat pump consumption, BTES capacity, and PVT production of thermal energy in July.

At last the results for the thermal energy output are displayed in Figure 43. As already shown many times, the heat demand for district heating in the summer is much lower than in the winter. Particularly in July, it is rarely higher than the minimum of 50 kW. The PCM-TES capacity is often at the maximum and the heat pump is shut-off quite frequently. When the heat pump is operating on the other hand, it works on full load mode, always delivering more than twice the demand of heat.

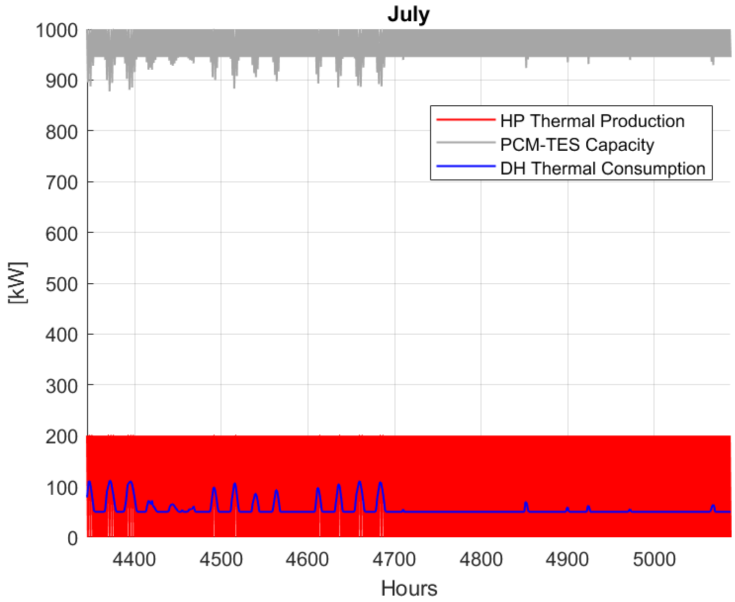

Figure 43: Trends of district heating consumption, PCM-TES capacity, and heat pump production of thermal energy in July.

5.4. Spring/Fall Results

The outcome of the simulation for both spring and fall periods are summarized in the results obtained in the month of April (see Figures 44-46).

The production of electrical energy by the PVT collector is intermediate between the winter and summer ones, and the battery capacity continuously oscillates between full capacity and 30-40% of the maximum. The production of thermal energy presents some isolate peaks of power that are not as high as the summer ones, to which correspond peaks of BTES capacity. The heat pump alternates its operation on all the possible modes during the month of April, and generally the full load operation can provide enough heat to satisfy the heat demand of district heating. To conclude, the capacity of the PCM-TES remains always close to the maximum, it experiences some negative peaks mainly correlated to the shut-off mode.

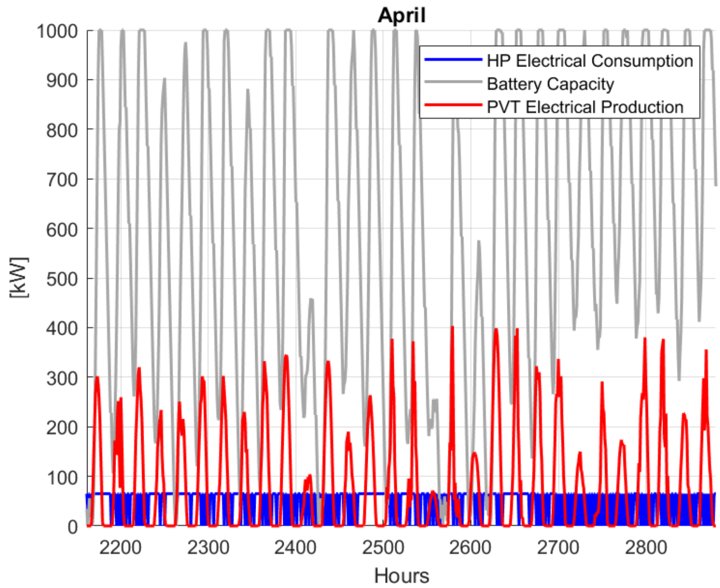

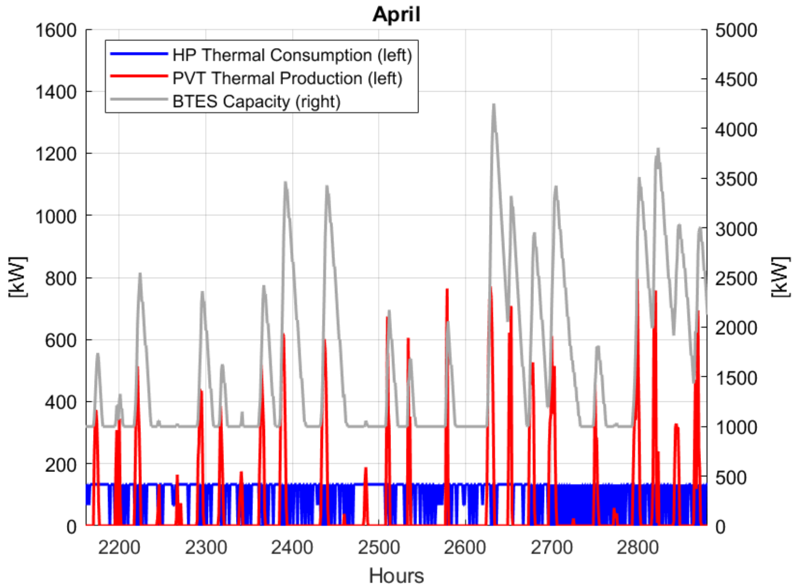

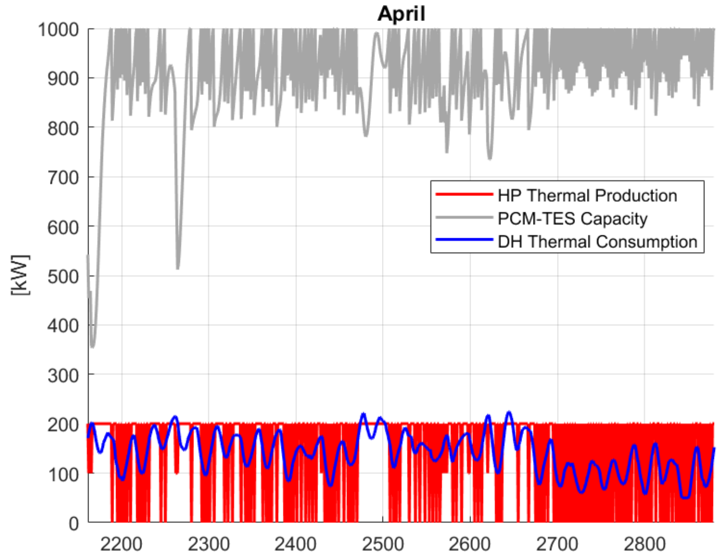

Figures 44-466: Trends of the parameters characterizing the integrated energy subsystems in April.

6. Discussion

6.1. Integrated Energy System Operation

During the winter the heat pump switches continuously between full load externally driven and part load mode. In the cold months there is little solar irradiance during the day, insufficient to drive the compressors and charge the battery. Thus electrical power is imported from the grid. When external supply is used, the heat pump works on full load and some power is used to charge the battery; hence, the heat pump will operate full load until the battery is full enough to sustain the part load operation or until the PVT collector produces enough electrical energy. The PCM-TES is loaded with the heat resulting from the difference between heat pump capacity and heat demand. In the winter the heat demand is often higher than the full load capacity, which means that rarely the PCM-TES gets loaded. This explains why in January the lost output heat is very low compared to the summer.

In the summer the heat pump operation oscillates between internally driven full load and shut-off modes. The shut-off operation is programmed to activate when the PCM-TES is at its full capacity, which happens when the heat demand is low. In the summer, it remains around the minimum of 50 kW most of the time. The solar irradiance during the summer is high enough to ensure the full load operation during the day, while in the night the battery is discharged to fulfill the energy requirements of the heat pump.

The fact that the total heat delivered is the highest in the winter, is a direct implication of the operating modes distribution. In the summer the heat pump is often shut-off. Thus, it does not produce heat, because the low demand is satisfied by the PCM-TES; while in the winter the heat pump is never shut-off. Hence, heat production is continuous.

During the warm months, the available heat remains stationary at around 1,100 kW. This is because the heat pump is usually operating on full load producing 200 kW. The PCM-TES is generally full at 1,000 kWh, while the heat demand remains between 50 and 100 kW. During the winter, the PCM-TES frequently runs low capacity, and the heat pump keeps switching between 200 kW and 100 kW of heat production; the availability of heat is therefore limited and often lower than the average demand. Having a heat available that is sometimes lower than the demand comes from the assumption made during design that the heat pump can cover at maximum 93.4% of the total demand.

A positive balance between exportation and importation of electrical energy from the grid means that, despite of 20% of energy loss for every charging/discharging of the battery, the system can sustain its operation during the year, thanks to the PVT panels. However, during the winter, the system cannot rely only on the solar energy. Particularly in a Nordic country as Norway, a connection with the electrical grid is essential. Furthermore, the PVT collector does not produce thermal energy during the winter. Due to the very low thermal efficiency, a huge underground heat storage is required, which might be an unfeasible solution for the high cost and construction difficulty. An alternative renewable energy source needs to be considered for fulfilling the thermal energy requirement of the heat pump during the cold period. Nevertheless, PV panels with thermal integration coupled with a BTES is an optimal solution in the summer, because the solar energy can be converted into heat with a good efficiency. Subsequently the heat surplus can be stored in the ground without the need of large storage facilities on the surface.

6.2. Model Limitations

Many limitations characterize the models used for simulating the integrated energy system. Focusing on the heat pump section, among the assumptions listed in Section 4.2.1, to completely neglect pressure drops is questionable. Particularly when a phase change occurs inside a heat exchanger, density and viscosity changes can be significant. Type and geometry of the equipment have not been chosen; thus, it is not possible to have an estimate of pressure drops, nor a prediction of the flow regime in the heat exchange units. For the same reason, it is convenient to assume perfect counterflow conditions. A real process based on the heat pump model built in this work will certainly have a lower coefficient of performance.

The PVT system was described with a very simple model. Shading, dirt and dust have not been accounted for; moreover, type and specific features of the PV cells have not been decided. The energy accumulation devices are modelled in an extremely simple way, considering a fixed efficiency of loading/unloading independent on the actual capacity. For the battery, many factors like cycling, aging, charge rate and memory effect can reduce the actual capacity deliverable. A specific phase-change material for the PCM-TES has not been selected and the heat transfer through the TES walls was neglected.

Finally the BTES is subject to the heaviest limitations, both in terms of total capacity and heat delivery. Number and dimension of the wells were not decided, physical and structural properties of the ground were not considered, and a continuous heat extraction directly from the ground was assumed.

7. Conclusions

In this thesis an integrated energy system has been built and its performances evaluated, as part of the bigger research project ChiNoZEN. The network comprises photovoltaic/thermal (PVT) panels, a borehole thermal energy storage (BTES), a battery, a phase-change material thermal energy storage (PCM-TES), a district heating (DH) section, and a cascade high temperature heat pump (HTHP) which uses zeotropic refrigerants and represents the core of the plant. The system was simulated using Matlab, with weather data retrieved from Meteonorm. The selected location was Oslo, in the reference year 2005. Operation and performance of all the subsystems have been investigated for every hour along the whole year. The results obtained from the steady-state simulation of the heat pump were excellent. Hot water at 100°C can be produced and delivered for district heating, with a temperature lift of 80°C. The cascade cycle has a very high energy efficiency, with a COP of 3.6. Due to the high variability of the atmospheric conditions during the year, a huge difference between winter and summer operation was highlighted. In the warm months, the heat pump is frequently shut-off because the heat demand is low, and the PCM-TES is usually at full capacity. Conversely, in the winter, the heat pump operates often on full capacity driven by external electricity from the grid. The PVT collector is not able to provide enough electrical and thermal energy due to the short duration of the winter days. Overall the system self-sustains its operation. In the winter, external power is required to drive the heat pump; but it is completely paid back in the summer, resulting in a positive balance. In conclusion, the integration of cascade high-temperature heat pumps within an energy system presents a promising avenue for sustainable and efficient energy utilization. The synergistic coupling of different temperature levels in the cascade system has proven to be a pivotal factor, enabling the harnessing of thermal energy across a broader spectrum. Through this comprehensive study, the multiple benefits of this innovative approach have been elucidated, ranging from enhanced energy efficiency to reduced environmental impact. In essence, the integration of cascade high-temperature heat pumps into the energy infrastructure represents a step towards a more sustainable and resilient energy future. Through ongoing innovation and collaboration, we can continue to push the boundaries of energy efficiency, contributing to a cleaner and more sustainable planet.

8. Further Work

As we move forward, it is imperative to consider further research and development to refine the technology, address any challenges that may arise during implementation, and to explore opportunities for wider adoption. There are several aspects that need to be improved from the model in this thesis. The heat pump model should be updated considering the actual variations in the temperature of the water entering the heat exchangers; thus, a transient simulation should be performed rather than a steady-state one. The models for the PVT system and district heating system need to be updated. The return temperature of both hot water and heat source should be thoroughly regulated and the mass flow rates of water and refrigerant should be adjusted to various scenarios. The sizes of various components such as heat exchanges and compressors should be optimized to improve the COP. Each component should be modelled in detail to fully understand how the heat pump functions. The energy consumed by all the side equipment constituting the heat pump should be calculated, rather than just the power consumption of compressors. Considering now the whole IES, an economic assessment should be performed. The capital cost of every part of the system must be estimated then, together with operative costs and revenues, the payback period can be calculated. With this last result, it will be possible to tell if the capital investment is profitable or not. Eventually, a deeper work on the system can be conducted, building a pilot plant of the HP to obtain experimental results and validate the theoretical study.

References

[1] Ryssdal, «High Temperature Heat Pumps in Integrated Energy Systems,» 2020.

[2] Skoglund, «High Temperature Heat Pumps Using Zeotropic Refrigerant in Integrated Energy Systems,» 2022.

[3] Ganesan, Eikevik, «New zeotropic CO2-based refrigerant mixtures for cascade high-temperature heat pump to reach heat sink temperature up to 180 °C,» *Energy Conversion and Management: X,* vol. 20, 2023.

[4] Ganesan, Eikevik, Hamid, Wang, Yan, «Thermodynamic analysis of cascade high-temperature heat pump using new natural zeotropic refrigerant mixtures: R744/R600 and R744/R601,» *International Journal of Refrigeration,* vol. 154, pp. 215-230, 2023.

[5] Slack, Tomlin, Barrett, Nonweiler, «Optimized Heat Pump System». Europe Brevetto EP 3 196 559 A1, 26 07 2017.

[6] Olympios, Mersch, Hoseinpoori, Pantaleo, «Optimal design of low-temperature heat-pumping technologies and implications to the whole-energy system,» 2020.

[7] Hays, «High temperature heat pump». USA Brevetto US 6 913 076 B1, 05 07 2005.

[8] Bamigbetan, Eikevik, Nekså, Bantle, Schlemminger, «Theoretical analysis of suitable fluids for high temperature heat pumps up to 125 °C heat delivery,» *International Journal of Refrigeration,* vol. 92, pp. 185-195, 2018.

[9] Urbanucci, Bruno, Testi, «Thermodynamic and economic analysis of the integration of high-temperature heat pumps in trigeneration systems,» *Applied Energy,* vol. 238, pp. 516-533, 2019.

[10] Choi, «Cascade type heat pump system and control method thereof». South Korea Brevetto KR 101 236 603 B1, 22 02 2011.

[11] Yerdesh, Toleukhanov, Mohanraj, «Air-to-Water Cascade Heat Pump Thermal Performance Modelling for Continental Climate Regions,» *Entropy: Thermodynamics – Energy – Environment – Economy,* vol. 3, n. 1, 2022.

[12] Jung, Kang, Yoon, Kim, «Performance comparison between a single-stage and a cascade multi-functional heat pump for both air heating and hot water supply,» *International Journal of Refrigeration,* vol. 36, n. 5, pp. 1431-1441, 2013.

[13] Boahen, Choi, «A Study on the Performance of a Cascade Heat Pump for Generating Hot Water,» *Energies,* vol. 12, p. 4313, 2019.

[14] Yilmaz, «Performance analysis of a vapor compression heat pump using zeotropic refrigerant mixtures,» *Energy Conversion and Management,* vol. 44, pp. 267-282, 2003.

[15] Navarro-Esbrí, Fernández-Moreno, Mota-Babiloni, «Modelling and evaluation of a high-temperature heat pump two-stage cascade with refrigerant mixtures as a fossil fuel boiler alternative for industry decarbonization,» *Energy,* vol. 254, n. B, 2022.

[16] Sezen, Gungor, «Comparison of solar assisted heat pump systems for heating residences: A review,» *Solar Energy,* vol. 249, pp. 424-445, 2023.

[17] Olabi, Mahmoud, Obaideen, Sayed, Ramadan, Abdelkareem, «Ground source heat pumps: Recent progress, applications, challenges, barriers, and role in achieving sustainable development goals based on bibliometric analysis,» *Thermal Science and Engineering Progress,* vol. 41, 2023.

[18] Lazzarin, Noro, «Photovoltaic/Thermal (PV/T)/ground dual source heat pump: Optimum energy and economic sizing based on performance analysis,» *Energy and Buildings,* vol. 211, 2020.

[19] Staffell, Brett, Brandon, Hawkes, «A review of domestic heat pumps,» *Energy & Environmental Science,* vol. 5, n. 11, pp. 9291-9306, 2012.

[20] Chua, Chou, Yang, «Advances in heat pump systems: A review,» *Applied Energy,* vol. 87, n. 12, pp. 3611-3624, 2010.

[21] de Boer, Marina, Zühlsdorf, Arpagaus, Bantle, Wilk, Elmegaard, Corberán, Benson, «Strengthening Industrial Heat Pump Innovation,» 2020. [Online]. Available: https://www.sintef.no/en/publications/publication/1921809/. [Consultato il giorno 14 12 2023].

[22] Sarbu, Advances in Building Services Engineering, Cham, Switzerland: Springer, 2021.

[23] Arpagaus, Bless, Uhlmann, Schiffmann, Bertsch, «High temperature heat pumps: Market overview, state of the art, research status, refrigerants, and application potentials,» *Energy,* vol. 152, pp. 985-1010, 2018.

[24] Bobelin, Bourig, Peureux, «Experimental results of a newly developed very high temperature industrial heat pump (140°C) equipped with scroll compressors and working with a new blend refrigerant,» 2012.

[25] Stene, «Residential CO2 Heat Pump System fpr Combined Space Heating and Hot Water Heating,» 2004.

[26] Dhilipan, Vijayalakshmi, Shanmugam, Ganesh, Kodeeswaran, Muralidharan, «Performance and efficiency of different types of solar cell material – A review,» *Materials Today: Proceedings,* vol. 66, n. 3, pp. 1295-1302, 2022.

[27] Dubey, Sarvaiya, Seshadri, «Temperature Dependent Photovoltaic (PV) Efficiency and Its Effect on PV Production in the World - A Review,» *Energy Procedia,* vol. 33, pp. 311-321, 2013.

[28] Lamnatou, Chemisana, «Photovoltaic/thermal (PVT) systems: A review with emphasis on environmental issues,» *Renewable Energy,* vol. 105, pp. 270-287, 2017.

[29] Ramos, Alcaso, Cardoso, «Photovoltaic-thermal (PVT) technology: Review and case study,» 2019.

[30] Sevela, Olesen, «Development and Benefits of Using PVT Compared to PV,» 2012.

[31] Sarbu, Sabarchievici, «A Comprehensive Review of Thermal Energy Storage,» *Sustainability,* vol. 191, n. 10, 2018.

[32] Schmidt, Technical Thermodynamics for Engineers Basics and Applications, Cham, Switzerland: Springer, 2019.

[33] Diersch, Bauer, «Analysis, modeling and simulation of underground thermal energy storage (UTES) systems,» in *Advances in Thermal Energy Storage Systems.*, Cambridge, UK, Elsevier, 2015, pp. 149-183.

[34] Schmidt, «Large scale heat storage for district heating,» 2020.

[35] Dong, McCartney, Lu, «Critical Review of Thermal Conductivity Models for Unsaturated Soils,» *Geotechnical and Geological Engineering,* vol. 33, n. 2, 2015.

[36] Lemmon, Bell, Huber, McLinden, «REFPROP Documentation,» 21 05 2018. [Online]. Available: https://www.nist.gov/system/files/documents/2018/05/23/refprop10a.pdf. [Consultato il giorno 15 12 2023].

[37] Sarkar, Bhattacharyya, «Assessment of blends of CO 2 with butane and isobutane as working fluids for heat pump applications,» *International Journal of Thermal Sciences,* vol. 48, pp. 1460-1465, 2009.

[38] Towler, Sinnott, Chemical Engineering Design - Principles, Practice and Economics of Plant and Process Desing, Burlington MA, USA: Elsevier, 2008.

[39] Turton, Bailie, Whiting, Schaeiwitz, Bhattacharyya, Analysis, Systesis and Design of Chemical Processes, Ann Arbor MI, USA: Prentice Hall, 2012.

[40] Herrando, Ramos, Zabalza, Markides, «A comprehensive assessment of alternative absorber-exchanger design for hybrid PVT-water collectors,» *Applied Energy,* vol. 235, pp. 1583-1602, 2019.

[41] Michaels, B. Jr, Vose, Knappenberger, «Analysis of trends in the variability of daily and monthly historical temperature measurements,» *Climate Research,* vol. 10, pp. 27-33, 1998.

[42] Dannevig, Hartsveit, «Klima i Norge,» Store Norske Leksikon, 28 10 2022. [Online]. Available: https://snl.no/klima_i_Norge#-Middeltemperaturer_(%C2%B0C)_i_Norge. [Consultato il giorno 15 12 2023].

Appendix: Draft Scientific Paper

Journal **XX** (XXXX) XXXXXX https://doi.org/XXXX/XXXX

Design of an integrated energy system using a cascade high temperature heat pump with zeotropic refrigerants.

Omar Volpato[1,2], Trygve M. Eikevik[1] and Ganesan Palanichamy[1]

[1] Department of Energy and Process Engineering, Norwegian University of Science and Technology, Trondheim, Norway
[2] Department of Industrial Engineering, University of Padova, Padova, Italy

E-mail: omar.volpato@studenti.unipd.it

Received xxxxxx
Accepted for publication xxxxxx
Published xxxxxx

Abstract

In the face of an escalating global energy demand, this thesis deals with the pivotal challenge of designing and modelling a self-sustainable integrated energy system. At its core, the system harnesses the power of a cascade high-temperature heat pump utilizing zeotropic refrigerants. The heat pump design is specifically sized to generate hot water for district heating with a temperature higher than 100°C, coupled with a Coefficient of Performance (COP) surpassing 3.6. This innovative system is tested in Oslo through a Matlab simulation, underlying the practical applicability to real-world scenarios. The results of this research demonstrate a noteworthy achievement: the proposed system not only meets the two design specifications, but is also a sustainable and efficient source of energy. The simulation is performed over a year on an hourly basis. The system proves capable of providing enough heat to satisfy the district heating demand for 9/12 months of the year while also achieving self-sustainability during its operation. In addition, the deployment of zeotropic mixtures as refrigerants adds an extra layer of efficiency and adaptability to the system thanks to their temperature glide. This remarkable success is a significant jump forward in clean and sustainable energy solutions, particularly for district heating. It demonstrates the potential of high temperature heat pumps to effectively address the energy needs of our world.

Keywords: high temperature heat pumps, zeotropic mixtures, integrated energy systems

1. Introduction

The world has been witnessing an unprecedented surge in the demand of energy prompted by rapid population growth, industrialization and technological progress. The investigation and development of sustainable and efficient solutions have become of primary importance to face this escalating need for energy. In the prospect of energy systems, the alignment with global initiatives such as the Sustainable Development Goals (SDGs) is now more pressing than ever. This work explores the possibility of building an integrated energy system with a particular emphasis on key SDGs, such as affordable and clean energy (SDG 7), industry, innovation, and infrastructure (SDG 9), and climate action (SDG 13). In the past decades, the use of fossil fuels for heating purposes has been the predominant solution worldwide; however, in the Net Zero Emissions by 2050 scenario, the use of green energy source must become the preferred choice for a substantial reduction of CO2 emissions in the atmosphere. The utilization of a heat pump for heat generation brings many benefits, both in terms of energy efficiency and mitigation of greenhouse gases release.

Industrial processes that require heating and waste heat disposal can benefit from the development of high temperature heat pumps. Both investment and operational cost of boilers and cooling towers can be potentially saved with a single more efficient and less complex energy system, at the same time reducing the environmental footprint. Furthermore, the employment of zeotropic refrigerants adds a layer of complexity and innovation to the conventional heat pump paradigm, enhancing the energy-efficiency thanks to their varying compositions and thermodynamic properties. Understanding and optimizing the interactions within this integrated system becomes crucial as it directly contributes to SDG 13. This exploration is not merely an academic pursuit; it is a stride towards a future where energy systems seamlessly align with environmental stewardship, economic viability, and technological innovation, all the while reflecting the interconnected objectives of the SDGs. The following chapters will delve into the theoretical foundations, design considerations, and empirical analyses necessary to comprehend and implement this integrated energy system, emphasizing its potential to significantly reduce CO2 emissions and contribute to a sustainable future. [1]

This work is part of the bigger project "Key technologies and demonstration of combined cooling, heating and power generation for low-carbon neighborhoods/buildings with clean energy" (ChiNoZEN). The project is the result of the cooperation of Norwegian and Chinese researchers within energy topics. The ChiNoZEN project supports the transition to a reliable, affordable, publicly accepted and sustainably built environment, aiming at reducing fossil fuel dependency in the face of increasingly scarce resources, growing energy needs, and threatening climate change. [2]

2. Methodology

2.1. About the Model

A model describing the integrated energy system is built using Matlab. The city of Oslo is the base location for building the system, meteorologic data (air temperature and solar irradiation) on hourly base were retrieved using Meteonorm for the year 2005. For the detailed simulation of the heat pump, the thermodynamic properties of the fluids are calculated using Refprop v9.1, coupled with Matlab.

It is assumed that the compressors are the only unit operation of the plant that require electrical energy to work, the consumption of all the other electrically-driven devices is neglected. The heat demand for district heating is divided into water heating and space heating demands. A base demand of 50 kW for water heating, independent of outside air temperature, is assumed; while, a temperature dependency exists for the space heating demand: it increases of 10.25 kW for every Celsius degree below 15°C. The mathematical relationship defining the heat demand is reported in Equation n.

$$D = \begin{cases} 50\ kW \quad if\ T_a \geq 15°C \\ [50 + 10.25(15 - T_a)]\ kW \quad if\ T_a < 15°C \end{cases} \quad (1)$$

T_a is the outside air temperature. [3] [4]

The integrated energy system (IES) is displayed in Figure 1.

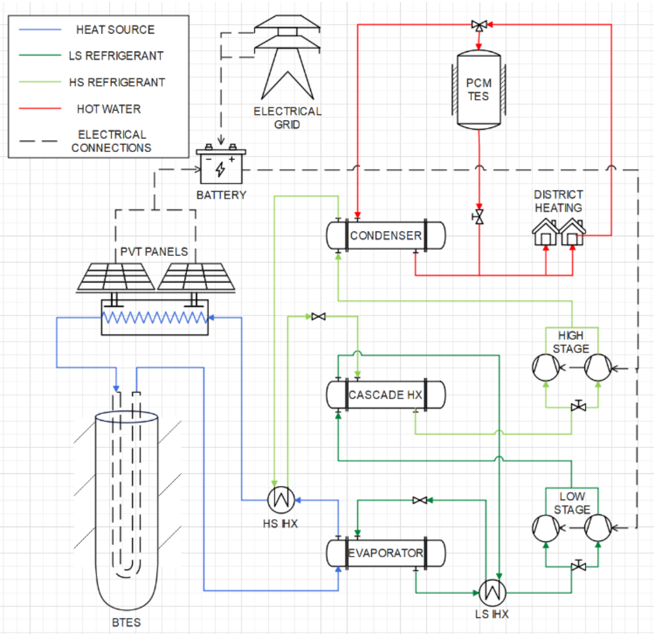

Figure 47: PFD of the integrated energy system.

2.2. PVT panels model

Photovoltaic/thermal (PVT) panels are used to collect solar energy from the sun and convert it into electrical and thermal energy, useful to drive the compressors and re-heat the heat source of the heat pump. The photovoltaic/thermal panels are described using a very simple model: the solar incident radiation that hits the solar collector is converted into both electrical energy and thermal energy with certain electrical and thermal efficiencies. With the solar irradiance data collected with Meteonorm, specific for Oslo in the year 2005, the electrical and thermal generation data on an hourly base can be obtained. Thermal and electrical efficiencies vary depending on the system conditions, and they are calculated according to the methods presented in the work of Herrando et al. The formulas for efficiency calculations are reported in Equations 2-3.

$$\eta_{th} = \eta_O - a_1 T_r - a_2 I_t T_r^{\,2} \qquad (2)$$

$$\eta_{th} = \eta_{ref}\left[1 - \beta_0\left(T_{PV} - T_{ref}\right)\right] \qquad (3)$$

η_O is the optical efficiency, a_1 is the linear heat loss coefficient, a_2 is the quadratic heat loss coefficient, I_t is the total solar irradiance per unit of area and T_r is the reduced temperature, η_{ref} is the reference PVT module efficiency tested at the reference temperature T_{ref} of 25°C and at a solar irradiance of 1000 W/m^2, β_0 is the temperature coefficient of the PVT module, while T_{PV} is the surface temperature of the PVT module, which is assumed to be 20°C higher than the air temperature. [5]

The PVT panel type will not be specified, but the total area of the panels is assumed to be 4000 m^2. The formulas for the calculation of electrical and thermal are reported in Equations 4-5.

$$\dot{P}_{el} = \eta_{el} I_t A_{PVT} \qquad (4)$$

$$\dot{P}_{th} = \eta_{th} I_t A_{PVT} \qquad (5)$$

2.3. Battery model

A solar-assisted heat pump cannot be independent from the electrical grid if one or more batteries are not integrated in the system. The energy that can be obtained from the sun with a solar collector is discontinuous during the day, due to day/night switch, variable cloud coverage, and other atmospheric factors. It is also variable throughout the year, particularly in Nordic countries, because of the difference in daytime duration between summer and winter. The battery is simulated according to a greatly simplified model. A battery type will not be specified and, its maximum capacity and charging/discharging efficiencies are assumed to be 1000 kWh and 80% respectively. These are the only two parameters characterizing the battery accumulator.

2.4. Borehole thermal energy storage (BTES) model

A borehole thermal energy storage (BTES) is integrated in the system to store the thermal energy produced by the PVT panels. A storage of thermal energy is necessary because of the significant variations in the supply from the PVT collector. The BTES is not designed in detail, the number and the features of the pipes in the borehole heat exchanger (BHE) have not been decided and the heat transfer within the BHE is not investigated. Furthermore, a strong assumption is made on the BTES: the heat stored in it never gets below 1% of the maximum capacity, because a small amount of heat can be extracted from the ground. The BTES is characterized only by its total storage capacity of 100,000 kWh and by a loading/unloading efficiency of 90%.

2.5. Phase-change material thermal energy storage (PCM-TES) model

A thermal energy storage, based on phase-change materials (PCM-TES), can be integrated into the system to store the surplus energy produced by the heat pump with respect to the heat demand of district heating. Conversely, in the winter months, when the heat pump capacity is insufficient, heat can be withdrawn from the TES to satisfy the demand. As for the other energy storage systems, also the PCM-TES is not designed in detail, the phase-change material is not selected and again only the maximum capacity and the loading/unloading efficiencies are assumed. Their values are 1000 kWh and 90% respectively.

2.6. District heating

The district heating is not modelled because the number and the type of building supplied with the heat produced by the heat pump are not decided upon. A mathematical expression is assumed for the heat demand composed of a water heating and a space heating contribution. The whole district heating system will be treated as if it was a heat exchanger. At every time iteration, the hot water leaving the heat pump ceases the sensible heat defined by the heat demand to the district heating, returning to the heat pump condenser at a lower temperature. Hence, the temperature reduction of the hot water can be calculated according to Equation 6.

$$\Delta T_{DH} = \frac{D}{\dot{m}_{hw} c_p} \tag{6}$$

$\dot{m}_{hw}$ is the heat source mass flow rate and c_p is the specific heat capacity of water.

2.7. Heat pump model

The zeotropic cascade high temperature heat pump consists of a low stage and a high stage, both comprise an evaporator, a condenser, two equal parallel compressors and an expansion valve. The two stages are nested together by means of a cascade heat exchanger, which serves as condenser for the low stage and as evaporator for the high stage. For both stages an internal heat exchanger (IHX) is present. A configuration with two parallel compressors for both stages is useful for load and capacity control, one of the compressors can be shut-off when the heat demand is low, increasing the plant's energy efficiency. The PFD of the heat pump section obtained after sizing and energy integration is shown in Figure 2.

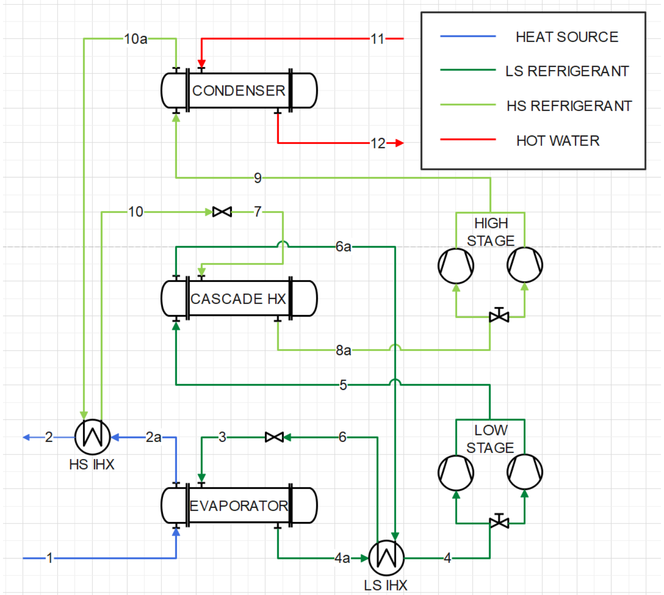

Figure 48: PFD of the heat pump section.

The following assumptions are made for modelling the heat pump:

- In the cascade heat exchanger, the low stage and the high stage refrigerants exchange the same heat capacity.
- Saturated vapor is present at the outlet of the evaporators.
- Saturated liquid is present at the outlet of the condensers.
- The expansion process is isenthalpic.
- The pressure drops and the heat losses in the system are neglected.
- All the heat exchangers have a counter-flow configuration. [6] [7]

A two-stage cascade heat pump requires the selection of two refrigerants such that the critical point of the one used in the high stage has a higher critical point than the one used in the low stage. Natural working fluids such as ammonia, carbon dioxide, light alkanes and alkenes, thanks to their negligible ODP, have a lower impact on the environment compared to synthetic refrigerants (HFCs and CFCs). Therefore, natural working fluids must be the primary choice as refrigerants.

3%/97% CO_2/butane and 2%/98% CO_2/pentane blends are selected for low stage and high stage respectively. The exact compositions are the ones ensuring the best temperature coupling between the refrigerants inside the heat exchangers (a difference between 5 and 10°C between the temperature profiles). [8]

The cascade heat pump is sized with two main design specifications: hot water temperature higher than 100°C and COP of the heat pump higher than 3.6. From the air temperature data in Oslo in year 2005, the heat demand for district heating can be calculated on an hourly basis and the load-duration curve (LDC) can be obtained (see Figure 3). The heat pump is sized to deliver 200 kW when operating full load. This will cover 93.4% of the total heat demand. A part load operating mode is defined too, it is characterized by half the capacity with respect to the full load mode.

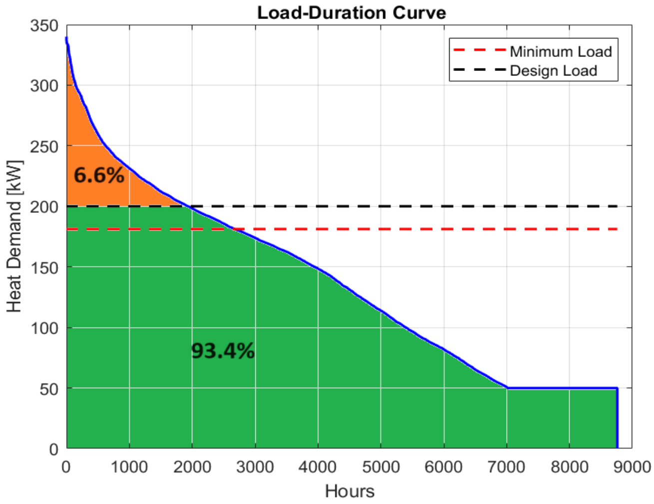

Figure 49: Load-duration curve.

From a sizing procedure followed by an energy integration, the values of all the construction parameters are calculated. The flow parameters of heat source and heat sink streams are calculated too. They are reported in Tables 1-2 respectively, for both full load and part load cases.

Design Parameter	Full Load	Part Load
Condenser Area	22 m^2	11 m^2
Cascade HX Area	12 m^2	6 m^2
Evaporator Area	13 m^2	6.5 m^2
LS IXH Area	1.1 m^2	0.55 m^2
HS IHX Area	0.5 m^2	0.25 m^2
LS Compressor Size	290 m^3/h	145 m^3/h
HS Compressor Size	300 m^3/h	150 m^3/h

Table 20: Values of the design parameters of the heat pump, for both full load and part load.

Stream	Flow Parameter	Full Load	Part Load
Heat Source	Inlet Temperature	40°C	40°C
	Mass Flow Rate	3.76 kg/s	1.88 kg/s
Heat Sink	Inlet Temperature	60°C	60°C
	Mass Flow Rate	1.19 kg/s	0.60 kg/s

Table 21: Values of the inlet flow parameter of heat source and heat sink for full load and part load.

Given the input conditions reported in Table 2, all the output variables (condenser capacity, compressor work, COP, and hot water outlet temperature) of the heat pump system are calculated with an iterative procedure. Each iteration starts with an estimate of the low stage evaporation temperature T_e^{LS}, the low stage condensation temperature T_c^{LS} and the high stage condensation temperature T_c^{HS}. Note that, since the refrigerants are zeotropic mixtures, evaporation and condensation temperatures are not unique; the evaporation temperature is taken equal to the mixture's dew point, while the condensation temperature is taken equal to the mixture's bubble point. All the state properties of the heat pump are calculated, with a superheating degree of 12°C and temperature difference between the stages of 8°C. The mass flow rate of the refrigerants is calculated according to Equation 7:

$$\dot{m}_{ref} = \rho_{in} \frac{V_c}{3{,}600} \eta_V \tag{7}$$

ρ_{in} is the vapor inlet density in the compressor, V_c is the compressor size, η_V is the volumetric efficiency of the compressor.

Then the capacities of the three main heat exchangers can be computed with the formulas reported in Equations 8-10:

$$\dot{Q}_c = \dot{m}_{ref}^{HS}(h_9 - h_{10a}) \tag{8}$$

$$\dot{Q}_{che} = \dot{m}_{ref}^{LS}(h_5 - h_{6a}) \tag{9}$$

$$\dot{Q}_e = m_{ref}^{LS}(h_{4a} - h_3) \tag{10}$$

The h_is are the enthalpies in the specific points of the plant (see Figure 2 for number references).

Every heat exchanger is characterized by a logarithmic mean temperature difference (LMTD), which has two mathematical expressions: one is the actual logarithmic mean of the temperature differences between inlet and outlet, the other comes from the global energy balance of the heat exchanger. The three equations based on the exchanger LMTDs are reported in Equations 11-13:

$$\Delta T_{ml}^{c} = \frac{\dot{Q}_c}{U_c A_c} = \frac{(T_9 - T_{12}) - (\boldsymbol{T_c^{HS}} - T_{11})}{\ln\left(\dfrac{T_9 - T_{12}}{\boldsymbol{T_c^{HS}} - T_{11}}\right)} \tag{11}$$

$$\Delta T_{ml}^{che} = \frac{\dot{Q}_{che}}{U_{che}A_{che}} = \frac{(T_5 - T_{8a}) - (\boldsymbol{T_c^{LS}} - T_7)}{\ln\left(\dfrac{T_5 - T_{8a}}{\boldsymbol{T_c^{LS}} - T_7}\right)} \tag{12}$$

$$\Delta T_{ml}^{e} = \frac{\dot{Q}_{e}}{U_{e}A_{e}} = \frac{(T_1 - \boldsymbol{T_e^{LS}}) - (T_2 - T_3)}{\ln\left(\dfrac{T_1 - \boldsymbol{T_e^{LS}}}{T_2 - T_3}\right)} \tag{13}$$

The T_is are the temperatures in the specific points of the plant (see Figure 2 for number references). The system of algebraic equations made of Equations 11-13 is solved with the fsolve solver of Matlab.

Once the values of the three unknowns are calculated, the power consumption of the two compressors can be calculated according to Equations 14-15:

$$\dot{W}_c^{LS} = \dot{m}_{ref}^{LS}(h_5 - h_4) \tag{14}$$

$$\dot{W}_c^{HS} = \dot{m}_{ref}^{HS}(h_9 - h_{8a}) \tag{15}$$

The COP of the cascade heat pump can be calculated according to Equation 16:

$$COP = \frac{\dot{Q}_c}{\dot{W}_c^{LS} + \dot{W}_c^{HS}} \tag{16}$$

Finally, the outlet temperature of heat source and hot water are calculated according to Equations 17-18:

$$T_{hs}^{out} = T_{hs}^{in} - \frac{\dot{Q}_e}{\dot{m}_{hs}c_p} \tag{17}$$

$$T_{hw}^{out} = T_{hw}^{in} + \frac{\dot{Q}_c}{\dot{m}_{hw}c_p} \tag{18}$$

$\dot{m}_{hs}$ is the heat source mass flow rate.

Parameter	Full Load	Part Load
Heat Capacity	200.6 kW	100.4 kW
Power Consumption	65.6 kW	32.7 kW
Hot Water Outlet Temperature	100.3°C	100.4°C
COP	3.60	3.61

Table 22: Results of the heat pump operation for both full load and part load operations.

The simulation of the heat pump, allows the calculation of all the outlet parameters, both for the full load and the part load operations. They are reported in Table 3. An energy efficiency of 85% is assumed for the compressors.

Given the exact values of the state properties in the heat pump system, the heat pump operation can be easily visualized in the T-s and P-h diagrams shown in Figures 4-5.

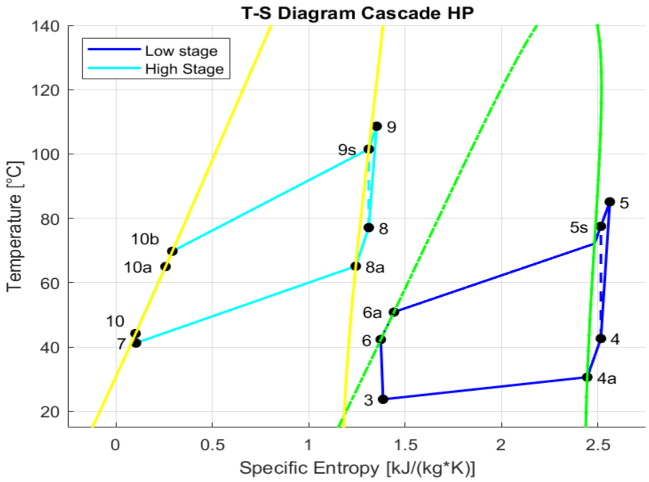

Figure 50: T-s diagram representing the heat pump.

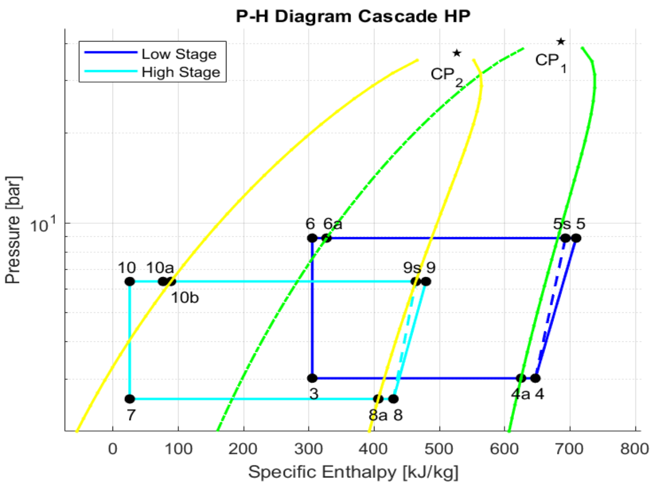

Figure 51: P-h diagram representing the heat pump.

Since the type of the heat exchangers have not been decided, it is assumed that the heat flux between contacted fluids is uniform and independent of the phase changes. The heat exchangers are divided in slices. A fraction of the total heat flow is transferred inside each slice, allowing to track the temperature profiles of the fluids and in turn the LMTDs values. All the profiles inside the three main heat exchangers (evaporator, cascade heat exchanger and condenser) are shown in Figures 6-11.

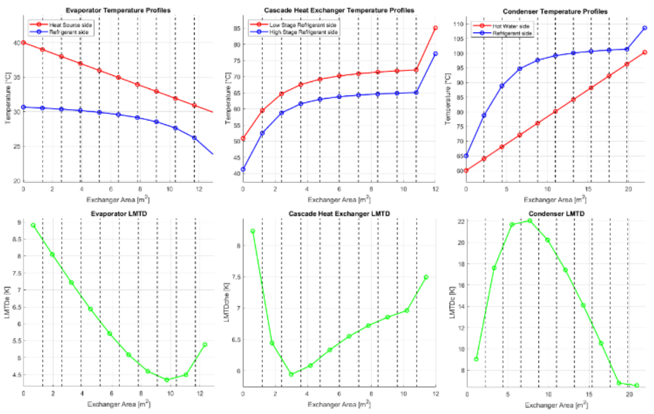

Figures 52-11: Temperature profiles (top) and LMTDs (bottom) inside the three main heat exchangers.

The refrigerants selected ensures a good temperature profile coupling, so that the internal LMTDs are never below 4°C. Inside the condenser the LMTD between high stage refrigerant and hot water reaches 22°C; this value is very high, and it is not possible to decrease it, due to the shape of the gliding temperature of the CO2/pentane mixture.

2.8. *Integrated energy system algorithm*

The integrated energy system works according to an algorithm that combines all the models developed for the subsystems. The BFD of the integrated energy system algorithm is shown in Figure 12.
First the weather data (air temperature and solar irradiance) on an hourly basis specific for Oslo in year 2005 are retrieved. From there it is possible to calculate heat demand for district heating, electrical and thermal power generation from the PVT panels throughout the year. The system is then initialized. For battery, BTES and PCM-TES the initial values of capacity are set. For all the time iteration, namely from the first to the last hours of year 2005, many system parameters are calculated: heat pump operational mode, condenser and evaporator capacities, power consumption, battery stored energy, BTES stored energy, PCM-TES stored energy, power imported or exported to the electrical grid and heat supplied to district heating.

At the beginning of an iteration, if the PCM-TES is at its maximum capacity, the heat pump is shut-off, because the thermal energy surplus produced would be wasted. In that case the heat demand is satisfied with the solely heat stored in the PCM-TES. Both capacities and power consumption are null, thus

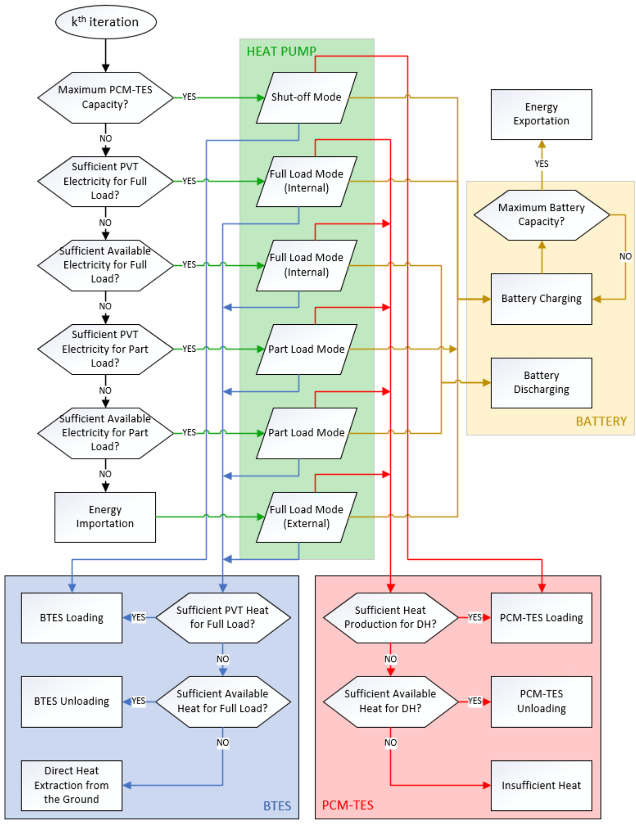

Figure 12: BFD of the algorithm used to simulate the integrated energy system (the sections are highlighted with different colors.

battery and BTES are loaded. If thermal energy can still be stored in the PCM-TES, then the operational mode of the heat pump at that time iteration is decided depending on the available electrical energy (power generated by the PVT panels plus energy stored in the battery). If the available electrical energy is sufficient, the heat pump runs on full load, and the battery can be either charged or uncharged. Otherwise, if the available electrical energy is enough to run the heat pump on part load, said operation is selected and again the battery can either be charged, when surplus electrical energy is produced, or uncharged instead. If at a certain iteration there is not enough available energy to run the heat pump on part load, energy is imported from the external and the heat pump is run on full load, charging the battery too. Every time the battery is charged, the maximum capacity might be reached, in that case the electrical energy that cannot be stored is exported to the outside through the electrical grid. When the BTES reaches its maximum capacity, then the thermal energy that would be added is assumed to be completely wasted. On the other hand, when the BTES reaches its minimum capacity, the heat source is assumed to be re-heated to 40°C, regardless of the thermal energy missing. Finally, when the PCM-TES reaches its maximum, the heat pump is shut-off to avoid thermal energy dissipation.

3. Results and discussion

The system was simulated in the city of Oslo during the year 2005 with the weather data retrieved from Meteonorm. A synthetic display of air temperature and solar irradiance is reported in Table 4.

Descriptor	Air Temperature	Solar Irradiance
Maximum	+29.8°C	868 kW/m^2
Minimum	-13.3°C	0 kW/m^2
Winter Average	-1.9°C	35 kW/m^2
Summer Average	+15.9°C	166 kW/m^2
Yearly Average	+7.1°C	102 kW/m^2

Table 23: Maximum, minimum, and average air temperature in Oslo during the year 2005.

The average temperature between winter and summer varies significantly. The air temperature usually remains above 15°C during the summer and between 0 and -5°C during the winter. The average solar irradiance shows an extreme variation during the year. This is due to the high latitude of Oslo, which ensures more than 200 monthly sunshine hours in the summer, but only 50 during the winter.

3.1. *Integrated energy system performance*

The simulation of the integrated energy system for the whole year gives results in terms of the performance of all the subsystems. For what concerns the heat pump, it can run on three different operational modes, depending on the overall energy availability and demand of district heating. The quantification of the hours in each mode, also divided for specific periods of the year, is reported in Table 5. For the sake of clarity, a distinction has been made between the system's full load operation driven by the directly available electrical energy (internal full load) and the full load operation driven by the electrical energy provided by the external grid (external full load).

Period	Hours Full Load		Hours Part Load	Hours Shut-off
	Internal	External		
January	53 (7.2%)	370 (49.7%)	321 (43.1%)	0 (0.0%)
April	540 (75.0%)	14 (1.9%)	13 (1.8%)	153 (21.3%)
July	380 (51.1%)	0 (0.0%)	0 (0.0%)	364 (48.9%)
October	220 (29.5%)	217 (29.2%)	197 (26.5%)	110 (14.8%)
Year	3497 (39.9%)	1770 (20.2%)	1540 (17.6%)	1953 (22.3%)

Table 24: Hours of full load, part load and shut-off operation in different periods of the year.

In Figure 13 the heat capacity of the heat pump is displayed together with the heat demand of district heating, the three operational modes of the heat pump are clearly distinguishable. The full load supplies 200 kW, the part load supplies 100 kW, while in shut-off mode the capacity is null. The heat demand highly exceeds the full load capacity of the heat pump in the winter months.

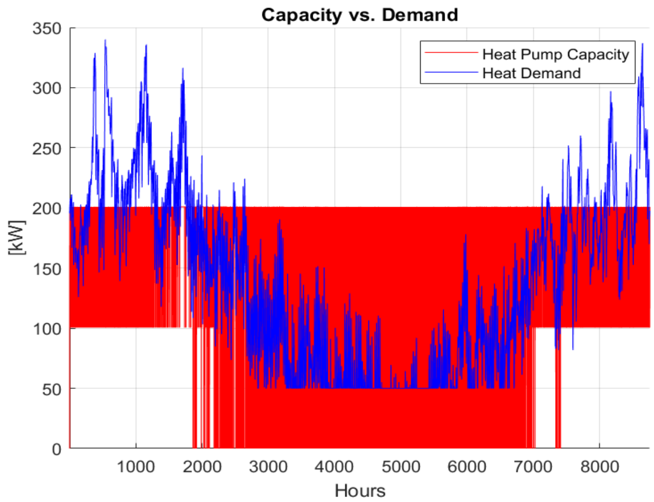

Figure 13: Heat pump capacity and heat demand during the year.

In Figure 14 the weekly averaged heat demand is compared to the weekly averaged heat available for district heating. The availability of heat, namely the one stored in PCM-TES plus the one produced on time by the heat pump, is always much higher than the demand in the summer, and in large part of spring and fall. In the winter, on the other hand, there are few weeks during which the heat demand surpasses the heat available.

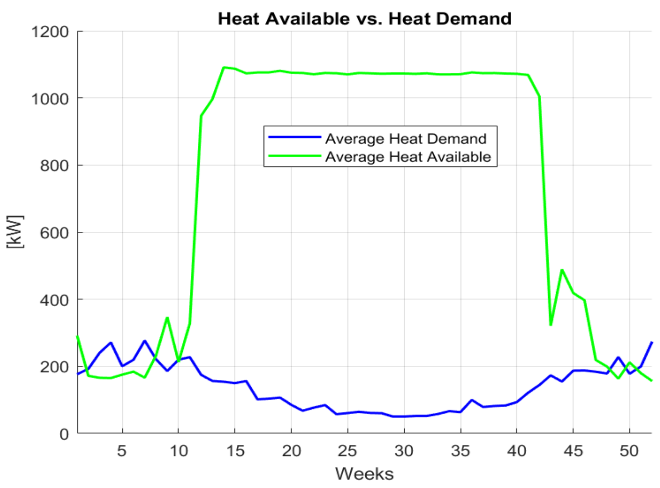

Figure 14: Weekly averaged heat demand and heat available during the year.

Period	Total Energy Imported	Total Energy Exported
January	36.90	0.00
April	1.40	15.79
July	0.00	67.03
October	21.70	0.91
Year	177.00	262.77

Table 25: Total electrical energy imported and exported to the grid for various periods of the year.

In Table 6 the results representing the import/export of electrical energy from/to the grid are reported. A positive balance between exportation and importation of electrical energy from the grid means that, despite of 20% of energy loss for every charging/discharging of the battery, the system can sustain its operation during the year, thanks to the PVT panels. However, during the winter, the system cannot rely only on the solar energy. Particularly in a Nordic country as Norway, a connection with the electrical grid is essential.

3.2. Winter period

Results specific for the winter period are displayed in Figures 15-17 in terms of the parameters characterizing each subsystem of the IES.
During the winter the heat pump switches continuously between full load externally driven and part load mode. In the cold months there is little solar irradiance during the day, insufficient to drive the compressors and charge the battery. Thus, electrical power is imported from the grid. When external supply is used, the heat pump works on full load and

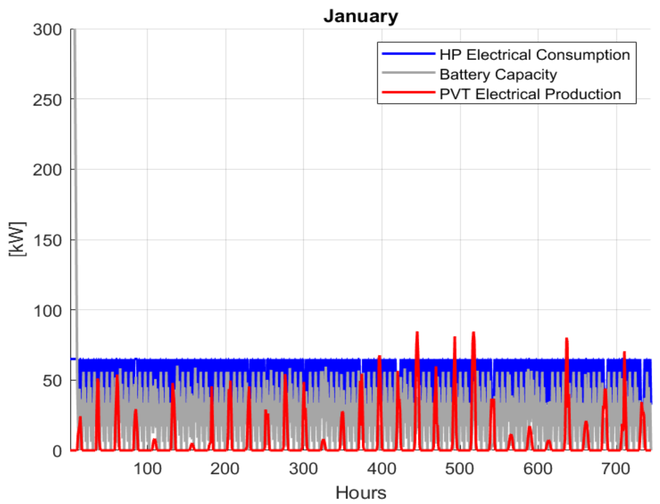

Figure 15: Trends of heat pump consumption, battery capacity, and PVT production of electrical energy in January.

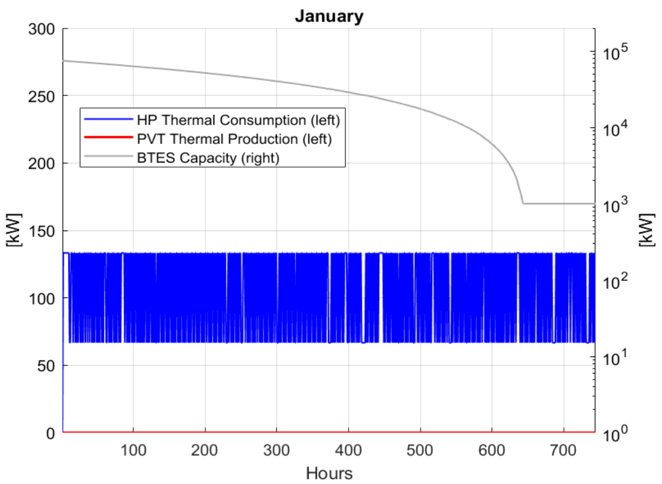

Figure 16: Trends of heat pump consumption, BTES capacity, and PVT production of thermal energy in January.

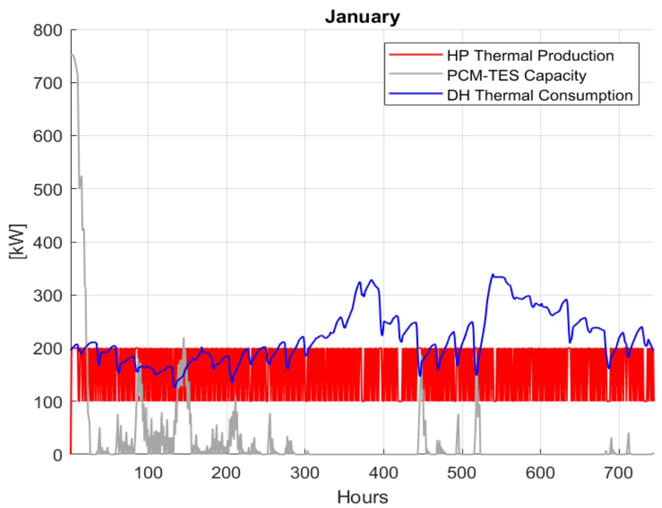

Figure 17: Trends of district heating consumption, PCM-TES capacity, and heat pump production of thermal energy in January.

some power is used to charge the battery; hence, the heat pump will operate full load until the battery is full enough to sustain the part load operation or until the PVT collector produces enough electrical energy. The PCM-TES is loaded with the heat resulting from the difference between heat pump capacity and heat demand. In the winter the heat demand is often higher than the full load capacity, which means that rarely the PCM-TES gets loaded. As shown in Figure 14, sometimes in the winter the heat available is lower than the demand.

The thermal energy produced by the PVT panels is null for the whole month of January. In fact, the air temperature is too low, and does not result in a positive thermal efficiency of the PVT collector. The heat pump is therefore thermally driven only by the heat stored in the BTES, which initially is 75 MWh (75% of the maximum), then decreases rapidly until reaching the 1% capacity before the end of January and simultaneously remains constant, since a continuous 1 MW of thermal energy is supplied by the ground.

3.3. Summer period

The results specific for the summer period are displayed in Figures 18-20 in terms of the parameters characterizing each subsystem of the IES.
In the summer the heat pump operation oscillates between internally driven full load and shut-off modes. The shut-off operation is programmed to activate when the PCM-TES is at its full capacity, which happens when the heat demand is low. In the summer, it remains around the minimum of 50 kW most of the time. As shown in Figure n, the available heat remains stationary at around 1,100 kW. This is because the heat pump operating on full load produces 200 kW and the PCM-TES is generally full at 1,000 kWh. Thus, the subtraction of the heat demand returns 1,100 kWh.

The fact that the total heat delivered is the lowest in the summer, is a direct implication of the operating modes distribution. In the warm months the heat pump is often shut-off. Thus, it does not produce heat, because the low demand is satisfied by the PCM-TES. This never happens in the winter, hence heat production is continuous in the summer.

The solar irradiance during the summer is high enough to ensure the full load operation during the day, while in the night the battery is discharged to fulfil the energy requirements of the heat pump. The PVT collector generates a huge amount of thermal energy during the day, usually much more than needed by the heat pump. Therefore, the BTES is often at its full capacity and, similarly to the battery, it is unloaded only during the night.

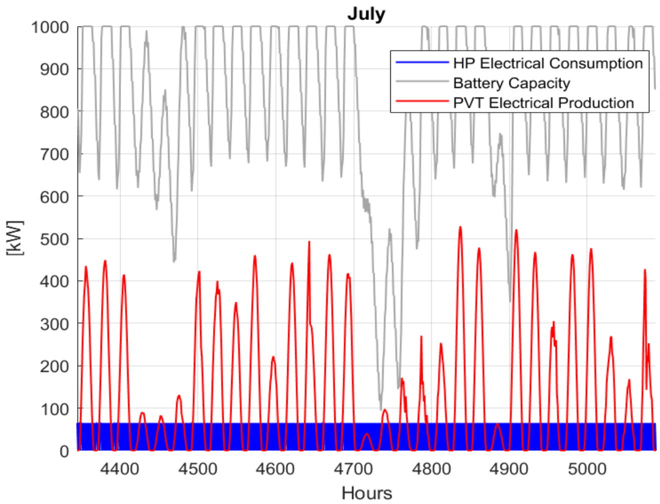

Figure 18: Trends of heat pump consumption, battery capacity, and PVT production of electrical energy in July.

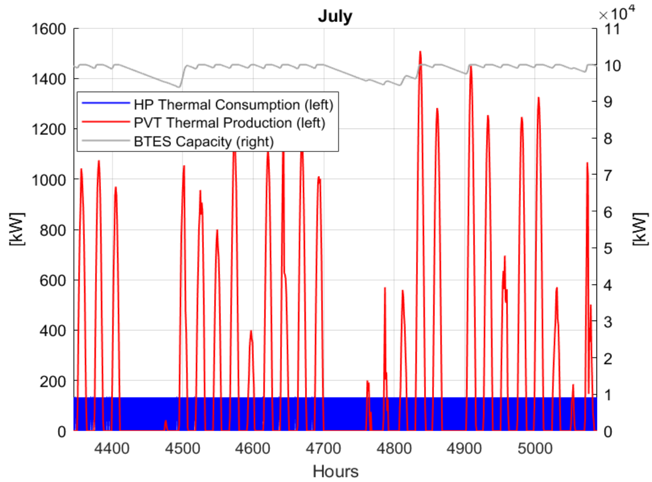

Figure 19: Trends of heat pump consumption, BTES capacity, and PVT production of thermal energy in July.

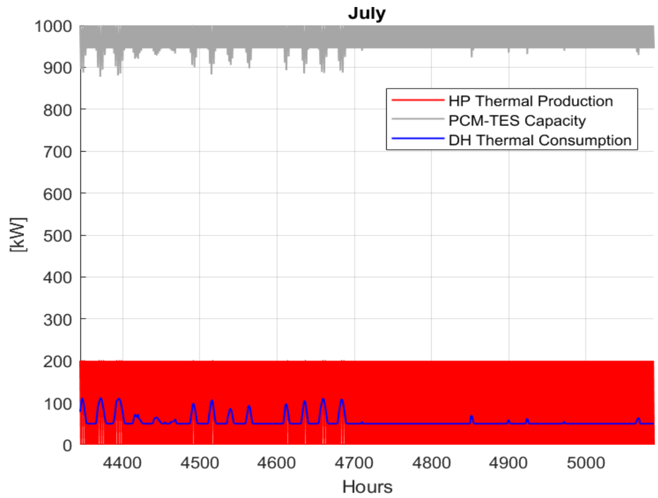

Figure 53: Trends of district heating consumption, PCM-TES capacity, and heat pump production of thermal energy in July.

4. Conclusions

In this work an integrated energy system has been built and its performances evaluated, as part of the bigger research project ChiNoZEN. The network comprises photovoltaic/thermal (PVT) panels, a borehole thermal energy storage (BTES), a battery, a phase-change material thermal energy storage (PCM-TES), a district heating (DH) section, and a cascade high temperature heat pump (HTHP) which uses zeotropic refrigerants and represents the core of the plant. Operation and performance of all the subsystems have been investigated for every hour along the whole year. The results obtained from the steady-state simulation of the heat pump were excellent. Hot water at 100°C can be produced and delivered for district heating, with a temperature lift of 80°C. The cascade cycle has a very high energy efficiency, with a COP of 3.6. Due to the high variability of the atmospheric conditions during the year, a huge difference between winter and summer operation was highlighted. In the warm months, the heat pump is frequently shut-off because the heat demand is low, and the PCM-TES is usually at full capacity. Conversely, in the winter, the heat pump operates often on full capacity driven by external electricity from the grid. The PVT collector is not able to provide enough electrical and thermal energy due to the short duration of the winter days. Overall, the system self-sustains its operation. In the winter, external power is required to drive the heat pump; but it is completely paid back in the summer, resulting in a positive balance.

In conclusion, the integration of cascade high-temperature heat pumps within an energy system presents a promising avenue for sustainable and efficient energy utilization. The synergistic coupling of different temperature levels in the cascade system has proven to be a pivotal factor, enabling the harnessing of thermal energy across a broader spectrum. Through this comprehensive study, the multiple benefits of this innovative approach have been elucidated, ranging from enhanced energy efficiency to reduced environmental impact. In essence, the integration of cascade high-temperature heat pumps into the energy infrastructure represents a step towards a more sustainable and resilient energy future. Through ongoing innovation and collaboration, we can continue to push the boundaries of energy efficiency, contributing to a cleaner and more sustainable planet.

5. Further Work

Many aspects of this research can be improved. The heat pump model should be updated considering the actual variations in the temperature of the water entering the heat exchangers; thus, a transient simulation should be performed rather than a steady-state one. The models for the PVT system and district heating system need to be updated. The return temperature of both hot water and heat source should be thoroughly regulated and the mass flow rates of water and refrigerant should be adjusted to various scenarios. The sizes of various components such as heat exchanges and compressors should be optimized to improve the COP. Each component should be modelled in detail to fully understand how the heat pump functions. The energy consumed by all the side equipment constituting the heat pump should be calculated, rather than just the power consumption of compressors. Considering now the whole IES, an economic assessment should be performed. The capital cost of every part of the system must be estimated then, together with operative costs and revenues, the payback period can be calculated. With this last result, it will be possible to tell if the capital investment is profitable or not. Eventually, a deeper work on the system can be conducted, building a pilot plant of the HP to obtain experimental results and validate the theoretical study.

Acknowledgements

This research work was funded by the Chinese-Norwegian collaboration project on Energy (ChiNoZEN) and National Key R&D Program of China (SQ2019YFE010256). The authors also gratefully acknowledge the financial support from the Research Council of Norway and user partners of High EFF (Centre for an Energy Efficient and Competitive Industry for the Future, an 8-year Research Centre under the FME-scheme).

References

United Nations, «The 17 Goals,» [Online]. Available: https://sdgs.un.org/goals. [Consultato il giorno 19 12 2023].

Norwegian University of Science and Technology, «About ChiNoZEN,» [Online]. Available: https://www.ntnu.edu/ept/chinozen#/view/about. [Consultato il giorno 19 12 2023].

Ryssdal, «High Temperature Heat Pumps in Integrated Energy Systems,» 2020.

Skoglund, «High Temperature Heat Pumps Using Zeotropic Refrigerant in Integrated Energy Systems,» 2022.

Herrando, Ramos, Zabalza e Markides, «A comprehensive assessment of alternative absorber-exchanger design for hybrid PVT-water collectors,» *Applied Energy,* vol. 235, pp. 1583-1602, 2019.

Ganesan e Eikevik, «New zeotropic CO2-based refrigerant mixtures for cascade high-temperature heat pump to reach heat sink temperature up to 180 °C,» *Energy Conversion and Management: X,* vol. 20, 2023.

Ganesan, Eikevik, Hamid, Wang e Yan, «Thermodynamic analysis of cascade high-temperature heat pump using new natural zeotropic refrigerant mixtures: R744/R600 and R744/R601,» *International Journal of Refrigeration,* vol. 154, pp. 215-230, 2023.

Sarkar e Bhattacharyya, «Assessment of blends of CO 2 with butane and isobutane as working fluids for heat pump applications,» *International Journal of Thermal Sciences,* vol. 48, pp. 1460-1465, 2009.

NTNU

Norwegian University of
Science and Technology